

**Cold Temperature Effect on the Acoustic Activity Emitted in Various  
Concrete Mixtures under Special Monitoring Conditions**

by

© Omar A. Kamel

A Thesis submitted to the School of Graduate Studies in partial fulfillment of the  
requirements for the degree of

**Master of Engineering**

**Faculty of Engineering and Applied Science – Civil Engineering**

Memorial University of Newfoundland

**August 2023**

St. John's, Newfoundland, Canada

## Abstract

Concrete mixtures with different microstructures and mechanical properties release different acoustic activity when they undergo cracking. This thesis aimed to investigate the effect of sub-freezing temperature ( $-20^{\circ}\text{C}$ ) on the waveforms of the acoustic emission (AE) in various concrete mixtures under flexural moment and abrasion forces. The study included many variables such as different coarse-to-fine aggregate ratios (C/F) (2.0 and 0.7), crumb rubber (CR) contents (0%, 10%, 20%, and 30%), rubber particle sizes (4.5 mm CR and 0.4 mm powder rubber), water-cement ratios (W/C) (0.4 and 0.55), fiber materials (polypropylene synthetic and steel), synthetic fiber lengths (19 mm and 38 mm), and volumes (0.2% and 1%), and sample temperatures ( $25^{\circ}\text{C}$  and  $-20^{\circ}\text{C}$ ). Samples from thirteen concrete mixtures were cast and tested under abrasion and monotonic four-point flexure moments, along with attaching piezoelectric AE sensors to monitor the AE activity throughout testing. Characteristics of AE signals such as the number of hits, signal amplitudes, cumulative signal strength (CSS), and wave rise time were collected and underwent various AE parameter-based analyses to correlate damage progression to the variation in the AE waveform. The results supported the ability of AE analysis to highlight abrasion damage progression and to detect the onset of micro- and macro-flexural cracks at both temperatures. Compared to  $25^{\circ}\text{C}$ , cooling down samples' temperature to  $-20^{\circ}\text{C}$  was found to decrease the values of the number of hits, CSS, severity ( $S_r$ ), and historic index ( $H(t)$ ) and to increase  $b$ -values for the waves emitted under abrasion and flexure. Noticeably, the reduction in samples' temperature decreased the emitted number of hits, CSS,  $S_r$ , and  $H(t)$ , and increased  $b$ -values till the onset of the first flexural macro-crack regardless of mixture composition. In addition, increasing CR

content (up to 30%) decreased wave signal amplitudes significantly at 25°C and was less noticeable at -20°C, which manifested the attenuation phenomenon at both temperatures. Eventually, the study developed user-friendly damage charts to estimate ranges of abrasion mass loss and wear depth and to classify the collected AE events, whether associated with flexure micro- or macro-cracks, exclusively considering temperature effect.

## Acknowledgments

I would like to thank my supervisor, Prof. Assem A. Hassan, co-supervisor Dr. Ahmed A. Abouhussien, and co-researcher Dr. Bassem H. Abdelaleem, for their guidance, patience, and support throughout this work, without which it would have been impossible to complete this work at this time. I'm really grateful to each one of you for all you have taught me during my Masters. Thank you for all your help over the courses, taking the first steps with me throughout the experimental, analytical, and writing process relieving the pressure, and making the mission easier. I'm also grateful to the technical services employees (Shawn Organ and Jamal Markov) at Memorial University of Newfoundland, who assisted me in the test setup, guided me in using the testing machines, and were on hand to offer assistance in the lab at all times. Without your cooperation and patience, the journey would have been more stressful.

The completion of this Journey wouldn't have been possible without the generous financial contributions through the NSERC-CRD. My Team and I are grateful for your support and belief in our work.

I would like to thank my dad, Alaa Kamel, my mom, and my brothers Ahmed and Mohamed for their love and continuous support while I pursued my graduate degree. I would also like to thank everyone who contributed to my research.

*Omar A. Kamel*

Omar A. Kamel

*August 16, 2023*

Date

## **Disclaimer**

It should be noted that the published versions of each paper presented in chapters 2, 3, and 4 have been slightly changed to fit the required thesis format.

## Co-authorship Statement

I, Omar A. Kamel, hold the principal author status for all the manuscript chapters (Chapters 2, 3, and 4) in this thesis. However, each manuscript is co-authored by my main supervisor (Prof. Assem A. A. Hassan), co-supervisor (Dr. Ahmed A. Abouhussien), and co-researcher (Dr. Bassem H. Abdelaleem), whose contributions have significantly facilitated the development of this work. Dr. Assem A. A. Hassan presented the idea for this project to me, and it was my task to carry out the work necessary to complete this thesis as part of the master's degree requirements.

In the papers presented in Chapters 2, 3, and 4, Dr. Bassem H. Abdelaleem and I performed all experimental work, including the preparation of the thirteen concrete mixtures, and test setup fabrication. Dr. Ahmed A. Abouhussien guided me to install the AE system, collect, filter, and analyze the AE data from those tests and formulate the results and conclusions presented in this thesis. Prof. Assem A. A. Hassan supervised all the stages of this research, including the experimental work, data analysis, and manuscript preparation.

Described below is a detailed breakdown of the work facilitated by the team.

- Paper 1 in Chapter 2: Omar A. Kamel, Ahmed A. Abouhussien, Assem A. A. Hassan, and Bassem H. Abdelaleem (2023) “Acoustic Emission Waves Propagation in Rubberized Concrete under Special Monitoring Conditions.” **Accepted for Publication in the Journal of Materials in Civil Engineering (ASCE)**

I was the primary investigator, with second, third, and fourth authors contributing to the idea, its formulation, development, and refinement of the format in which it has been presented.

- Paper 2 in Chapter 3: Omar A. Kamel, Ahmed A. Abouhussien, Assem A. A. Hassan, and Bassem H. Abdelaleem (2023) “Behavior of Acoustic Emission Waves in Rubberized Concretes under Flexure in a Sub-Freezing Environment.”  
**Submitted for Publication in the Journal of Cold Regions Engineering.**

I was the primary author, with second, third, and fourth authors contributing to the idea, its formulation, development, and refinement of the format in which it has been presented.

- Paper 3 in Chapter 4: Omar A. Kamel, Ahmed A. Abouhussien, Assem A. A. Hassan, and Bassem H. Abdelaleem (2023) “Assessment of Abrasion Resistance of Fiber-Reinforced Concrete at Cold Temperature via Acoustic Emission Analysis.” **Accepted for Publication in ACI Materials Journal, DOI: 10.14359/51738806**

I was the primary author, with second, third, and fourth authors contributing to the idea, its formulation, development, and refinement of the format in which it has been presented.

*Omar A. Kamel*

Omar A. Kamel

*August 16, 2023*

Date

# Table of Contents

<b>Abstract</b> .....	<b>ii</b>
<b>Acknowledgments</b> .....	<b>iv</b>
<b>Disclaimer</b> .....	<b>v</b>
<b>Co-authorship Statement</b> .....	<b>vi</b>
<b>List of Tables</b> .....	<b>xi</b>
<b>List of Figures</b> .....	<b>xiii</b>
<b>List of Symbols, Nomenclature, or Abbreviations</b> .....	<b>xvi</b>
<b>1.Introduction and Overview</b> .....	<b>1</b>
1.1 Background on AE analysis technology .....	2
1.2 Research Objectives.....	4
1.3 Thesis Outline .....	4
1.4 Chapter References .....	6
<b>2. Acoustic Emission Waves Propagation in Rubberized Concrete under Special Monitoring Conditions</b> .....	<b>10</b>
2.1 Abstract.....	10
2.2 Introduction.....	11
2.4 Experimental program .....	16
2.4.1 Mixture design .....	16
2.4.2 Materials properties .....	17
2.4.7 AE Intensity analysis .....	22
2.5.1 Impact of cold temperature on the abrasion experimental measurements.....	26

2.5.6 Abrasion damage charts of rubberized mixtures using AE intensity analysis parameters.....	36
2.6 Conclusions.....	38
2.7 Chapter References.....	40
<b>3. Behavior of acoustic emission waves in rubberized concretes under flexure in a sub-freezing Environment.....</b>	<b>46</b>
3.1 Abstract.....	46
3.2 Introduction.....	46
3.3 Experimental program.....	50
3.3.1 Mixture design.....	50
3.3.7 Built-in and amplitude-duration AE data filtering.....	54
3.3.8 AE <i>b</i> -value analysis.....	56
3.3.9 AE Intensity analysis.....	57
3.4.3 Effect of C/F ratio on micro- and macro-crack onset loads and associated AE parameters at a sub-freezing temperature.....	68
3.4.4 Effect of CR content on micro- and macro-crack onset load and associated AE parameters at a sub-freezing temperature.....	70
3.4.5 Effect of rubber particle size on micro- and macro-crack onset load and associated AE parameters at a sub-freezing temperature.....	71
3.4.6 Crack level detection chart based on intensity analysis parameters.....	72
3.4.7 Micro- and macro-crack classification using RA analysis.....	73
3.5 Conclusions.....	74
3.6 Chapter References.....	77

## **4. Assessment of Abrasion Resistance of Fiber-Reinforced Concrete at Cold**

<b>Temperature via Acoustic Emission Analysis.....</b>	<b>83</b>
4.1 Abstract.....	83
4.2 Introduction.....	83
4.3 Experimental Investigation.....	87
4.3.1 Materials properties and mixture design.....	87
4.3.2 Abrasion test setup.....	90
4.3.3 AE data filtering.....	91
4.3.5 AE Intensity analysis.....	93
4.4 Experimental Results and Discussion.....	94
4.4.3 Effect of cold temperature on the abrasion performance and AE data.....	104
4.4.6 Effect of fiber volume on the abrasion and AE data at room and cold temperature.....	109
4.4.7 Effect of fiber type on the abrasion and AE data at room and cold temperatures.....	109
4.4.8 Effect of fiber length on the abrasion and AE data under different temperatures.....	110
4.4.9 Abrasion damage quantification charts using AE intensity analysis parameters.....	111
4.5 Conclusions.....	114
4.6 Chapter References.....	116
<b>5. Summary and Recommendations.....</b>	<b>122</b>
<b>5.1 Summary.....</b>	<b>122</b>
<b>5.2 Potential Applications and Recommendations for Future Research.....</b>	<b>125</b>
<b>Bibliography.....</b>	<b>126</b>

## List of Tables

Table 2-1 Concrete mixture proportions.....	17
Table 2- 2 Chemical properties of all cement/cementitious materials.....	18
Table 2- 3 Physical properties of all cement/cementitious materials. ....	18
Table 2- 4 Average weight loss (gms) Throughout abrasion testing at 25°C and -20°C...	20
Table 2- 5 AE system details. ....	21
Table 2- 6 Average Compressive Strength and Wear Depth at 25°C and -20°C.....	25
Table 2- 7 Average Values of AE Parameters after 1 min & 6 mins of Abrasion Testing of all mixtures at 25°C and -20°C.....	26
Table 3- 1 Concrete mixture proportions.....	50
Table 3- 2 Chemical properties of all used binders. ....	51
Table 3- 3 Physical properties of all used binders. ....	52
Table 3- 4 AE system details. ....	55
Table 3- 5 Acceptance limits for AE amplitude-duration filter.....	55
Table 3- 6 Examples of K-values obtained in concrete-based specimens tested under a four-point flexure test. ....	60
Table 3- 7 Average results of cylinder compressive strength, first micro-crack loads, maximum flexure load, and flexure strength for all mixtures at 25°C and -20°C..	61

Table 3- 8 AE parameters at the micro-cracking stage at 25°C and -20°C.....	62
Table 3- 9 AE parameters at the macro-cracking stage at both temperatures. ....	63
Table 4- 1 Mixture proportions.....	88
Table 4- 2 The physical and mechanical properties of fibers. ....	88
Table 4- 3 Average values of L-box ratio, T <sub>50</sub> , V-funnel time, compressive strength, and wear depth of all samples at room and cold temperatures. ....	89
Table 4- 4 AE system details. ....	92
Table 4- 5 The percentage of weight loss after testing sample-2 of mixture 550-SynF38 (M5) at 25°C under smooth-roller and rotating cutter test. ....	96
Table 4- 6 Average AE parameters collected when testing sample-2 of mixture 550-SynF38 at 25°C under smooth-roller and rotating cutter test.....	97
Table 4- 7 Average values of AE parameters after 1 min & 6 min abrasion testing of all samples at room and cold temperatures. ....	105
Table 4- 8 Average percentage of weight loss after testing at room and cold temperatures for all samples. ....	105

## List of Figures

Fig. 2- 1 Research approach/highlights. ....	15
Fig. 2- 2 Rotating cutter abrasion test setup. ....	20
Fig. 2- 3 Average Weight Loss percentage (%) after 6 mins Abrasion at 25°C and -20°C. .....	25
Fig. 2- 4 Variation of AE Parameters along with Weight Loss (%) of Mixture M5 S2: a) number of hits, b) CSS, c) $H(t)$ , d) $S_r$ and e) $b$ -value.....	31
Fig. 2- 5 Average Signal Amplitudes throughout the Abrasion Tests.....	34
Fig. 2- 6 Ranges of Weight Loss (%) Quantification Chart. ....	37
Fig. 2- 7 Ranges of Wear Depth (mm) Quantification Chart. ....	37
Fig. 3- 1 Pictures of the rubber particles used: a) 0.4 mm powder rubber, b) 4.5 mm crumb rubber.....	52
Fig. 3- 2 Four-point load flexure setup, AE sensors' locations and samples' positioning. .....	53
Fig. 3- 3 RA-value vs. AF-value chart to classify tensile and shear cracks. ....	59

Fig. 3- 4 The change in AE parameters throughout flexure test versus applied load on sensor-1 sample-1 mixture 20%CR tested at -20°C: a) Number of hits, b) CSS, c) $S_r$ , d) $H(t)$ , e) $b$ -value.....	65
Fig. 3- 5 Average values of signal amplitudes at 25°C and -20°C at the onset of: a) micro-crack stage, b) macro-crack stage. ....	69
Fig. 3- 6 Crack level classification chart using intensity analysis parameters for all-in mixtures.....	73
Fig. 3- 7 Crack level classification chart based on average values of RA and A-FRQ for the non-rubberized mixtures. ....	74
Fig. 3- 8 Crack level classification chart based on average values of RA and average frequency for the rubberized mixtures.....	74
Fig. 4- 1 AE and rotating cutter abrasion test setup.....	91
Fig. 4- 2 Verification abrasion test setup using a smooth roller. ....	95
Fig. 4- 3 Mixture M5 samples after 6 minutes of testing under a) rotating cutter abrasion test, b) smooth roller abrasion test. ....	96
Fig. 4- 4 Average percentage of weight loss (%) of all mixtures at: a) Room temperature (25°C) and b) Cold temperature (-20°C). ....	98

Fig. 4- 5 Variations in AE parameters for 500-0.55w/b (S2) tested at cold temperature: a) Number of hits, b) CSS c)  $b$ -value, d)  $H(t)$ , and e)  $S_r$ ..... 101

Fig. 4- 6 Relation between  $b$ -value and weight loss for 550-0.55W/B (S2) at cold and room temperatures. .... 103

Fig. 4- 7 Average percentage of weight loss of all samples after 6 mins abrasion at room and cold temperatures. .... 104

Fig. 4- 8 Average signal amplitude values of all samples at room and cold temperature. .... 107

Fig. 4- 9 Percentage of weight loss (%) quantification chart..... 113

Fig. 4- 10 Wear depth (mm) quantification chart. .... 113

## List of Symbols, Nomenclature, or Abbreviations

<b>AE</b>	refers to “acoustic emission.”
<b>ASTM</b>	refers to “the American Society for Testing and Materials.”
<b>C.A.</b>	refers to “the coarse aggregate.”
<b>C/F</b>	refers to “the coarse to fine aggregate ratio.”
<b>CR</b>	refers to “the crumb rubber.”
<b>CSS</b>	refers to “the cumulative signal strength.”
<b>dB</b>	refers to “the decibel unit.”
<b>F.A.</b>	refers to “the fine aggregate.”
<b>FA</b>	refers to “the fly ash.”
<b><i>H (t)</i></b>	refers to “the historic index.”
<b>HRWRA</b>	refers to “the high-range water-reducer admixture.”
<b>MK</b>	refers to “the metakaolin”
<b>N</b>	refers to “number of hits.”
<b>NC</b>	refers to “normal concrete.”
<b>NDT</b>	refers to “non-destructive testing.”
<b>SCC</b>	refers to “self-consolidating concrete.”
<b>SCM</b>	refers to “supplementary cementing material.”
<b>SCRC</b>	refers to “self-consolidating rubberized concrete.”
<b>Syn-F</b>	refers to “synthetic fiber.”
<b>SHM</b>	refers to “structural health monitoring.”
<b><i>Sr</i></b>	refers to “the severity index.”
<b>W/B</b>	refers to “water to binder ratio.”

## **1. Introduction and Overview**

The existing public infrastructure of Canada and the United States (US) have suffered from decades of neglect and overuse, leading to the accelerated deterioration of civil infrastructure including bridges and roads (Halsall et al. 2016). Governments began to place more attention on inspection plans and maintenance to detect deficiencies early, reduce rehabilitation costs, and prolong the service lives of the infrastructure. According to the Canadian infrastructure (Halsall et al. 2016), Canada needed to spend \$50 billion in the replacement and maintenance of bridges in 2016. Similar maintenance was required for more than 68,000 existing bridges in the US, costing \$70.9 billion. A large amount of these expenses was going to the fixed-interval inspections and maintenance plans that can improve human resource efficiency (Sommer et al. 1993) but was found not cost-effective. A difficult decision in the allocation of a maintenance budget lies in choosing the optimum intervals between inspections of bridge members (Lovejoy 2003). These inspections at fixed intervals could be unnecessarily short for bridges in excellent condition and precariously long for those in poor conditions.

The development of structural health monitoring (SHM) technology over the past two decades has opened up an exciting field in civil engineering. SHM refers to the broad concept of assessing the in-service structural performance of structures using a variety of measurement techniques. Those structures which incorporate numerous SHM sensors are called “smart structures” and this approach has shown promise for detecting infrastructure damage. Consequently, determining the urgency of an inspection visit will lower inspection costs, especially in offshore infrastructure where inspection visits have high cost.

## 1.1 Background on AE analysis technology

Along with the nucleation of a localized source or sources of damage within a material, a rapid release of energy is emitted, and transient elastic waves are generated in a phenomenon called “the acoustic emission (AE)” (ASTM E1316, 2014). When AE is performed in a passive mode, AE transducers continuously capture acoustic waves generated by the formation of cracks or microcracks throughout loading. These acoustic waves properties are highly dependent on the source of damage (for example, crack size), and when analyzed, the type and magnitude of the resulting damage can be identified (Shigeishi and Ohtsu 2001; Yuyama et al. 1999). The continuous monitoring and analysis of the damage-associated AE waves can provide continuous measurement of crack formation and then evaluate the integrity of concrete structures.

Two types of AE analysis are most common: waveform analysis that can provide more information about source allocation, and parameter-based analysis that can quantify damage severity (Aggelis et al. 2012). For instance, the parameter-based analysis, rise time/maximum amplitude versus average frequency was used to characterize the fracture process and cracking evolution in various concrete mixtures (Aggelis 2011; Aggelis et al. 2012; Aggelis et al. 2013). Another parameter based technique, *b*-value analysis, was used to monitor crack growth in concrete and to identify stages of stress-induced cracking in cement mortar (Sagar et al. 2012), evaluate damage due to corrosion in concrete (Zaki et al. 2015), detect early corrosion in prestressed concrete piles (Vélez et al. 2015), monitor cracking behavior of steel fiber reinforced concrete under bending (Soulioti et al. 2009), assess the bond performance of corroded reinforced concrete (RC) beams (Abouhussien and Hassan 2017), and evaluate bond integrity of RC under pull out tests (Abouhussien and Hassan 2017).

Since the characteristics of the AE waves are related to the properties of the transfer medium, AE researchers have some concerns regarding AE technique integrity in different concrete mixtures. One of those concerns is that incorporating components in concrete production with noticeable acoustic absorption capacity such as rubber particles or high doses of synthetic polypropylene fibers, can affect the integrity of such a technique. Previous studies reported a reduction in wave signal amplitudes along with increasing rubber particles content in rubberized concretes (Abouhussien and Hassan 2020; Ridgley et al. 2018). However, AE analysis technique was still capable of detecting micro- and macro-cracking onset in rubberized concrete mixtures (Xu et al. 2018), evaluate abrasion resistance of self-consolidated rubberized concrete (Ridgley et al. 2018), evaluate the fracture process of crumb rubber basalt fiber reinforced concrete (Liu et al. 2020), and evaluate the post-peak softening behavior of rubberized concretes (Liu et al. 2021).

Another concern is that concrete mixtures with different microstructures and mechanical properties produce different types of acoustic activity when they undergo cracking (Pollock 2011). Hence factors that can affect concrete microstructure, such as extremely cold temperature, are anticipated to change the behavior of AE waves emitted in concrete mixtures similar to that effect on ultrasonic waves (Shang et al. 2014). Hence, such potential effects can impact the AE analysis if not properly considered. Whilst the properties of the acoustic waves emitted in room temperature are well documented under abrasion (Ridgley et al. 2018; Ridgley et al. 2018) and flexure (Abouhussien and Hassan 2019; Abouhussien and Hassan 2020; Behnia et al. 2014), the literature lacks information regarding the behavior when the temperature decreases to sub-freezing levels.

## 1.2 Research Objectives

This thesis aimed to investigate the change in the parameters of AE signals emitted under abrasion and flexure tests in various concrete mixtures at sub-freezing temperatures. The developed concrete mixtures contained different sizes and contents of rubber particles and fibers which are known to have noticeable acoustic absorption capacity and may affect the AE waves behavior. The experimental program included testing thirteen concrete mixtures with various crumb rubber contents and sizes, various fiber dosages, lengths and materials, different W/B, and different C/F. Besides, the study aimed to develop user-friendly charts that can allow engineers to roughly estimate the cracking level (micro- or macro-cracking) under flexure and ranges of mass loss percentages or wearing depths due to abrasion.

## 1.3 Thesis Outline

The Experimental program of this thesis is divided into three experimental studies and discussed into the following chapters:

- **Chapter 2** titled “*Acoustic Emission Waves Propagation in Rubberized Concrete under Special Monitoring Conditions*” addresses the effect of different W/B ratios, rubber particle sizes, and crumb rubber contents on the parameters of the AE waves emitted under abrasion forces at -20°C and 25°C.
- **Chapter 3** titled “*Behavior of acoustic emission waves in rubberized concretes under flexure in a sub-freezing Environment*” investigates the behavior of AE waves emitted in rubberized concrete mixtures under flexure in a sub-freezing environment.
- **Chapter 4** titled “*Assessment of Abrasion Resistance of Fiber-Reinforced Concrete at Cold Temperature via Acoustic Emission Analysis*” investigates the behavior change of the AEs

emitted in concrete mixtures with different C/F, fiber types (steel and polypropylene synthetic), and different fiber length and contents.

- **Chapter 5** includes summary, potential applications for the current study, and recommendations for future studies.

## 1.4 Chapter References

- Abouhussien, A. A., and Hassan, A. A. (2017). "Application of acoustic emission monitoring for assessment of bond performance of corroded reinforced concrete beams." *Structural Health Monitoring*, 16(6), 732-744.
- Abouhussien, A. A., and Hassan, A. A. (2019). "Crack Growth Monitoring in Fiber-Reinforced Self-Consolidating Concrete via Acoustic Emission." *ACI Materials Journal*, 116(5), 181-191.
- Abouhussien, A. A., and Hassan, A. A. A. (2017). "Acoustic emission monitoring for bond integrity evaluation of reinforced concrete under pull-out tests." *Advances in structural engineering*, 20(9), 1390-1405.
- Abouhussien, A. A., and Hassan, A. A. A. (2020). "Classification of damage in self-consolidating rubberized concrete using acoustic emission intensity analysis." *Ultrasonics*, 100, 105999-105999.
- Aggelis, D. G. (2011). "Classification of cracking mode in concrete by acoustic emission parameters." *Mechanics research communications*, 38(3), 153-157.
- Aggelis, D. G., Soulioti, D. V., Barkoula, N. M., Paipetis, A. S., and Matikas, T. E. (2012). "Influence of fiber chemical coating on the acoustic emission behavior of steel fiber reinforced concrete." *Cement and Concrete Composites*, 34(1), 62-67.
- Aggelis, D. G., Soulioti, D. V., Gatselou, E. A., Barkoula, N. M., and Matikas, T. E. (2013). "Monitoring of the mechanical behavior of concrete with chemically treated steel fibers by acoustic emission." *Construction and Building Materials*, 48, 1255-1260.
- Behnia, A., Chai, H., Yorikawa, M., Momoki, S., Terazawa, M., and Shiotani, T. (2014). "Integrated non-destructive assessment of concrete structures under flexure by acoustic emission and travel time tomography." *Construction and Building Materials*, 67, 202-215.

- E1316, A. (2014). "terminology for nondestructive examinations." *ASTM International*(west conshohocken, PA).
- Halsall, P., Cavicchia, L., and McDonough, A. (2016). *Canadian Infrastructure Report Card : Informing the Future*, Johnson-Shoyama Graduate School of Public Policy, Regina, SK, CA.
- Liu, H., Li, W., Luo, G., Liu, S., and Lyu, X. (2020). "Mechanical properties and fracture behavior of crumb rubber basalt fiber concrete based on acoustic emission technology." *Sensors (Basel, Switzerland)*, 20(12), 1-21.
- Liu, M., Lu, J., Ming, P., and Yin, Y. (2021). "Study of fracture properties and post-peak softening process of rubber concrete based on acoustic emission." *Construction & building materials*, 313, 125487.
- Lovejoy, S. C. (2003). "Determining Appropriate Fatigue Inspection Intervals for Steel Bridge Members." *Journal of bridge engineering*, 8(2), 66-72.
- Pollock, A. A. "Material Brittleness and the energetics of acoustic emission." *Proc., Experimental Mechanics on Emerging Energy Systems and Materials, Volume 5: Proceedings of the 2010 Annual Conference on Experimental and Applied Mechanics*, Springer, 73-79.
- Ridgley, K. E., Abouhussien, A. A., Hassan, A. A., and Colbourne, B. (2018). "Assessing abrasion performance of self-consolidating concrete containing synthetic fibers using acoustic emission analysis." *Materials and Structures*, 51, 1-17.
- Ridgley, K. E., Abouhussien, A. A., Hassan, A. A., and Colbourne, B. (2018). "Evaluation of abrasion resistance of self-consolidating rubberized concrete by acoustic emission analysis." *Journal of Materials in civil Engineering*, 30(8), 04018196.

- Sagar, R. V., Prasad, B. R., and Kumar, S. S. (2012). "An experimental study on cracking evolution in concrete and cement mortar by the *b*-value analysis of acoustic emission technique." *Cement and Concrete Research*, 42(8), 1094-1104.
- Shang, H.-s., Yi, T.-h., and Guo, X.-x. (2014). "Study on Strength and Ultrasonic Velocity of Air-Entrained Concrete and Plain Concrete in Cold Environment." *Advances in materials science and engineering*, 2014, 1-7.
- Shigeishi, M., and Ohtsu, M. (2001). "Acoustic emission moment tensor analysis: development for crack identification in concrete materials." *Construction and Building Materials*, 15(5), 311-319.
- Sommer, A. M., Nowak, A. S., and Thoft-Christensen, P. (1993). "Probability-Based Bridge Inspection Strategy." *Journal of structural engineering (New York, N.Y.)*, 119(12), 3520-3536.
- Soulioti, D., Barkoula, N., Paipetis, A., Matikas, T., Shiotani, T., and Aggelis, D. (2009). "Acoustic emission behavior of steel fibre reinforced concrete under bending." *Construction and Building Materials*, 23(12), 3532-3536.
- Vélez, W., Matta, F., and Ziehl, P. (2015). "Acoustic emission monitoring of early corrosion in prestressed concrete piles." *Structural control and health monitoring*, 22(5), 873-887.
- Xu, J., Fu, Z., Han, Q., Lacidogna, G., and Carpinteri, A. (2018). "Micro-cracking monitoring and fracture evaluation for crumb rubber concrete based on acoustic emission techniques." *Structural Health Monitoring*, 17(4), 946-958.
- Yuyama, S., Li, Z.-w., Ito, Y., and Arazoe, M. (1999). "Quantitative analysis of fracture process in RC column foundation by moment tensor analysis of acoustic emission." *Construction and Building Materials*, 13(1), 87-97.

Zaki, A., Chai, H. K., Aggelis, D. G., and Alver, N. (2015). "Non-destructive evaluation for corrosion monitoring in concrete: A review and capability of acoustic emission technique." *Sensors*, 15(8), 19069-19101.

## 2. Acoustic Emission Waves Propagation in Rubberized Concrete under Special Monitoring Conditions

### 2.1 Abstract

This study investigates the change in the acoustic emission (AE) parameters emitted in rubberized concrete under abrasion action at a sub-freezing temperature (-20°C). Seven concrete mixtures were developed with different coarse-to-fine aggregate (C/F) ratios (2.0 and 0.7), various crumb rubber (CR) content (0%, 10%, 20%, 30%), and different rubber particle sizes (4.5 CR and 0.4 mm powder rubber (PR)). 100 mm cubic samples from each mixture were tested at -20°C and 25°C for comparison while being monitored via an AE system. AE parameters such as amplitude, number of hits, and signal strength were collected and underwent two parameter-based analyses: *b*-value and intensity analysis approaches, resulting in three additional parameters: *b*-value, severity ( $S_r$ ), and the historic index ( $H(t)$ ). Results showed that cooling down samples' to -20°C and testing under abrasion was accompanied by a decrease in the emitted number of hits, CSS,  $S_r$ ,  $H(t)$ , and an increase in the *b*-values compared to testing at 25°C. Furthermore, incorporating rubber particles was found to decrease the AE signals' amplitudes significantly at 25°C and slightly at -20°C, which manifested wave attenuation occurrence at both temperatures. Besides, AE analysis showed a decrease in the abrasion resistance for mixtures with higher C/F, higher CR content, and larger rubber particle size. These decreases were more noticeable at 25°C compared to -20°C. Finally, the study developed two damage classification charts to estimate the ranges of abrasion mass loss percentage and wear depth in terms of the intensity analysis parameters:  $S_r$  and  $H(t)$ .

## 2.2 Introduction

Concrete surfaces in roadways, parking lots, airfield runways, and/or other rigid pavement applications suffer from inescapable impact and erosive forces. As larger vehicles and/or increased speed limits became more common recently, the erosive forces became more aggressive. Degradation in such infrastructure, especially in arctic regions, which are also characterized by extremely adverse climates, can cause significant disruption to people's daily lives. As a result, concrete has to possess proper abrasion resistance, impact absorption, and durability properties relevant to its use.

Abrasion damage occurs in concrete due to sliding or friction with aggressive movement. The American Society for Testing and Materials (ASTM) provides standard tests to evaluate concrete's abrasion performance. These standard methods include the rotating cutter method (ASTM, 2012a), the rotating desk test (ASTM, 2012b), and sandblasting test (ASTM, 2012c). The results of each procedure are used for a comparative analysis to evaluate the hardness or the abrasion resistance of the tested surface. Abrasion resistance of concrete is significantly influenced by many factors such as hardness and volume fraction of coarse aggregate (Liu, 1981), the use of supplementary cementing materials in the mixture (Laplante et al., 1991), and/or type and duration of concrete curing (Nanni, 1989). Abrasion damage can also be alleviated by the proper design, handling, and placement of concrete. For instance, self-consolidating concrete (SCC), which has a more homogeneous and denser microstructure, due to the better dispersion of the cementitious particles in the matrix, was found to have better mechanical properties and abrasion resistance compared to normal vibrated concrete (Ghafoori et al., 2014).

Using crumb rubber (CR) as a fine aggregate replacement in concrete has been shown to improve the impact resistance and ductility of concrete (Bignozzi and Sandrolini, 2006). The use of CR also

allows the development of eco-friendly concrete (Su et al., 2015), with reduced self-weight. Nearly one billion waste tires are discarded each year, and this number is predicted to reach 1.2 billion per year in 2030 (Rahman et al., 2012). These tires are disposed of in landfills and empty yards, burnt, or even dumped illegally. Rubber particles have a lower stiffness modulus compared to other concrete constituents. The presence of rubber acts as large pores in the concrete matrix, which reduces the effective cross-section area and overall strength of concrete. In addition, the non-uniform texture of rubber particles contributes to entrapping a higher volume of air voids in the concrete mixture, which further weakens the strength of concrete (Ismail and Hassan, 2016a).

Reducing the size of rubber particles reduces the negative effect of rubber on concrete strength (Osama et al. 2020). However, the positive effect of rubber on improving impact resistance and energy absorption is also reduced when reducing the size of rubber particles (Osama et al. 2020). Therefore, it is essential to select the proper size of rubber based on the intended structure application. To alleviate the negative effects of CR in the concrete mixture, researchers suggested adding supplementary cementing materials such as fly ash, silica fume (AbdelAleem and Hassan, 2018), ground granulated blast furnace slag (Ozbay et al., 2011), and/or metakaolin, which was proven to enhance the mechanical properties, mixture viscosity, particles suspension, and reduce coarse aggregate and CR segregation (Ismail and Hassan, 2016b; Madandoust and Mousavi, 2012).

Acoustic emission (AE) monitoring has been proven to be a more suitable non-destructive testing technique over other traditional forms of monitoring. In areas with extreme adverse weather such as the Arctic region, AE can be the best choice to save time and high costs for routine maintenance and inspection in hard-to-reach locations. AE monitoring has been successfully employed in many studies related to rubberized concretes. For instance, AE has been recently used to assess the abrasion damage in SCC containing rubberized materials (Ridgley et al., 2018); to classify damage

and detect micro and macro cracks in rubberized SCC (Abouhussien and Hassan, 2020); to evaluate the impact resistance and acoustic absorption capacity in rubberized SCC (Ismail and Hassan, 2016a); to investigate the fatigue damage process in rubberized SCC (Wang et al., 2013); and to monitor micro-cracking and fracture process in rubberized SCC (Xu et al. 2018).

Ridgley et al. (2018) performed a preliminary study on AE monitoring to assess the abrasion damage in rubberized concrete at room temperature. They noticed changes in the AEs' behavior when adding CR to the mixture. A significant decrease in signal amplitudes was observed with the increase in CR content, which manifested the attenuation phenomenon, as supported in other studies (Wang et al., 2013; Xu et al., 2018). Rubber particles have a high sound absorption property. As the percentage of CR increases, the intensity of the sound travels from the source of damage is expected to decrease (Ismail and Hassan, 2016). It is anticipated that the rubber sound absorption properties would be different at sub-freezing temperatures, and this could affect the wave attenuation and the accuracy of AE readings in cold regions similar to the behavior change of ultrasonic waves (Shang et al., 2014).

To date, there are no studies in the literature that monitored the behavior of AE waves emitted in rubberized concretes at a sub-freezing temperature; consequently, further investigations are warranted. The goal of this investigation is to evaluate the change in AE readings in rubberized concretes at sub-zero temperatures. The study particularly focuses on monitoring abrasion damage using AE signal analysis as a new and innovative monitoring technique. The effect of using various coarse-to-fine aggregate ratios (C/F) (2.0 and 0.7), different rubber contents (0%, 10%, 20%, and 30%), and different rubber sizes (4.5 mm CR and 0.4 mm PR) on AE wave propagation are highlighted in this study. The investigation also aims to provide charts to estimate the ranges of abrasion mass loss and wearing depth using AE intensity analysis parameters:  $S_r$  and  $H(t)$ . The

outcome of this study can enrich the AE analysis technique to provide real-time monitoring in hard-to-reach structures such as offshore platforms, especially those structures are often subjected to abrasion at extremely low temperatures.

### **2.3 Research methodology**

**Fig. 2-1** shows the research approach/highlights of the conducted study. From the figure, it can be seen that the research went through six main stages: development of mixtures; curing and preparing of samples before testing; conducting rotating cutter abrasion test in conjunction with AE monitoring; collecting experimental data and recording AE parameters; filtering the recorded AE parameters and conducting parameter-based analysis; discussing the obtained results and draw the research conclusion. Each stage is discussed in further detail in the following sections.

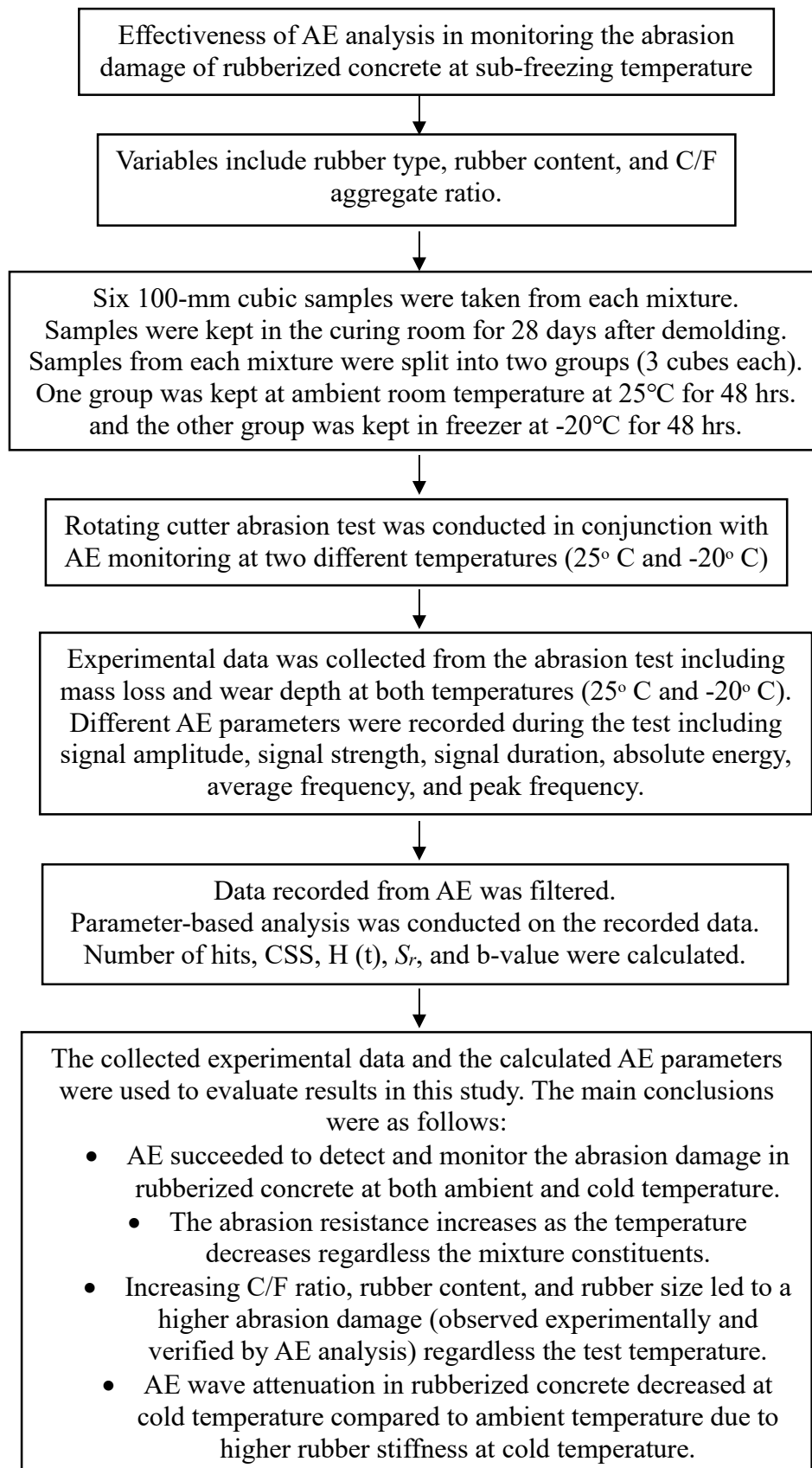


**Fig. 2- 1** Research approach/highlights.

## 2.4 Experimental program

### 2.4.1 Mixture design

**Table 2-1** shows the proportions of all mixtures used in this study. The tested mixtures included two non-rubberized concrete mixtures with different C/F (M1 and M2), one control mixture with 0% rubber content (M3), and four rubberized SCC mixtures (M4-M7). M1 mixture had a relatively high C/F of 2.0, whilst all other mixtures (M2-7) had 0.7 C/F. This difference in the C/F was selected to magnify the effect of lower coarse aggregate content (which is frequently used in SCC mixtures) on the AE spread behavior if any. Mixture M3 was developed as a control SCC mixture for all the rubberized mixtures (M4-7) to assess the effect of rubber content and size on the abrasion damage and associated AE wave parameters. Three of the rubberized SCC mixtures (M4-6) contained 4.5 mm CR as a fine aggregate replacement with a percentage of 10%, 20%, and 30% by volume of sand, respectively. These values were selected based on previous studies performed by the authors (Ismail and Hassan, 2016a; Ismail and Hassan, 2016b; Ismail and Hassan, 2017) aimed to optimize the fresh and mechanical properties of rubberized SCC mixtures. In these studies, it wasn't possible to develop SCC with acceptable fresh properties, as per ASTM C1611 (ASTM, 2009), when the percentage of CR exceeded 30%. M7 mixture (PR size 0.4 mm) was included in this study to be compared with M5 to study the effect of PR compared to CR on the abrasion resistance and spread of AE signals. It should be noted that in rubberized mixtures, the binder content was increased from 500 kg/m<sup>3</sup> to 550 kg/m<sup>3</sup> to compensate for the reduction in the strength that results from the inclusion of rubber. All mixtures were designated as per their binder content and either C/F or percentage of CR. For example, a mixture containing 550 kg/m<sup>3</sup> binder content and 10% CR would be designated as 550-10%CR.

**Table 2-1** Concrete mixture proportions.

Mixture no.	Mixture type	Cement (kg/m <sup>3</sup> )	MK (kg/m <sup>3</sup> )	FA (kg/m <sup>3</sup> )	C.A. (kg/m <sup>3</sup> )	F.A. (kg/m <sup>3</sup> )	Water content (kg/m <sup>3</sup> )	Rubber content (kg/m <sup>3</sup> )	C/F	W/C	HRWRA (kg/m <sup>3</sup> )
M1	500-2.0C/F-0.4w/c	500	-	-	1111.54	555.77	200	-	2.0	0.4	1.72
M2	500-0.7C/F0.4w/c	500	-	-	686.53	980.76	200	-	0.7	0.4	1.51
M3	550-control	275	110	165	620.2	886.2	220	-	0.7	0.4	3.44
M4	550-10%CR	275	110	165	620.2	797.4	220	32.5	0.7	0.4	4.36
M5	550-20%CR	275	110	165	620.2	708.8	220	64.9	0.7	0.4	4.67
M6	550-30%CR	275	110	165	620.2	620.2	220	97.3	0.7	0.4	5.82
M7	550-20%PR	275	110	165	620.2	708.8	220	58.7	0.7	0.4	4.61

### 2.4.2 Materials properties

All mixtures utilized general-use Portland cement (type GU) with a specific gravity of 3.15 gm/cm<sup>3</sup>, in accordance with ASTM type I (ASTM C150-12, 2012e). Metakaolin (MK) (provided by Advanced Cement Technologies LLC) conforming to ASTM C618 class N (ASTM C618, 2012) and fly ash (FA) conforming to ASTM C618 class N (ASTM C618, 2012) were used in mixtures M3-7. The MK and FA used had a specific gravity of 2.26 gm/cm<sup>3</sup> and 2.51 gm/cm<sup>3</sup>, respectively. The chemical and physical properties of the binders used were provided by the manufacturer and are shown in **Tables 2-2** and **2-3**. It's worth noting that adding MK and FA to the mixtures aimed mainly to improve the workability and strength of the mixtures and to compensate for the adverse impact of CR on these properties. All mixtures included natural crushed aggregate with a maximum aggregate size of 10 mm and natural fine aggregate with a maximum size of 4.75 mm. Both aggregates had a specific gravity of 2.61 and water absorption of 1.1%. The rubber used in all mixtures had a specific gravity of 0.94 and negligible water absorption. Two sizes of rubber were used: 4.5 mm CR and 0.4 mm PR. The target slump flow for all SCC mixtures was 700 ± 50 mm, as per ASTM C1611 (ASTM 1611, 2009), and was obtained by using poly-carboxylate-based high-range-water-reducing-admixtures, in accordance with ASTM C494 type F (ASTM, 2013). The high-range-water-reducing admixtures had a specific

gravity of 1.21, a volatile weight of 62%, and a pH level of 9.5. For all mixtures, the water-binder (W/B) ratio was set to a constant value of 0.4 which was recommended in previous studies (Ismail and Hassan, 2016; Ismail and Hassan, 2016; Ismail and Hassan, 2017).

**Table 2- 2** Chemical properties of all cement/cementitious materials.

Chemical properties %	Cement	MK	Fly ash
SiO <sub>2</sub>	19.63	51–53	51
Al <sub>2</sub> O <sub>3</sub>	5.48	42–44	23
Fe <sub>2</sub> O <sub>3</sub>	2.37	<2.2	12
FeO	--	--	--
TiO <sub>2</sub>	--	<3.0	--
C	--	--	--
Cr <sub>2</sub> O <sub>3</sub>	--	--	--
MnO	--	--	--
P <sub>2</sub> O <sub>5</sub>	--	<0.21	--
S <sub>2</sub> O	--	--	--
BaO	--	--	--
SO <sub>4</sub>	--	<0.5	--
CaO	62.43	<0.2	5
MgO	2.47	<0.1	--
Na <sub>2</sub> O	--	<0.05	--
C <sub>3</sub> S	52.33	--	--
C <sub>2</sub> S	16.82	--	--
C <sub>3</sub> A	10.51	--	--
C <sub>4</sub> AF	7.23	--	--
K <sub>2</sub> O	--	<0.40	--
L.O.I	2.04	<0.50	--

**Table 2- 3** Physical properties of all cement/cementitious materials.

	Cement	Metakaolin	Fly ash
Specific gravity	3.15	2.5	2.38
Blaine fineness (m <sup>2</sup> /kg)	410	19,000	420

### 2.4.3 Test samples details

To evaluate the compressive strength, six cylinders (100 mm diameter and 200 mm height) were prepared from each mixture to be tested at both temperatures according to ASTM C39 (ASTM C39-12, 2012). In addition, six 100 mm cubes were cast for each mixture for the abrasion test according to the rotating-cutter standard (ASTM, 2012a). All specimens were kept in a moist-curing room at approximately 25°C for 28 days. To evaluate the change in AE propagation behavior as a result of turning water inside the voids into ice, all samples were submerged in water for 48 hrs to guarantee full saturation then the surface was dried to reach a saturated surface dry moisture state. Then, samples from each mixture were divided into two groups, each containing three cylinders and three cubes. One group was kept at ambient room temperature (25°C), and the other group was kept in a freezer at -20°C for at least 48 hours before the test to reach a steady-state temperature (Zaki et al., 2020). For each mixture, the abrasion test was conducted on three samples, and the average percentages of weight loss were recorded in **Table 2-4**.

#### **2.4.4 Abrasion test setup**

Rotating-cutter method, mentioned in ASTM C944 (2012), was implemented for the abrasion test. Three faces were tested in each mixture at each temperature condition. The rotating-cutter method uses a spindle that carries a constant load of 98 N (10 Kg) and rotates directly on the face of the cubic sample, as shown in **Fig. 2-2**. In this study, each face was continuously scraped for 6 intervals (1 minute each) and the weight loss was measured after each interval with a digital scale of 0.02 gm resolution. Besides, the wear depth due to abrasion was measured for each face at the end of the test (after 6 mins) using electronic calipers having a sensitivity of 0.01 mm.



**Fig. 2- 2** Rotating cutter abrasion test setup.

**Table 2- 4** Average weight loss (gms) Throughout abrasion testing at 25°C and -20°C.

Mixture no.	Mixture	Average weight loss (gms)											
		1 min		2 min		3 min		4 min		5 min		6 min	
		25°C	- 20°C	25°C	- 20°C	25°C	- 20°C	25°C	- 20°C	25°C	- 20°C	25°C	-20°C
M1	500-2C/F-0.4w/c	4.56	3.60	7.92	6.72	10.32	8.88	12.00	11.04	13.92	12.24	16.08	13.44
M2	500-0.7C/F-0.4w/c	4.04	2.84	6.20	5.24	9.32	7.40	11.00	9.56	12.92	11.48	14.84	13.19
M3	550-MK/FA-control	2.77	2.05	4.93	4.21	7.57	6.37	9.49	7.57	11.17	9.73	12.85	11.55
M4	550-10%CR	3.95	3.23	6.59	5.63	8.51	7.31	10.19	9.23	12.35	11.29	15.23	12.83
M5	550-20%CR	5.39	4.43	7.79	6.59	9.95	8.99	11.39	9.95	13.83	11.89	17.87	14.37
M6	550-30%CR	6.35	4.67	8.75	7.79	11.39	9.47	13.31	11.63	14.94	13.07	19.79	15.47
M7	550-20%PR	4.91	4.43	7.31	6.59	9.47	8.51	10.91	9.95	12.35	11.39	15.71	13.89

#### **2.4.5 AE data monitoring setup**

AE software called AEwin was used to monitor and record the signals being emitted during abrasion testing. As shown in **Fig. 2-2**, one piezoelectric AE sensor (model number R6I-AST)

with an integral preamplifier (acoustics, 2005) was attached to each cube with a two-part epoxy adhesive and then connected via a cable to the data acquisition system made by Mistras group (Mistras Group, 2007). These sensors have high sensitivity and low resonant frequency, making them suitable for multiple applications, including metals, FRPs, and concrete structures (Abouhussien and Hassan 2017). An amplitude threshold of 40 dB was set in the AEWin software to record different AE signal parameters emitted during the abrasion testing period. A full list of the AE parameters and filtering criteria predefined in the system can be seen in **Table 2-5**. The analog and digital filter ranges shown in **Table 2-5** were selected based on a preliminary study completed by the authors to evaluate the abrasion damage in concrete using AE analysis (Ridgley et al., 2018). This AE data acquisition setup in **Table 2-5** has also been implemented in other previous studies conducted by the authors and allowed the detection of various damage mechanisms in concrete (Abouhussien and Hassan, 2017; Abouhussien and Hassan, 2017). The system recorded a wide variety of AE signal parameters including amplitude, signal strength, signal duration, absolute energy, counts, rise time, average frequency, and peak frequency. A full description of these parameters is discussed in further detail in ASTM E1316 (ASTM, 2014).

**Table 2- 5** AE system details.

AE setup parameters	
Threshold	40 dB <sub>AE</sub>
Sample rate	1 MSPS
Pre-trigger	256 μs
Length	1000 points
Preamp gain	40 dB
Preamp voltage	28
Analog filter	1-50 kHz
Digital filter	100-400 kHz
Peak definition time	200 μs
Hit definition time	800 μs
Hit lockout time	1000 μs
Maximum duration	1000 μs

#### 2.4.6 AE *b*-value analysis

The various traditional AE parameters such as signal amplitudes, number of hits, and cumulative signal strength were collected, filtered, and analyzed throughout the test. In addition, signal amplitudes and the number of hits underwent a *b*-value analysis to evaluate the abrasion damage progression for all samples resulting in a subsidiary parameter referred to as the *b*-value. The *b*-value analysis was adapted from seismic magnitude-frequency equations in the first place and then extended to concrete and was effectively utilized in many studies to indicate the changes in the frequency level of the AE waves to assess several damage mechanisms in concrete (Abdelrahman et al., 2015; Abouhussien and Hassan, 2019; Abouhussien and Hassan, 2020; Colombo et al., 2003; Du et al., 2019). The *b*-value was calculated throughout the abrasion tests for all specimens according to **Eq. 1** and correlated to the different damage stages in all samples.

$$\text{Log NA} = a - b \log A \quad \text{Eq. 1}$$

In this equation, NA. = the number of hits having amplitudes larger than A (before the indicated time); A = the signal amplitude of the specific hit at the specific time (dB), a = an empirically derived constant (a is the vertical axis intercept with the line induced when plotting the values of Log NA on the vertical axis and log A on the horizontal axis. The value of a (calculated in this study) = 3.8 and *b* = the *b*-value (Abdelrahman et al., 2015; Abouhussien and Hassan, 2019; Abouhussien and Hassan, 2020; Colombo et al., 2003; Du et al., 2019).

#### 2.4.7 AE Intensity analysis

Another AE analysis approach called intensity analysis was performed on the signal strength of the collected AE signals to calculate two more parameters namely: the historic index  $H(t)$  and severity ( $S_r$ ). These two parameters were originally developed for the classification of damage of FRP vessels (Fowler, 1989). These two parameters are very sensitive to the extent of damage,

which made them effective for the quantifiable assessment of the different damage mechanisms of concrete in several previous studies (Abouhussien and Hassan, 2017; ElBatanouny et al., 2014; Nair and Cai, 2010; Vélez et al., 2015). In this study, these parameters have the potential to highlight the effects of varying temperatures, C/F, and rubber particle size/dosage on the AE data parameters and to correlate to the damage.

The  $H(t)$  could measure any sudden peaks in the cumulative signal strength (CSS) versus time and be calculated using **Eq. 2** below:

$$H(t) = \frac{N}{N-K} \frac{\sum_{i=K+1}^N S_{oi}}{\sum_{i=1}^N S_{oi}} \quad \text{Eq. 2}$$

In this equation,  $N$  = the cumulative number of hits until the time ( $t$ ),  $S_{oi}$  = the signal strength of the  $i$ th event. On the other hand, the severity ( $S_r$ ) was calculated according to **Eq. 3**.

$$S_r = \sum_{i=1}^J \frac{S_{oi}}{J} \quad \text{Eq. 3}$$

Severity ( $S_r$ ) value was based on the average signal strength of the  $J$  number of hits. The constants ( $K$  and  $J$ ) in **Eqs. 2 and 3** used in this study were determined based on previous studies regarding AE analysis in concrete (Fowler, 1989).

The constant  $K$  used in **Eq. 2** may affect the magnitude of  $H(t)$  and subsequently the associated damage progression in terms of capturing any pronounced AE activity. In this analysis,  $K$  was calculated as follows:

- a)  $K = 0$ : if  $N \leq 50$ , b)  $K = N - 30$ : if  $51 \leq N \leq 200$ , c)  $K = 0.85 N$ : if  $201 \leq N \leq 500$ , and
- d)  $K = N - 75$ : if  $N \geq 501$ .

The previously mentioned ranges of  $K$  are dependent on the type of material under testing and were adapted from the first standard AE intensity analysis made by Fowler et al. (1989). The values of  $J$  have a similar effect on the  $S_r$  to that  $K$  has on  $H(t)$ . A range of values of  $J$  of 25-75

has been studied to calculate  $S_r$ , which was also followed in previous studies (Fowler, 1989). In this study, J was set to an average constant value of 50 based on an analysis performed in preliminary studies conducted by the authors (Ridgley et al., 2018).

## 2.5 Results and Discussion

The parameters of the emitted AE signals during the abrasion test were analyzed along with the experimental lab measurements. **Table 2-4** presents the average values of abrasion mass loss after each 1-minute interval for all mixtures at both temperatures. **Fig. 2-3** is a bar chart that shows the average percentage of mass loss at the end of the 6 minutes test for all mixtures and highlights the variation in performance at  $-20^{\circ}\text{C}$  compared to  $25^{\circ}\text{C}$ . **Table 2-6** lists the wear depth measured at the end of the test and the average 28-day compressive strength. **Table 2-7** summarizes the average values of the emitted AE parameters throughout the first and last abrasion intervals for all samples at  $25^{\circ}\text{C}$  and  $-20^{\circ}\text{C}$ . The coefficient of variance of wear depth and weight loss values was calculated and listed in **Table 2-6** to evaluate the significance and acceptability of those measurements. According to ASTM C944 (ASTM, 2012a), the values could be considered significant and acceptable since the test was normal load condition and the coefficient of variance of all samples was less than 59%. The results presented in these tables are further discussed in the following subsections.

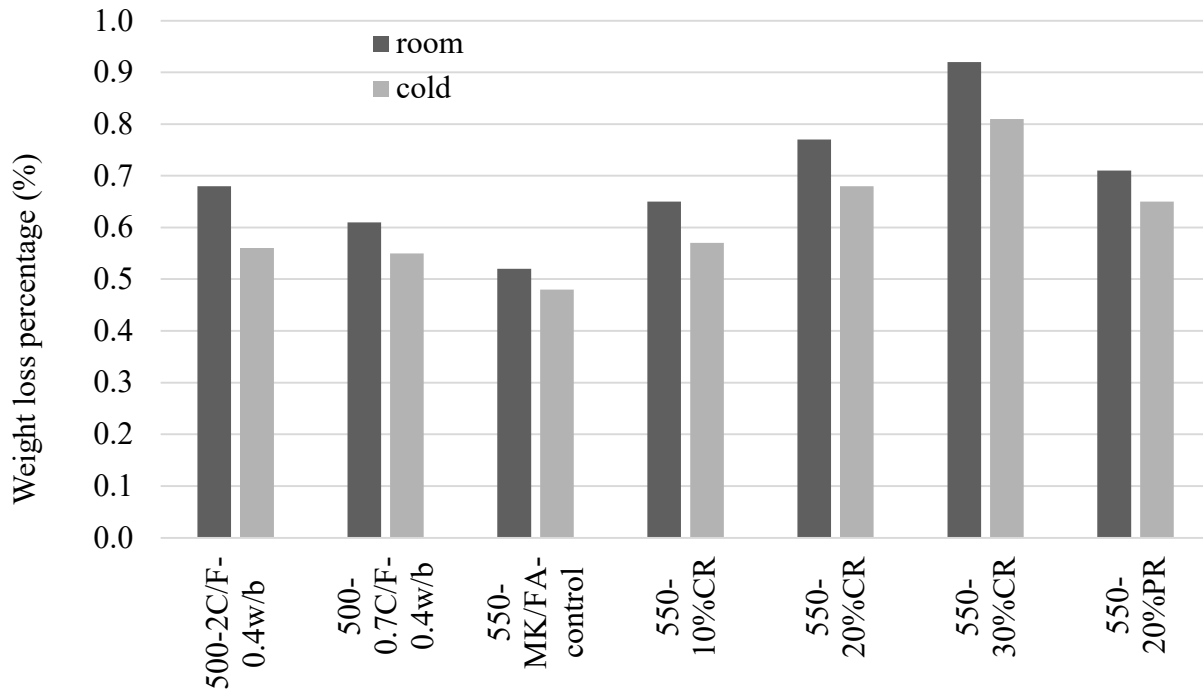


**Fig. 2- 3** Average Weight Loss percentage (%) after 6 mins Abrasion at 25°C and -20°C.

**Table 2- 6** Average Compressive Strength and Wear Depth at 25°C and -20°C.

Mixture no.	Mixture type	Testing temperature	Compressive strength (MPa)	Wear depth (mm)	Weight loss / compressive strength (gms/MPa)	Coeff. Of variance of mass loss values (%)	Coeff. Of variance of wear depth values (%)
M1	500-2C/F-0.4w/c	Room	56.48	1.04	0.28	3.4	12.8
		Cold	73.36	0.81	0.18	5.1	9.7
M2	500-0.7C/F-0.4w/c	Room	64.42	0.91	0.23	4.9	13.3
		Cold	79.64	0.80	0.17	2.7	11.5
M3	550-MK/FA-control	Room	73.65	0.81	0.17	6.1	7.4
		Cold	82.84	0.71	0.14	5.3	10.1
M4	550-10%CR	Room	62.48	0.92	0.24	13.1	16.3
		Cold	71.91	0.76	0.18	11.2	9.8
M5	550-20%CR	Room	42.4	1.24	0.42	18.1	22.3
		Cold	53.13	1.02	0.27	13.5	14.7
M6	550-30%CR	Room	31.86	1.51	0.62	21.3	29.6
		Cold	42.23	1.19	0.37	17.1	18.9
M7	550-20%PR	Room	48.21	1.11	0.33	11.4	14.4
		Cold	56.84	0.98	0.24	8.5	11.9

**Table 2- 7** Average Values of AE Parameters after 1 min & 6 mins of Abrasion Testing of all mixtures at 25°C and -20°C.

Mixture no.	Mixture type	Testing temperature	Average signal amplitude (dB)		Number of hits		CSS × 10 <sup>3</sup> (mV.s)		H (t)		S <sub>r</sub> (mV.s)		b-value	
			1 min	6 min	1 min	6 min	1 min	6 min	1 min	6 min	1 min	6 min	1 min	6 min
M1	500-2C/F-0.4w/b	25°C	81	80	126	631	0.51	2.32	2.15	2.77	4.29	5.99	1.29	1.09
		-20°C	84	83	72	410	0.39	1.8	1.53	1.82	3.34	4.17	1.38	1.22
M2	500-0.7C/F-0.4w/b	25°C	85	84	111	541	0.38	2.13	2.02	2.38	4.14	5.51	1.37	1.19
		-20°C	86	84	67	397	0.21	1.76	1.29	1.7	3.30	4.71	1.49	1.27
M3	550-MK/FA-control	25°C	84	84	93	389	0.24	1.81	1.46	1.57	3.83	4.87	1.39	1.27
		-20°C	86	85	64	337	0.21	1.68	1.26	1.47	2.95	3.67	1.54	1.34
M4	550-10%CR	25°C	79	76	156	486	0.39	1.91	2.33	2.91	4.36	4.97	1.19	1.06
		-20°C	87	82	62	411	0.22	1.47	2.03	2.34	3.03	3.64	1.31	0.95
M5	550-20%CR	25°C	75	71	203	561	0.51	2.03	2.54	2.93	4.97	6.26	0.98	0.84
		-20°C	85	78	62	434	0.16	1.97	2.31	2.59	3.92	5.83	1.14	0.91
M6	550-30%CR	25°C	72	66	243	641	0.63	2.23	2.68	2.09	5.89	5.55	0.84	0.76
		-20°C	84	75	503	498	0.59	1.87	2.37	1.84	5.04	4.93	0.96	0.91
M7	550-20%PR	25°C	81	72	161	517	0.38	1.71	2.43	2.72	4.03	5.79	1.03	0.95
		-20°C	86	82	86	422	0.29	1.53	2.09	2.33	3.84	4.89	1.23	1.09

### 2.5.1 Impact of cold temperature on the abrasion experimental measurements

By comparing the mass loss for all samples at both temperatures, it can be stated that cooling down the mixtures to a sub-freezing temperature (-20°C) generally enhanced the abrasion resistance (in terms of a decrease in weight loss and wear depth) and increased the compressive strength regardless of the mixture composition as shown in **Tables 2-4** and **2-6** and **Fig. 2-3**. For instance, the control mixture (M3) experienced 12.85 gms abrasion weight loss when tested at room temperature, and this loss decreased to 11.55 gms when tested at -20°C. In addition, the average weight loss for the rubberized mixtures (M4-M7) at room temperature was 17.15 gms, and this average loss decreased to reach 14.14 gms when samples were tested at -20°C. This behavior could be attributed to the fact that at -20°C, gels and water pores were turned into ice, which in

turn strengthened the bond between the aggregate and the surrounding mortar, limited crack growth, and provided a solid substance (ice) that had an extra bearing capacity to resist abrasion forces (Cai et al., 2011; Zaki et al., 2020). Moreover, the shrinkage of concrete due to freezing reduced the atomic distance and increased the attraction forces between the atoms, which resulted in a higher compressive and abrasion resistance (Cai et al., 2011; Banthia et al., 1998).

The results also showed that the enhancement in the abrasion resistance with the decrease in temperature (at  $-20^{\circ}\text{C}$ ) was more pronounced in the mixture with higher C/F. For example, mixture M1 with a C/F of 2.0 experienced a 16.4% reduction in weight loss (enhancement in abrasion resistance) when cooled down to  $-20^{\circ}\text{C}$ , while this reduction was only 11.1% in mixture M2 with a C/F of 0.7. This observation could be attributed to the fact that increasing the volume of coarse aggregate increases the volume of the interface zone between the aggregates and cement mortar. This zone is known to have a higher water-to-cement ratio and larger water pores compared to the rest of the concrete matrix (Kim et al., 2012). Therefore, reducing the temperature to subzero in mixtures with higher C/F (higher volume of interface zone) turns more water into ice which results in more enhancement in the strength and abrasion resistance. It's worth noting that the tested samples were frozen only once. Hence, the results of this study were not affected by freeze-thaw cycling, which would have decreased the abrasion resistance of the tested samples (Amorim Júnior et al., 2018; Shang, 2013). Future studies on the same rubberized mixtures under abrasion test after being subjected to freeze-thaw cycles are recommended to address the change in AE behavior and wave propagation.

**Fig. 2-3** and **Table 2-4** also show that the mixture with a larger rubber particle size (4.5 mm CR) experienced more enhancement in the abrasion when cooled down to  $-20^{\circ}\text{C}$ , compared to a mixture with a smaller rubber size (0.4 PR). As seen in **Table 2-4**, the weight loss in the mixture

with larger rubber size (M5) (4.5 mm CR) dropped by 19.6% (enhancement in abrasion) when cooled down to -20°C while this drop was only 11.6% in the mixture with smaller rubber size (M7) (0.4 mm PR). Larger rubber particles have lower stiffness modulus compared to smaller rubber. Decreasing the temperature to sub-zero increases the stiffness and strength of rubber, which increases the strength and abrasion of the concrete. Therefore, reducing the temperature to sub-zero in a mixture with larger rubber particles (CR) showed more enhancement in the abrasion resistance compared to the mixture with smaller rubber (PR).

### 2.5.2 Cold temperature effect on the AE parameters in rubberized mixtures

The variation in AE parameters, along with abrasion mass loss values throughout the tests at 25°C and -20°C, were analyzed. **Table 2-7** lists the average values of the recorded parameters during the first and last testing intervals at both temperatures. **Fig. 2-4** shows the variation of the number of hits, CSS,  $H(t)$ ,  $S_r$ , and  $b$ -values over the test, along with weight loss progression for sample 2 of mixture M5 (taken as an example) when tested at -20°C. It was noticed that AE parameter values varied following a specific pattern at both temperature conditions. Along with abrasion damage progress, there was an increase in the number of hits, CSS,  $H(t)$ , and  $S_r$ , and there was a slight decrease in  $b$ -values in all tested mixtures (similar to the mixture shown in **Fig. 2-4**). For instance, the increase in weight loss for mixture M3 at a -20°C from 2.05 gm after 1 min to 11.55 gms after 6 mins coincided with an increase in the number of hits from 64 to 367, CSS from 210 to 1680 mV.s,  $H(t)$  from 1.26 to 1.47, and in  $S_r$  from 2.95 to 3.67, and a decrease in  $b$ -value from 1.54 to 1.34 (see **Table 2-7**). The aforementioned values manifested the sensitivity of AE parameters to abrasion damage at sub-freezing temperature for rubberized concrete mixtures.

The results also revealed that the amplitude values for rubberized mixtures witnessed a slight increase trend when tested at -20°C compared to 25°C. This increasing trend (at -20°C compared

to 25°C) was not noticeable in non-rubberized mixtures (M1-2). This confirms the signal wave attenuation due to rubber, which decreased the wave signal amplitude in various mixtures. For instance, signal amplitudes for waves emitted in rubberized mixtures, when temperature varied from 25°C to -20°C, changed from 79 to 87 for mixture M4, from 75 to 85 for mixture M5, from 72 to 84 for mixture M6, and from 81 to 86 for mixture M7. This behavior could be attributed to the fact that the stiffness of rubber particles increased at -20°C and mitigated the attenuation effect. Besides, turning water into ice supported a solid transfer medium which could have affected the propagation of waves and relieved the signal attenuation phenomenon (Shang et al., 2014).

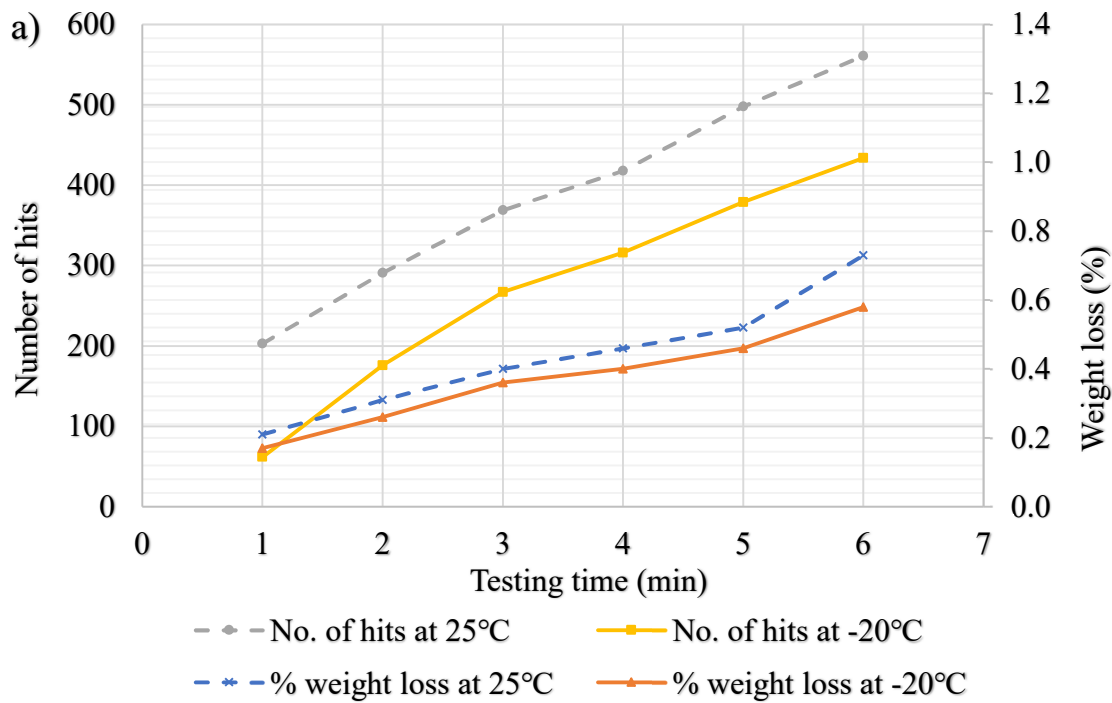


**Fig. 2- 4** Variation of AE Parameters along with Weight Loss (%) of Mixture M5 S2: a) number of hits, b) CSS, c)  $H(t)$ , d)  $S_r$  and e)  $b$ -value.

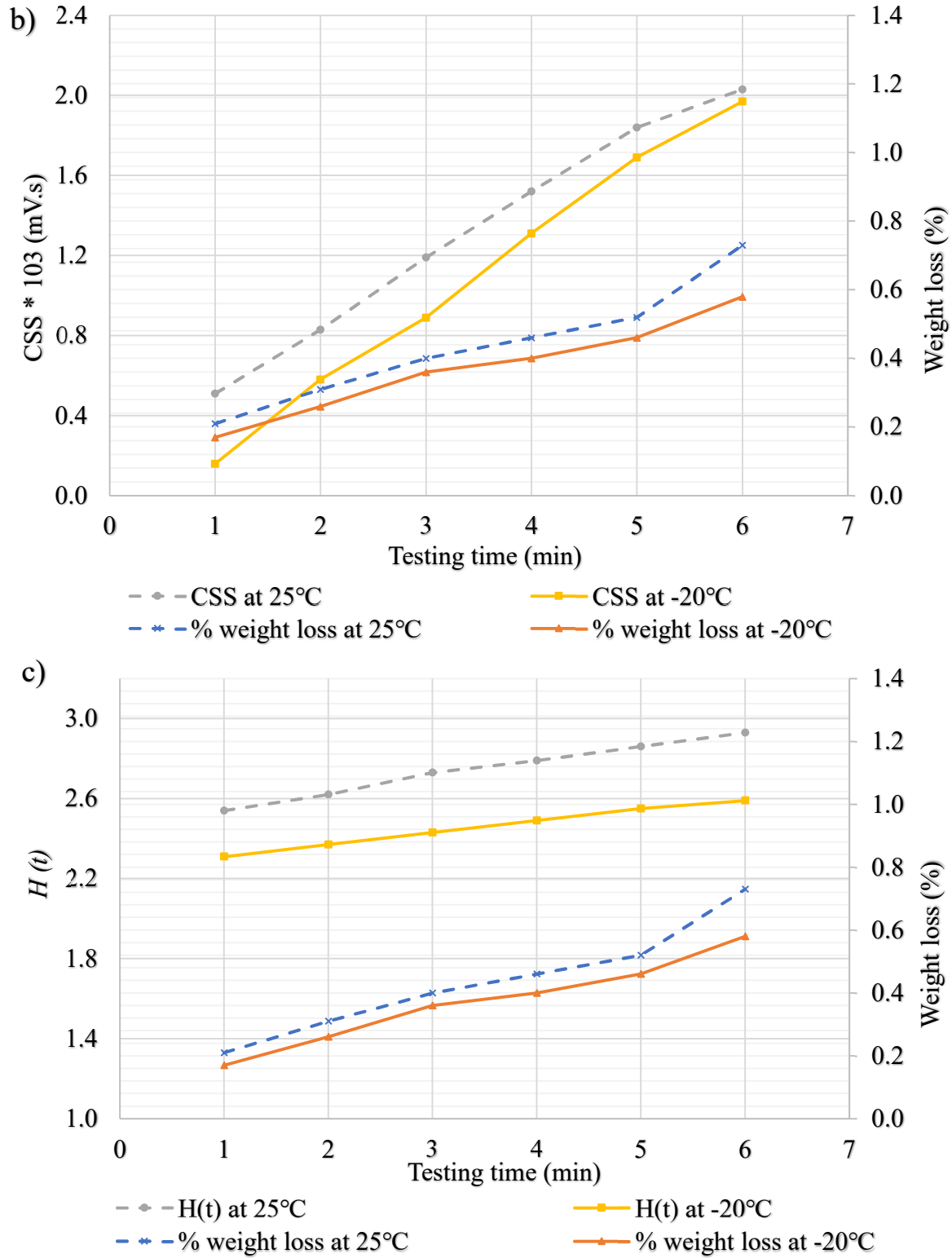


**Fig. 2- 5** Variation of AE Parameters along with Weight Loss (%) of Mixture M5 S2: a) number of hits, b) CSS, c)  $H(t)$ , d)  $S_r$  and e)  $b$ -value. (cont').

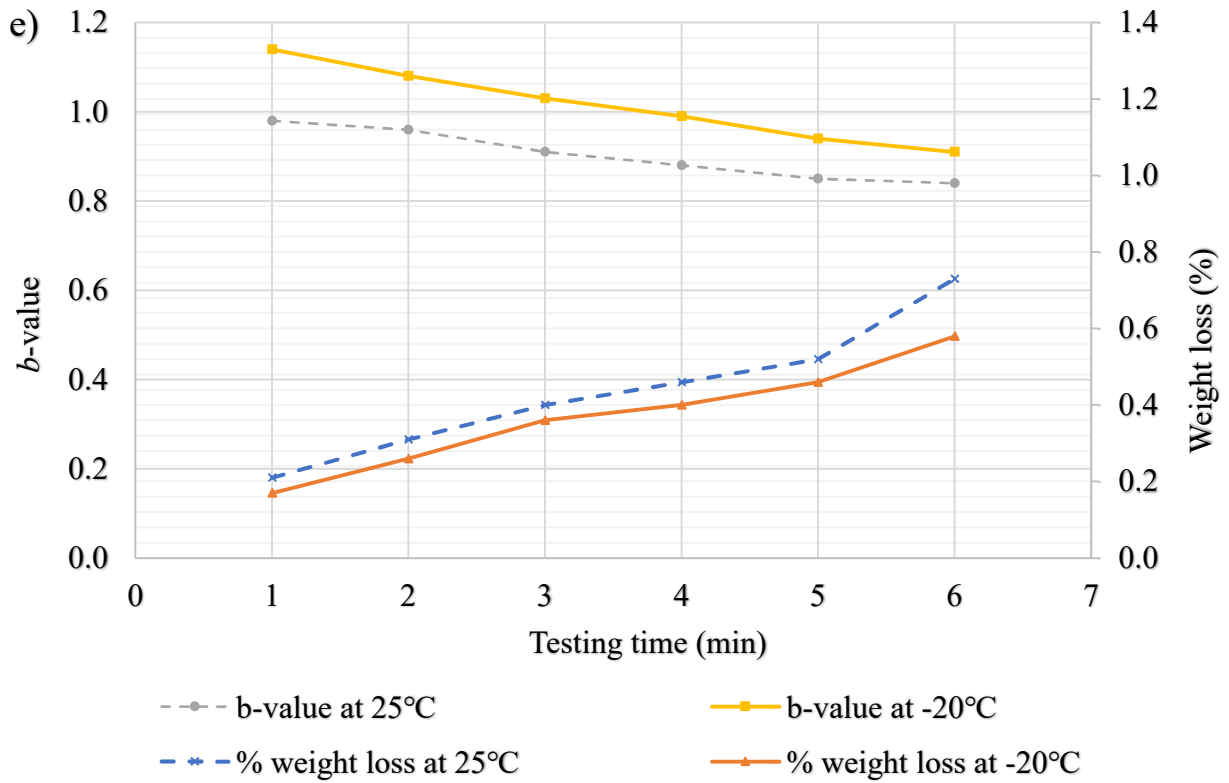
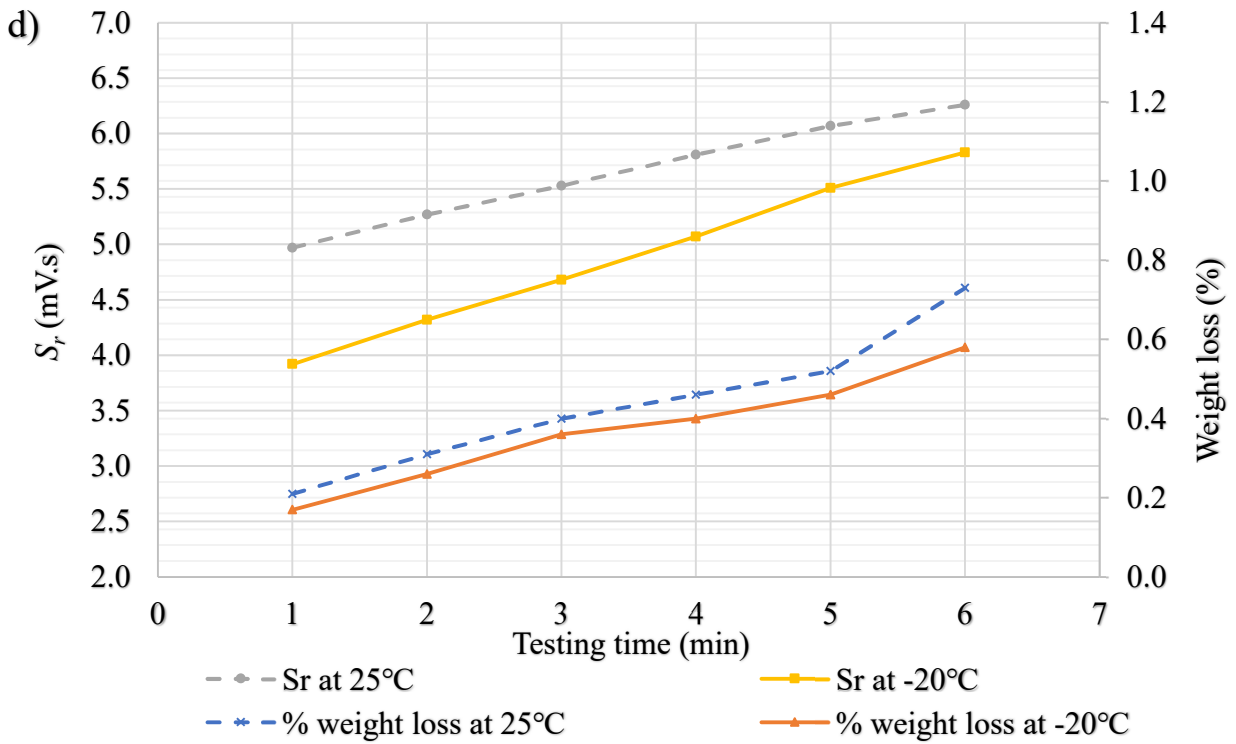


**Fig. 2- 6** Variation of AE Parameters along with Weight Loss (%) of Mixture M5 S2: a) number of hits, b) CSS, c)  $H(t)$ , d)  $S_r$  and e)  $b$ -value (cont').

### **2.5.3 Influence of C/F on abrasion resistance and AE parameters at a sub-freezing temperature**

Two concrete mixtures with different C/F were studied: M1 with 2.0 C/F and M2 with a lower C/F of 0.7. By evaluating both lab results and the collected AE parameters, it could be concluded that mixtures with higher C/F had lower abrasion resistance regardless of the temperature of the tested samples (see **Table 2-4**). Meanwhile, the enhancement in the abrasion performance due to freezing was more pronounced in the mixtures with higher C/F compared to lower C/F. For instance, the weight loss/compressive strength of mixture M1 with 2.0 C/F dropped by 35.7% (from 0.28 gms/MPa to 0.18 gms/MPa ) when cooled down from 25°C to -20°C, while this drop was only 26% in mixture M2 with 0.7 C/F (indicating more enhancement in the abrasion resistance for mixture with 2.0 C/F at cold temperature compared to mixture with 0.7 C/F). Similarly, the wear depth of the 2.0 C/F mixture (M1) dropped by 22.1% when cooled down from 25°C to -20°C, while this drop was 12% in the 0.7 C/F mixture (M2). The better enhancement in the abrasion resistance due to freezing in a mixture with higher C/F (compared to the mixture with less C/F) could be related to the higher volume of water voids that turns into ice in mixtures with higher C/F, as previously explained.

**Table 2-7** also shows that there was a change in the collected AE parameters as a result of cooling down samples, which indicates that AE analysis supports the same conclusions. For example, the AE parameters witnessed a decrease of 26.6% VS 35% in the number of hits, 17.3% VS 22.4% in CSS, 28.5% VS 34% in  $H(t)$ , and 14.5% VS 30.3% in  $S_r$ , and an increase of 6.7% VS 12% in  $b$ -value in M2 VS M1, when cooled down from 25°C to -20°C. The aforementioned values confirm the more significant effect of cold temperature on enhancing the abrasion resistance in mixtures

with higher C/F compared to lower C/F. In terms of signal amplitudes, there was no noticeable variation in wave signals' amplitudes for mixtures M1 and M2. It should be noted that these outcomes are valid within the range of C/F tested in this study (0.7-2).

#### **2.5.4 Influence of CR content on abrasion resistance and AE parameters at the sub-freezing temperature**

Generally, increasing the rubber content was found to significantly increase the abrasion damage in terms of weight loss and wear depth at both temperatures (**Tables 2-4 and 2-6**). Meanwhile, the decline in the abrasion resistance due to increasing the CR content at  $-20^{\circ}\text{C}$  was not as significant as at room temperature. For instance, when tested at room temperature, mixtures M4-M6 with CR contents of 10%, 20%, and 30%, respectively, experienced 18.5%, 39.1%, and 54% more weight loss compared to the control mixture (M3). The same mixtures (M4-M6) experienced only 11.1%, 24.4%, and 33.9%, respectively, more weight loss compared to the control mixture (M3) when tested at  $-20^{\circ}\text{C}$ . The escalating abrasion damage due to increasing CR content could be attributed to the noticeable reduction in compressive strength and the poor bond between rubber particles and the surrounding mortar. Furthermore, the increase in voids content, which is associated with the increase in rubber content (Ismail and Hassan, 2016), further reduces the strength of the mixture and makes it easier for particles to be pulled out during abrasion tests. In addition, the noticeable effect of cold temperature in alleviating the abrasion damage (associated with the increase in CR content) could be related to the increased stiffness of rubber particles and better bond with the surrounding mortar at cold temperature, which has a direct effect on improving the strength and abrasion resistance of the mixture.

The average signal amplitudes at both temperatures over the test period for all mixtures were compared in **Fig. 2-4**. This figure shows that, at room temperature, the average signal amplitudes

for all rubberized mixtures significantly decreased along with the increase in rubber content, indicating significant signal wave attenuation at 25°C compared to the wave attenuation at -20°C. For instance, increasing the CR content from 0% to 30% (M3 to M6) resulted in a 21.4% decrease in signal amplitudes when tested at room temperature, while this decrease reached 11.8% at -20°C (Table 2-7).

The results also showed that varying the CR content had a noticeable effect on the AE studied parameters, with a more pronounced effect at room temperature compared to cold temperature. For instance, increasing the CR content from 0% to 30% (M3 to M6) resulted in a 64.8% increase in the number of hits, 56.4% in CSS, 96.8% in  $H(t)$ , 55% in  $S_r$ , and 40.1% decrease in  $b$ -value when tested at room temperature. These numbers dropped to 47.8%, 11.3%, 25.2%, 34.3%, and 32% (increase in the number of hits, CSS,  $H(t)$ ,  $S_r$ , and decrease in  $b$ -value, respectively) when tested at -20°C (Table 2-7). The above findings highlight the sensitivity of the studied AE parameters to the abrasion damage for all mixtures at both temperatures.

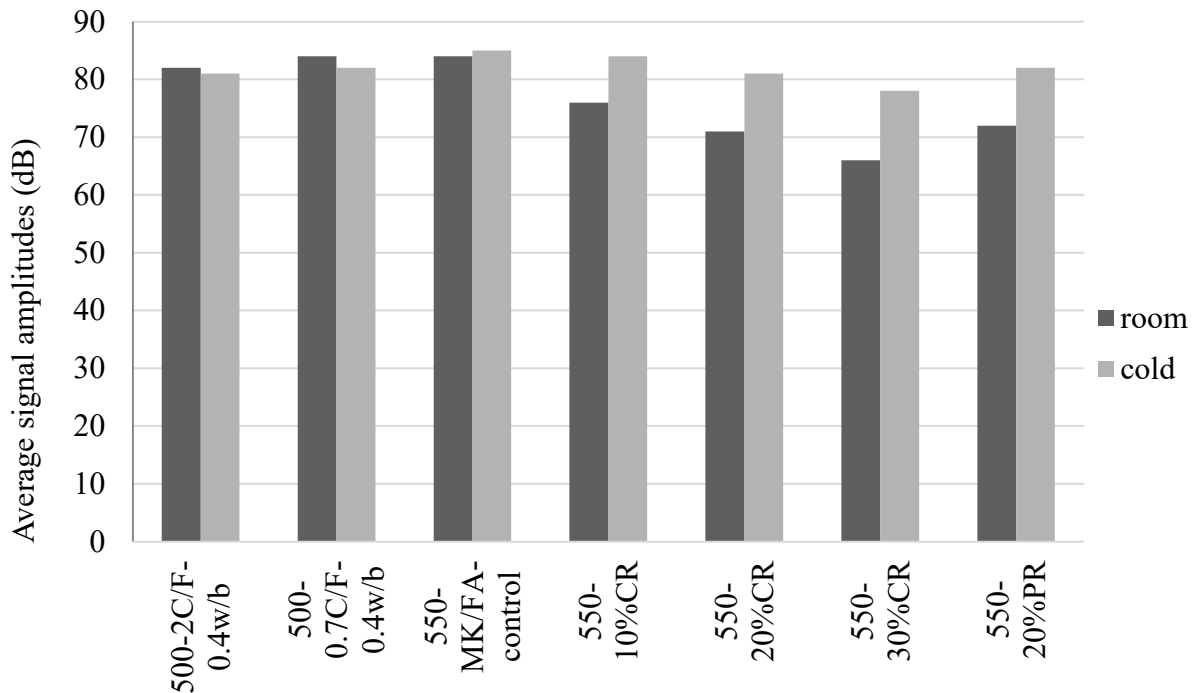


Fig. 2- 7 Average Signal Amplitudes throughout the Abrasion Tests.

### **2.5.5 Influence of rubber particles size on abrasion resistance and associated AE parameters at the sub-freezing temperature**

The study included two SCC mixtures with 20% rubber content: mixture M5 containing 4.5 mm CR and mixture M7 containing 0.4 mm PR. By evaluating the abrasion experimental results along with the collected AE parameters for both mixtures, it was found that increasing the rubber size decreased the abrasion resistance in terms of weight loss and wear depth and decreased the compressive strength regardless of the test temperature (see **Tables 2-4 and 2-6**). The results also indicated that the enhancement of the abrasion resistance as a result of low temperature (-20°C) was more pronounced in mixtures with larger rubber particles (CR) compared to smaller ones (PR). For instance, mixture M5 (with 4.5 mm CR) experienced 8% more weight loss, 12% more wear depth, and 13.7% less compressive strength compared to mixture M7 (with 0.4 mm PR), when tested at room temperature. This mixture (M5) witnessed only 3.5% more weight loss, 4% more wear depth, and 6.5% less compressive strength compared to mixture M7 (with PR) when tested at -20°C. As mentioned earlier, larger rubber particles have lower stiffness modulus compared to smaller ones. This could be attributed to the fact that larger CR particles have lower stiffness modulus, which has a higher negative effect on the strength and abrasion resistance of concrete. In addition, larger rubber particles have rougher surface area compared to smaller ones, which increases the tendency to trap more air in the mixture (Su et al., 2015). This higher air content in a larger rubber mixture contributes more to decrease the strength and abrasion resistance of the mixture. Reducing the temperature to -20°C relatively increases the stiffness of CR, which alleviate the negative effect of CR in reducing the strength and abrasion resistance.

The same conclusions could be deduced by evaluating the AE collected parameters of mixtures M5 and M7. For instance, mixture M5 witnessed 26% more number of hits, 18.7% more CSS,

7.7% more  $H(t)$ , 55% more  $S_r$ , and 11.6% less  $b$ -value when tested at room temperature, compared to a smaller rubber mixture (M7). These results manifested the negative effect of larger rubber particles on the abrasion resistance. The enhancement ratio in the abrasion resistance as a result of decreasing the temperature was also clear in the variation of the collected AE parameter values. For instance, mixture M5 with CR witnessed a decrease of 22.6% in the number of hits, 3% in CSS, 13.1% in  $H(t)$ , 7.4% in  $S_r$ , and a 16.3% increase in  $b$ -value when cooled down to -20°C. These numbers were 18.4%, 10.5%, 14.3%, 10.5%, and 13.7% (decrease in the number of hits, CSS,  $H(t)$ ,  $S_r$  and increase in the  $b$ -value, respectively) in mixture M7 with PR. The above changes in the collected AE parameters highlight the enhancement in performance of both mixtures at cold temperature, which was more significant in mixture M5 with larger rubber particles.

### **2.5.6 Abrasion damage charts of rubberized mixtures using AE intensity analysis parameters.**

Intensity analysis parameters ( $H(t)$  and  $S_r$ ) after 6 mins abrasion were used to develop two damage quantification charts to infer the ranges of wear depth (mm) and weight loss (%) at both temperatures, as shown in **Figs. 2-6 and 2-7**. Both of these charts indicate the abrasion damage in three ranges, which were determined based on the distribution of  $H(t)$  and  $S_r$  values. The chart in **Fig. 2-6** is based on the calculated values of  $H(t)$  and  $S_r$  (calculated from Eqs. 2 and 3). This chart has three ranges of mass loss percentage: 0.44-0.6%, 0.61-0.76%, and 0.77-0.94%. The corresponding ranges for  $H(t)$  and  $S_r$  are 1.3-3.8 and 3.5-8.1 mV/s, respectively (**Fig. 2-6**). For instance, if  $H(t)$  value was 2.7 and  $S_r$  value was 6 mV.s, then the predicted percentage of weight loss due to abrasion could be at the range of 0.61-0.76%. It should be highlighted that the test temperature wasn't included as a factor in the chart. This is because the test temperature has

already affected the output AE parameter values.

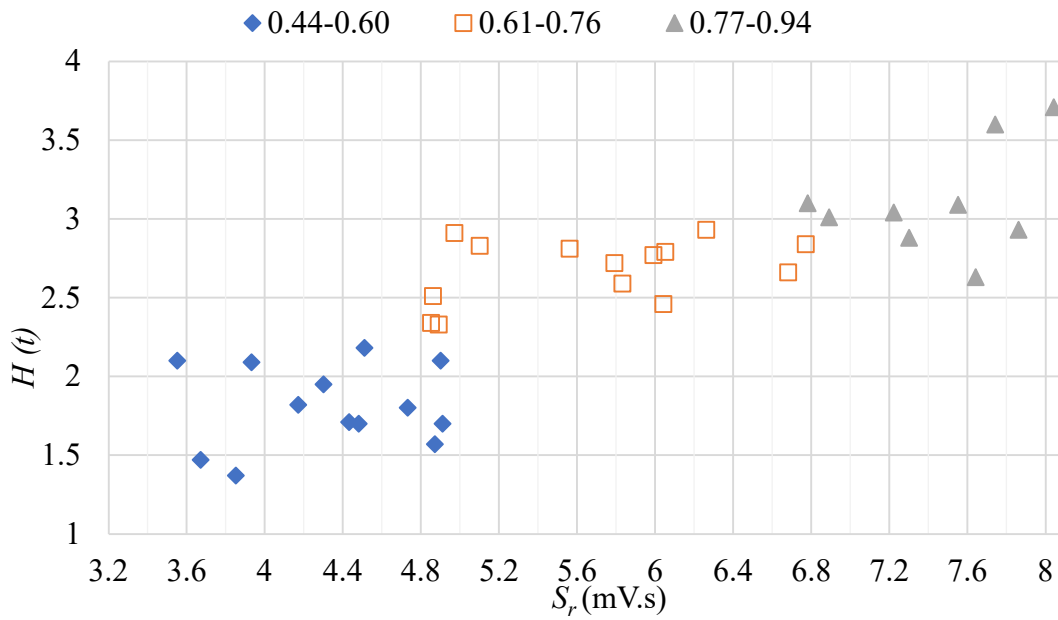


**Fig. 2- 8** Ranges of Weight Loss (%) Quantification Chart.

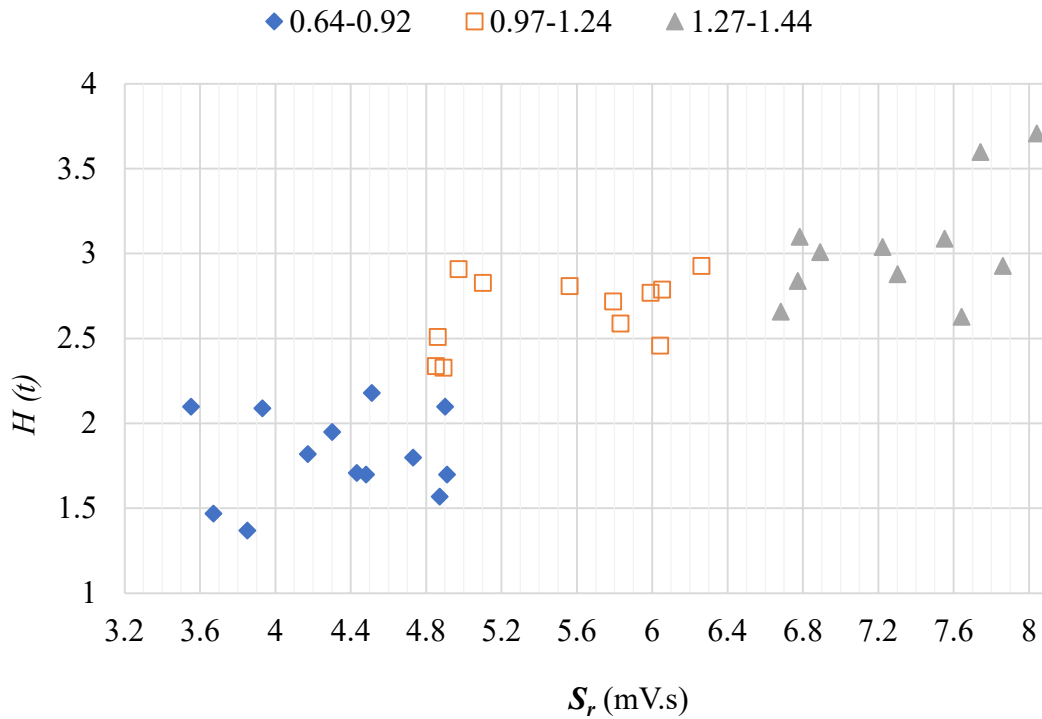


**Fig. 2- 9** Ranges of Wear Depth (mm) Quantification Chart.

Similarly, the chart shown in **Fig. 2-7** could be used to determine the wear depth due to abrasion using the same intensity analysis parameters:  $H(t)$  and  $S_r$  (calculated from Eqs. 2 and 3). This chart has three ranges of wear depth (mm): 0.64-0.92 mm, 0.97-1.24 mm, and 1.27-1.44 mm.  $H(t)$  and  $S_r$  have the same ranges mentioned in the previous chart and could be used in the same way to predict the wear depth. For the case mentioned in the previous example, with  $H(t)$  of 2.7 and  $S_r$  of 6 mV.s, according to this chart, the anticipated wear depth could be in the range of 0.97-1.24 mm. It's worth noting that some limitations exist for the use of these charts regarding the mixture proportions and testing temperature. The mixtures included in this study contained CR replacement of up to 30% and PR replacement of 20%. Therefore, further investigation is warranted to develop more refined charts that can predict the abrasion damage for mixtures with different mixture compositions.

## 2.6 Conclusions

This chapter aimed to investigate the change in the behavior of the AE waves emitted in rubberized concretes under abrasion forces when the samples' temperature was cooled down to -20°C. Seven mixtures with various C/F, different sizes and volumes of CR were tested at both 25°C and -20°C along with collecting the associated AE signals during the tests. The parameters of the emitted AE waves were analyzed and correlated to the weight loss progression in a trial to identify any potential patterns. The following conclusions were obtained:

1. AE parameters followed specific patterns along with the progression of abrasion damage despite the presence of rubber particles at room (25°C) and sub-freezing (-20°C) temperatures. The number of hits, CSS,  $H(t)$ , and  $S_r$  increased along with abrasion damage progression. Meanwhile,  $b$ -value kept fluctuating with an overall declining trend indicating a clear

correlation to damage propagation regardless of samples temperature or composition during the test.

2. Signal amplitudes significantly decreased along with increasing the CR content, as a clear indication of signal wave attenuation. Meanwhile, signal wave attenuation in rubberized mixtures was found to decrease when samples were tested at  $-20^{\circ}\text{C}$ . This effect could be attributed to the increase in CR stiffness at sub-zero temperatures.
3. Neither rubber particles' size nor C/F were found to have any effect on changing signal amplitudes in the tested mixtures. In addition, all recorded signals with amplitudes more than 40 dB could properly characterize the abrasion damage in all mixtures in terms of the studied AE parameters.
4. Increasing C/F, CR content, and size were found to decrease the abrasion resistance regardless of the test temperature. Increasing C/F and CR content/size was accompanied by an increase in the number of hits, CSS,  $H(t)$ , and  $S_r$  values, and a decrease in  $b$ -values of the collected AE waves.
5. Decreasing samples' temperature to  $-20^{\circ}\text{C}$  was found to increase the abrasion resistance regardless of the mixture constituents. Meanwhile, this increase in abrasion resistance at  $-20^{\circ}\text{C}$  was more pronounced in mixtures with higher C/F, larger CR particles, and higher CR contents.
6. The AE intensity analysis parameters:  $H(t)$  and  $S_r$  could be utilized to characterize abrasion damage in terms of both weight loss and wear depth at both temperatures using the developed damage classification charts in this study. These charts could be adequately used to predict the abrasion damage ranges (mass loss and wear depth) using both parameters in the ranges of 1.29–3.75 for  $H(t)$  and 3.5–8.1 for  $S_r$ . Meanwhile, further lab, and field investigations are

recommended on other rubberized mixtures with variable mixture ingredients to check the validity of the charts presented in this study.

## 2.7 Chapter References

- AbdelAleem, B. H., and Hassan, A. A. A. (2018). "Development of self-consolidating rubberized concrete incorporating silica fume." *Construction & building materials*, 161, 389-397.
- Abdelrahman, M., ElBatanouny, M. K., Ziehl, P., Fasl, J., Larosche, C. J. and Fraczek, J. (2015). "Classification of alkali-silica reaction damage using acoustic emission: A proof-of-concept study." *Construction & building materials*, 95, 406-413.
- Abouhussien, A. A., and Hassan, A. A. A. (2017). "Acoustic emission monitoring for bond integrity evaluation of reinforced concrete under pull-out tests." *Advances in structural engineering*, 20(9), 1390-1405.
- Abouhussien, A. A., and Hassan, A. A. A. (2017). "Application of acoustic emission monitoring for assessment of bond performance of corroded reinforced concrete beams." *Structural health monitoring*, 16(6), 732-744.
- Abouhussien, A. A., and Hassan, A. A. A. (2019). "Crack growth monitoring in fiber-reinforced self-consolidating concrete via acoustic emission." *ACI materials journal*, 116(5), 181-191.
- Abouhussien, A. A., and Hassan, A. A. A. (2020). "Classification of damage in self-consolidating rubberized concrete using acoustic emission intensity analysis." *Ultrasonics*, 100, 105999-105999.
- ASTM C1611-09, "Standard Test Method for Slump Flow of Self-Consolidating Concrete," *ASTM International*, West Conshohocken (2009).
- ASTM C944/C944M-12, "Standard Test Method for Abrasion Resistance of Concrete or Mortar Surfaces by the Rotating-Cutter Method," *ASTM International*, West Conshohocken (2012a).

ASTM C779/C779M-12, “Standard Test Method for Abrasion Resistance of Horizontal Concrete Surfaces,” *ASTM International*, West Conshohocken (2012b).

ASTM C418-12, “Standard Test Method for Abrasion Resistance of Concrete by Sandblasting,” *ASTM International*, West Conshohocken (2012c).

ASTM C150-12, “Standard Specification for Portland Cement,” *ASTM International*, West Conshohocken (2012e).

ASTM C39-12, “Standard Test Method for Compressive Strength of Cylindrical Concrete Specimens,” *ASTM International*, West Conshohocken (2012f).

ASTM C618, “Standard Specification for Coal Fly Ash and Raw or Calcined Natural Pozzolan for Use in Concrete,” *ASTM International*, West Conshohocken, PA, USA (2012).

ASTM C494-13, “Standard Specification for Chemical Admixtures for Concrete,” *ASTM International*, West Conshohocken (2013).

ASTM E1316-14, “Standard Terminology for Nondestructive Examinations,” *ASTM International*, West Conshohocken (2014).

Banthia, N., Yan, C., and Sakai, K. (1998). “Impact resistance of fiber reinforced concrete at subnormal temperatures.” *Cement & concrete composites*, 20(5), 393-404.

Bignozzi, M. C., and Sandrolini, F. (2006). “Tire rubber waste recycling in self-compacting concrete.” *Cement and concrete research*, 36(4), 735-739.

Cai, X. P., Yang, W. C., Yuan, J., Ge, Y., and Zhang, B. S. (2011). “Effect of Low Temperature on Mechanical Properties of Concrete with Different Strength Grade.” *Key Engineering Materials*, 477, 308-312.

- Colombo, I. S., Main, I. G., and Forde, M. C. (2003). "Assessing damage of reinforced concrete beam using "b-value" analysis of acoustic emission signals." *Journal of materials in civil engineering*, 15(3), 280–286.
- Du, F., Li, D., and Li, Y. (2019). "Fracture Mechanism and Damage Evaluation of FRP/Steel–Concrete Hybrid Girder Using Acoustic Emission Technique" *Journal of materials in civil engineering*, 31(7), 4019111.
- ElBatanouny, M. K., Mangual, J., Ziehl, P. H., and Matta, F. (2014). "Early corrosion detection in prestressed concrete girders using acoustic emission." *Journal of materials in civil engineering*, 26, 504–511.
- Fowler, T., Blessing, J., and Conlisk, P. (1989). "New directions in testing." *Proc., Int. Conf. of Acoustic Emission from Composite Materials*, K. Ono, ed., Acoustic Emission Working Group, Memphis, TN, 16–27.
- Ghafoori, N., Najimi, M., and Aqel, M. A. (2014). "Abrasion resistance of self-consolidating concrete." *Journal of materials in civil engineering*, 26(2), 296–303.
- Ismail, M. K., and Hassan, A. A. A. (2016a). "Impact resistance and acoustic absorption capacity of self-consolidating rubberized concrete." *ACI materials journal*, 113(6), 725–736.
- Ismail, M. K., and Hassan, A. A. A. (2016b). "Use of metakaolin on enhancing the mechanical properties of SCC containing high percentages of crumb rubber." *J. Clean. Prod.*, 125, 282–295.
- Ismail, M. K., and Hassan, A. A. A. (2016). "Influence of Mixture Composition and Type of Cementitious Materials on Enhancing the Fresh Properties and Stability of Self-Consolidating Rubberized Concrete." *Journal of materials in civil engineering*, 28(1), 4015075.

- Ismail, M. K., and Hassan, A. A. A. (2017). "Impact Resistance and Mechanical Properties of Self-Consolidating Rubberized Concrete Reinforced with Steel Fibers." *Journal of materials in civil engineering*, 29(1), 4016193.
- Kim, J. J., Dong J. K., Su, T. K., and Jang, H. L. (2012). "Influence of Sand to Coarse Aggregate Ratio on the Interfacial Bond Strength of Steel Fibers in Concrete for Nuclear Power Plant." *Nuclear Engineering and Design*, 252, 1–10.
- Laplante, P., Aitcin, P. C., and Vézina, D. (1991). "Abrasion Resistance of Concrete." *Journal of materials in civil engineering*, 3(1), 19-28.
- Liu, T. C. (1981). "Abrasion resistance of concrete." *In: Journal Proceedings*, 78, 341-350.
- Madandoust, R., and Mousavi, S. Y. (2012). "Fresh and hardened properties of self-compacting concrete containing metakaolin." *Construction & building materials*, 35, 752-760.
- Mistras Group. (2007). "PCI-2 based AE system 1 user's manual." Physical Acoustics Corporation, Princeton Junction, NJ, USA.
- Nair, A., and Cai, C. S. (2010). "Acoustic emission monitoring of bridges: Review and case studies." *Eng. Struct.*, 32(6), 1704–1714.
- Nanni, A. (1989). "Abrasion resistance of roller compacted concrete." *ACI materials journal*, 86 (6), 559-565.
- Youssf, O., Mills, J.E., Benn, T., Zhuge, Y., Ma, X., Roychand, R. and Gravina, R. (2020) "Development of crumb rubber concrete for practical application in the residential construction sector—design and processing." *Construction and Building Materials*, 260, p.119813.
- Ozbay, E., Lachemi, M., and Sevim, U. K. (2011). "Compressive Strength, abrasion resistance and energy absorption capacity of rubberized concrete with and without slag." *Mater. Struct.*, 44(7), 1297–1307.

- Physical Acoustics. (2005). "R6I-AST sensor." *Physical Acoustics Corporation*, Princeton Junction, NJ, USA.
- Rahman, M. M., Usman, M., and Al-Ghalib, A. A. (2012). "Fundamental properties of rubber modified self-compacting concrete (RMSCC)." *Construction & Building Materials*, 36, 630–637.
- Ridgley, K. E., Abouhussien, A. A., Hassan, A. A. A., and Colbourne, B. (2018). "Evaluation of Abrasion Resistance of Self-Consolidating Rubberized Concrete by Acoustic Emission Analysis." *Journal of materials in civil engineering*, 30(8), 4018196.
- Shang, H.-s., Yi, T.-h., and Guo, X.-x. (2014). "Study on Strength and Ultrasonic Velocity of Air-Entrained Concrete and Plain Concrete in Cold Environment." *Advances in materials science and engineering*, 2014, 1-7.
- Su, H., Yang, J., Ling, T., Ghataora, G. S., and Dirar, S. (2015). "Properties of concrete prepared with waste tyre rubber particles of uniform and varying sizes." *Journal of Cleaner Production*, 91, 288–296.
- Rahman, M. M., Usman, M., and Al-Ghalib, A. A. (2012). "Fundamental properties of rubber modified self-compacting concrete (RMSCC)." *Construction & building materials*, 36, 630–637.
- Sukontasukkul, P., and Chaikaew, C. (2006). "Properties of concrete pedestrian block mixed with crumb rubber." *Construction & building materials*, 20(7), 450-457.
- Vélez, W., Matta, F., and Ziehl, P. (2015). "Acoustic emission monitoring of early corrosion in prestressed concrete piles." *Structural control and health monitoring*, 22(5), 873-887.
- Wang, C., Zhang, Y., and Ma, A. (2013). "Investigation into the fatigue damage process of rubberized concrete and plain concrete by AE analysis." *Journal of materials in civil engineering*, 23(7), 886–892.

Xu, J., Fu, Z., Han, Q., Lacidogna, G., and Carpinteri, A. (2018). "Micro-cracking monitoring and fracture evaluation for crumb rubber concrete based on acoustic emission techniques." *Structural health monitoring*, 17(4), 946-958.

Zaki, R. A., AbdelAleem, B. H., Hassan, A. A. A., and Colbourne, B. (2020). "Abrasion Resistance of Fiber-Reinforced Concrete under Cold Temperatures." *ACI materials journal*, 117(5), 221-232.

### **3. Behavior of acoustic emission waves in rubberized concretes under flexure in a sub-freezing Environment.**

#### **3.1 Abstract**

This study attempts to evaluate the change in the behavior of the acoustic waves associated with flexure cracks developed in rubberized concretes in a sub-freezing environment. Seven normal and rubberized concrete mixtures were developed with different compositions. Prism samples from each mixture were tested at two temperatures (25°C and -20°C) under a four-point monotonic flexure test while being monitored via two attached acoustic emission (AE) sensors to collect the emitted AEs till failure. AE signal characteristics such as signal amplitudes, number of hits, and cumulative signal strength (CSS) were collected and underwent three AE parameter-based analyses:  $b$ -value, intensity, and rise time-amplitude (RA) analysis. Analyzing the acoustic activity could detect micro- and macro-cracks nucleation, which were found to be associated with a noticeable spike in CSS, historic index ( $H(t)$ ), severity ( $S_r$ ) values, and a significant dip in the  $b$ -values. In addition, cold temperature was found to increase the micro- and macro-cracking onset load and time regardless of mixture composition. Besides, mixtures with a lower C/F, less CR content, and/or smaller rubber particle size witnessed higher micro- and macro-crack load and time thresholds. Noticeably, the AE signal attenuation effect caused by the high CR content (up to 30%) at 25°C was significantly relieved when samples were tested at -20°C. Three charts were developed to classify the cracking level based on the values of the intensity analysis parameters ( $H(t)$  and  $S_r$ ) and RA analysis.

#### **3.2 Introduction**

The physical mobility of people, goods, and services in the US and Canada depends on an intricate and interconnected network of infrastructure that has long been neglected and overused. For

instance, 40% of the concrete bridges still in service in Canada were constructed more than 50 years ago, and a sizable portion requires strengthening or replacement (Bisby et al., 2005). Unsatisfactory monitoring or inspection is one of the main factors that led such structures to need urgent repair with a cost-approaches to replacement. Recently, many innovative techniques have been proposed to provide real-time structural health monitoring (SHM) for concrete structures. AEs associated with any damage or crack nucleation can lead to valuable structural performance information if properly handled and analyzed. This is possible because the number of AE events is more or less proportional to the number of growing cracks. Besides, the AE wave amplitudes (or energy) are proportional to the size of crack growth in materials such as concrete and rocks (Colombo et al., 2003; Ohtsu, 1987; Rao et al., 2011). Since concrete materials have discrete and non-uniform characteristics, stress concentration can easily occur when a load is applied, resulting in micro or macro-cracks. Local transitory energy is produced as a result of this process, and the wave causes mechanical vibration when it reaches the surface. The vibration is then converted into an electrical signal by the AE detectors (Li et al., 2020). After the electrical signal is processed by an amplifier, the AE parameters are recorded as waveforms. According to the AE signal parameters change, any internal damage or crack development can be identified, giving early warning in case of severe damage.

The analysis of the AE signals can take the form of parameter-based or waveform-based. Waveform-based AE analysis can offer more information regarding source identification and signal characterization (Abouhussien and Hassan, 2017). However, parameter-based analysis techniques such as the *b*-value, intensity, and RA (which stands for rise time divided by average amplitude) approaches may offer quantifiable outcomes that can be utilized to assess the severity of damage and then evaluate the structural integrity to make decisions. Previous studies

characterized the fracture process and cracking mode in various concrete mixtures by performing RA analysis of the collected AEs (Aggelis et al., 2012; Aggelis et al., 2013). Sagar et al. (2012) tracked the development of cracks in concrete and cement mortar and identified distinct stress-induced cracking via *b*-value analysis. Most of these studies were performed on either normal or fiber-reinforced concrete, while few studies examined rubberized concrete (Abouhussien and Hassan, 2020; Aggelis, 2011).

In keeping with the global need for an eco-friendly construction industry, incorporating rubber particles manufactured from end-of-life rubber tires in concrete production has become widely accepted. The fact that rubber particles are not easily biodegradable (Sadek and El-Attar, 2015), burning them releases air-toxic fumes (Garrick, 2005), and their rapid accumulation provides a mosquito breeding medium has been the reason for serious environmental concerns and imposed a dire need to reuse them (Mohammed et al., 2012). Even though the incorporation of rubber particles in concrete has been found to be associated with a general drop in mechanical properties, it improves ductility, strain capacity, flexure toughness, and fracture energy (Ismail and Hassan, 2016; Najim and Hall, 2012). As a result of the substitution of rubber particles in concrete, Najim and Hall (2012) found a notable improvement in the strain capacity that reduced the displacement of the crack mouth opening. It is also worth noting that reducing the size of rubber particles reduces the negative effect of rubber on concrete strength (Youssf et al., 2020). However, the positive effect of rubber on improving impact resistance and energy absorption is also reduced when the size of rubber particles is reduced (Youssf et al., 2020). Therefore, it is essential to select the optimum size of rubber based on the intended structure application.

One concern reported regarding the integrity of the AE technique to monitor the structural performance of rubberized concrete was that the AEs emitted in concrete highly depend on the

acoustic absorption properties of the transfer medium. Hence, using rubber particles in concrete was anticipated to have some effect on the AE properties due to their noticeable acoustic absorption property. Earlier research (Ridgley et al., 2018; Wang et al., 2013; Xu et al., 2018) investigated similar issues and found that rubberized concrete emits AE waves under flexure stresses with lower signal amplitudes than non-rubberized concrete. This reduction was attributed to the wave attenuation phenomenon. Yet, the AE analysis technique was still valid for classifying damage detecting micro- and macro-cracks in rubberized concrete (Abouhussien and Hassan, 2020), investigating the fatigue damage process in rubberized concrete (Wang et al., 2013), and monitoring the micro-cracking and fracture process in rubberized concrete (Xu et al., 2018).

Extremely low temperatures, such as in Arctic regions, could change the stiffness of rubber particles in rubberized concrete and turn water inside the pores into ice. This change is anticipated to affect the behavior of the AEs emitted in rubberized concrete in such temperatures, similar to the behavior change in ultrasonic wave propagation noticed in concrete at cold temperatures (Shang et al., 2014). The behavior of the AEs emitted in rubberized concrete at ambient room temperature is well documented in the literature. Meanwhile, there is a lack of information regarding the change in AE parameters emitted in rubberized concrete at extremely low (sub-freezing) temperatures.

This research examined how cooling concrete prism samples to below-freezing temperature ( $-20^{\circ}\text{C}$ ) altered the behavior of the AE waves released under flexure test conditions. The tested samples contained various C/Fs and various contents and sizes of rubber particles. The study also investigated the attenuation phenomenon at  $-20^{\circ}\text{C}$  compared to at  $25^{\circ}\text{C}$ . In an effort to identify the commencement of micro- and macro-cracking stages, three AE parameter-based analyses—*b*-value, intensity, and RA analysis—were applied. The ultimate goal of this research was to create

damage characterization charts that could categorize rubberized concrete damage under varied temperatures.

### 3.3 Experimental program

#### 3.3.1 Mixture design

Seven concrete mixtures were investigated in this study, as listed in **Table 3-1**. The mixtures included M1 with a C/F of 2.0 and M2 with a C/F of 0.7. Mixtures M1 and M2 were included without rubber to study the effect of changing the C/F on AE behavior. In addition, four mixtures, M3-M6, were included with various 4.5 mm crumb rubber contents (0%, 10%, 20%, and 30%), respectively. These mixtures were selected to investigate the effect of various CR contents on the AEs' behavior and crack growth. The CR percentage was expressed as a replacement of fine aggregate by volume. More details about these selected mixtures' fresh and mechanical properties can be found in (Ismail and Hassan, 2016). Mixture M7 with 20% powder rubber (0.4 mm particle size) was also included to study the effect of CR particle size on the AE behavior. It should be mentioned that metakaolin (MK) and fly ash (FA) were added to mixtures M3-M7 to enhance coarse aggregate suspension and counteract the negative effects of adding CR on the structural performance.

**Table 3- 1** Concrete mixture proportions.

Mixture no.	Mixture type	Cement (kg/m <sup>3</sup> )	MK (kg/m <sup>3</sup> )	FA (kg/m <sup>3</sup> )	C.A. (kg/m <sup>3</sup> )	F.A. (kg/m <sup>3</sup> )	Water content (kg/m <sup>3</sup> )	Rubber content (kg/m <sup>3</sup> )	C/F	W/C	HRWRA (kg/m <sup>3</sup> )
M1	500-2C/F-0.4w/c	500	-	-	1111.54	555.77	200	-	2.0	0.4	1.72
M2	500-0.7C/F-0.4w/c	500	-	-	686.53	980.76	200	-	0.7	0.4	1.51
M3	550-control	275	110	165	620.2	886.2	220	-	0.7	0.4	3.44
M4	550-10%CR	275	110	165	620.2	797.4	220	32.5	0.7	0.4	4.36
M5	550-20%CR	275	110	165	620.2	708.8	220	64.9	0.7	0.4	4.67
M6	550-30%CR	275	110	165	620.2	620.2	220	97.3	0.7	0.4	5.82
M7	550-20%PR	275	110	165	620.2	708.8	220	58.7	0.7	0.4	4.61

Note: 1 kg/m<sup>3</sup> = 0.06243 lb/ft<sup>3</sup>

### 3.3.2 Materials properties

General-use Canadian Portland cement (type GU) with a specific gravity of 3.15 was used in all mixtures in accordance with ASTM type I (ASTM C150-12, 2012). Advanced Cement Technologies provided fly ash and metakaolin from the eastern United States, and both binders conformed to ASTM C618 class N (ASTM C618, 2012). The specific gravity of MK and FA were 2.26 and 2.52, respectively. All the chemical and physical properties of the binders used are shown in **Tables 3-2** and **3**. Two types of aggregate were deployed in all mixtures: coarse aggregate (C.A) and fine aggregate (F.A). The C.A used was natural crushed stone with a maximum aggregate size of 10 mm, and the F.A was natural sand with a 3.1 fineness modulus. Both aggregates had a specific gravity of 2.6 and 1% water absorption. The rubber used had a specific gravity of 0.96, minimal water absorption, and two particle sizes of 4.5 mm (CR) and 0.4 mm (powder rubber), as shown in **Fig. 3-1**. The target slump flow for all SCC mixtures was  $700 \pm 50$  mm, as per ASTM C1611 (ASTM, 2009), and was obtained by using poly-carboxylate-based high-range-water-reducing-admixtures, in accordance with ASTM C494 type F (ASTM C, 2013). The high-range-water-reducing admixtures had a specific gravity of 1.21, a volatile weight of 62%, and a pH level of 9.5. For all mixtures, W/C was set to a constant value of 0.4 which was recommended in previous studies (Ismail and Hassan, 2016; Ismail and Hassan, 2016; Ismail and Hassan, 2017).

**Table 3- 2** Chemical properties of all used binders.

Chemical properties %	Cement	MK	Fly ash
SiO <sub>2</sub>	19.63	51–53	51
Al <sub>2</sub> O <sub>3</sub>	5.48	42–44	23
Fe <sub>2</sub> O <sub>3</sub>	2.37	<2.2	12
FeO	--	--	--
TiO <sub>2</sub>	--	<3.0	--
C	--	--	--

<b>Cr<sub>2</sub>O<sub>3</sub></b>	--	--	--
<b>MnO</b>	--	--	--
<b>P<sub>2</sub>O<sub>5</sub></b>	--	<0.21	--
<b>SrO</b>	--	--	--
<b>BaO</b>	--	--	--
<b>SO<sub>4</sub></b>	--	<0.5	--
<b>CaO</b>	62.43	<0.2	5
<b>MgO</b>	2.47	<0.1	--
<b>Na<sub>2</sub>O</b>	--	<0.05	--
<b>C<sub>3</sub>S</b>	52.33	--	--
<b>C<sub>2</sub>S</b>	16.82	--	--
<b>C<sub>3</sub>A</b>	10.51	--	--
<b>C<sub>4</sub>AF</b>	7.23	--	--
<b>K<sub>2</sub>O</b>	--	<0.40	--
<b>L.O.I</b>	2.04	<0.50	--

**Table 3- 3** Physical properties of all used binders.

	Cement	MK	Fly ash
Specific gravity	3.15	2.5	2.38
Blaine fineness (m <sup>2</sup> /kg)	410	19,000	420

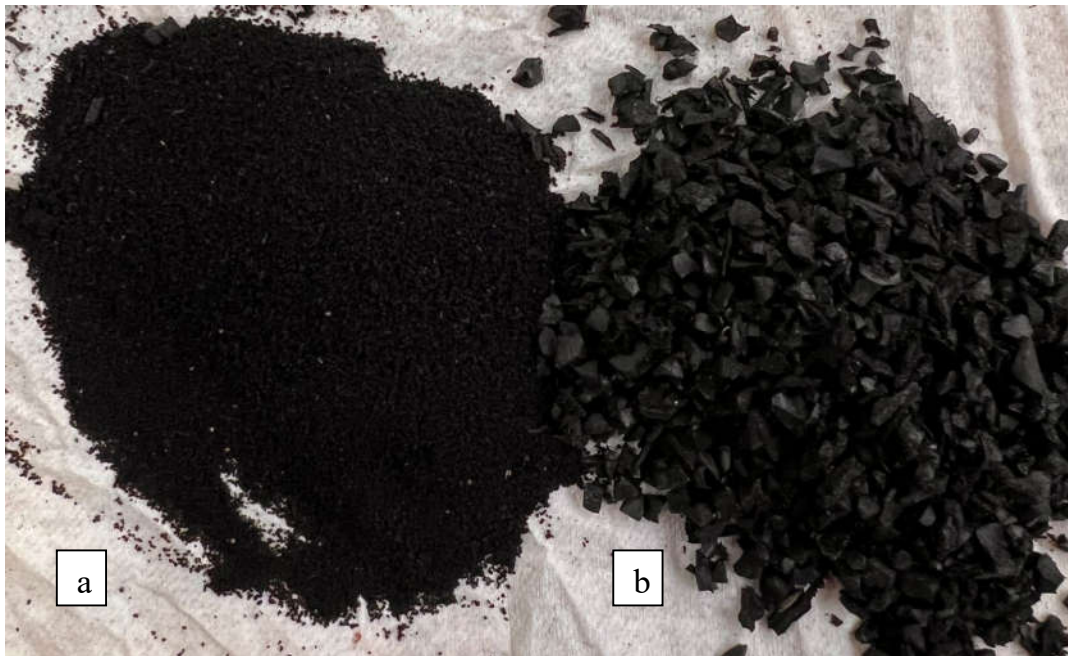


**Fig. 3- 1** Pictures of the rubber particles used: a) 0.4 mm powder rubber, b) 4.5 mm crumb rubber.

### 3.3.4 Description of tested samples

For each mixture, samples were cast as follows: six cylinders (100 mm diameter and 200 mm height) to evaluate the mixture's compressive strength according to ASTM C39 (ASTM C39-12, 2012) and four prisms (100 × 100 × 400 mm) to monitor flexure behavior according to ASTM C78 (ASTM C78, 2016). Samples were kept at ambient room temperature for 24 hours before demolding. Then the samples were de-molded and kept at 25°C in a moist curing room for 28 days to reach the target strength. After reaching maturity, samples were divided into two groups. Each group consisted of three cylinders and two prisms. For each mixture, one group was tested at room temperature (25°C), and the other group was kept in a freezer for 48 hours to reach a steady-state temperature of -20°C before testing (Zaki et al., 2020).

### 3.3.5 Four-point flexure test setup

A Tinius Olsen universal hydraulic machine was used to perform the four-point flexure test, as shown in Fig. 3-2. The machine conducted the test in a deflection control mode at a constant displacement rate of 0.2 mm/min until failure according to ASTM C78 (ASTM C78, 2016). The loading rate was determined based on the displacement of the machine loading arm. The load resisted by the specimens with time was recorded with the aid of a data-acquisition system.

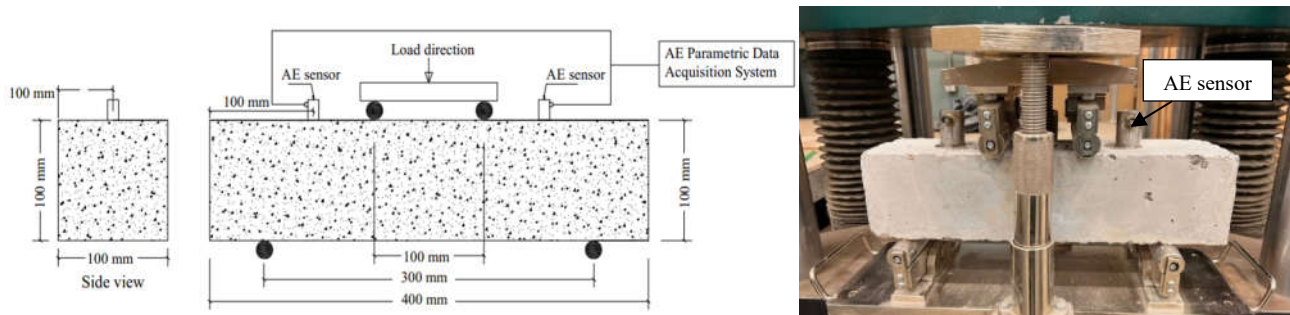


**Fig. 3- 2** Four-point load flexure setup, AE sensors' locations and samples' positioning.

### **3.3.6 AE monitoring setup**

An amplitude threshold was set to 40 dB to filter noise data, which was also set in earlier similar studies, proving its validity (Abouhussien and Hassan, 2019a; Aggelis et al., 2013; Li et al., 2015; Sagar et al., 2012). **Table 3-4** presents the limits of the parameters used to set up the AE data acquisition system, which were kept constant during all tests. The analog and digital filter values shown in **Table 3-4** were chosen at values below half of the sampling rate to enable waveform analysis, according to the manufacturer (Mistrass Group, 2007). This was done to allow the isolation of the individual AE modes with different wave velocities (Mistrass group, 2007; Li et al., 2015). This range of analog and digital filters was found to be compatible with the AE sensors used herein based on a similar recent study completed by the authors (Abouhussien and Hassan, 2016). Similarly, the hit definition parameters (peak definition time, hit definition time, hit lockout time, and maximum duration) were chosen based on the recommended values by the manufacturer and previous studies performed by the authors (Abouhussien and Hassan, 2015; Abouhussien and Hassan, 2016; Abouhussien and Hassan, 2017; Abouhussien and Hassan, 2019b; Mistrass group, 2007). The following AE signal parameters were recorded during all tests: amplitude, energy, duration, signal strength, absolute energy, rise time, counts, average frequency, and peak frequency. The contextual importance and implications of the abovementioned AE parameters used in this study can be found in ASTM E1316 (E1316, 2014).

### **3.3.7 Built-in and amplitude-duration AE data filtering**

The data acquisition system had built-in analog and digital filters to eliminate noise data and vast wave reflections within the boundaries of samples, as shown in **Table 3-4**. Moreover, an amplitude-duration-based filter (Swansong II filter) was applied post-testing on the data collected during the four-point flexure test, as can be seen in **Table 3-5**. This filter is based on the concept

that the real high amplitude AE signals are typically associated with long values of signal duration and vice versa. The limits of this filter were identified by means of the visual inspection of the resulting AE signals, as can be seen in **Table 3-5**. This filter was effective in isolating the noise resulting from the contact between loading heads and specimens, and it was successfully adapted in many previous AE-based studies (Abdelrahman et al., 2014; Abouhussien and Hassan, 2017; Abouhussien and Hassan, 2019b).

**Table 3- 4** AE system details.

<b>AE setup parameters</b>	
Threshold	40 dB <sub>AE</sub>
Sample rate	1 MSPS
Pre-trigger	256 $\mu$ s
Length	1000 points
Preamp gain	40 dB
Preamp voltage	28
Analog filter	1-50 kHz
Digital filter	100-400 kHz
Peak definition time	200 $\mu$ s
Hit definition time	800 $\mu$ s
Hit lockout time	1000 $\mu$ s
Maximum duration	1000 $\mu$ s

**Table 3- 5** Acceptance limits for AE amplitude-duration filter.

Amplitude range (dB)	Duration ( $\mu$ s)		Amplitude range (dB)	Duration ( $\mu$ s)	
	Lower	Upper		Lower	Upper
$40 \leq A < 45$	0	400	$60 \leq A < 65$	300	1,000
$45 \leq A < 48$	0	500	$65 \leq A < 70$	500	2,000
$48 \leq A < 52$	0	600	$70 \leq A < 80$	1,000	4,000
$52 \leq A < 56$	0	700	$80 \leq A < 90$	2,000	7,000
$56 \leq A < 60$	100	800	$90 \leq A < 100$	3,000	10,000

### 3.3.8 AE *b*-value analysis

In the parameter-based approach, any signal is reduced to a few sets of parameters, and the evolution of these parameters with time or any external parameter (e.g., the applied load or crack width development) is investigated to establish a specific correlation that might exist between damage progression and the investigated AE parameters. This paper adopted a set of parameter-based analyses as follows:

Initially, signal amplitudes, number of hits, and cumulative signal strength (CSS) were analyzed versus testing time. Then, additional *b*-value analysis on the amplitudes and number of hits was performed, yielding an additional parameter (*b*-value). This approach is based on seismic magnitude-frequency equations, where the *b*-value denotes the frequency versus magnitude distribution of AE events indicative of the degree of damage. This analysis was successfully implemented to assess the cracking development in various concrete mixtures (Abouhussien and Hassan, 2020; Colombo et al., 2003; ElBatanouny et al., 2014; Li et al., 2015; Sagar et al., 2012). This study used *b*-values on a comparative basis to assess the performance of all tested mixtures and highlight the effect of the studied parameters (C/F and CR content and size) on the AE parameters. The *b*-value was calculated throughout the flexure tests for all specimens according to **Eq. 1** and correlated to the different damage stages in all samples.

$$\text{Log NA} = a - b \log A \quad \text{Eq. 1}$$

Where *A* = the signal amplitude of a specific hit at a specific time (dB); *NA* = the number of hits having amplitudes larger than *A* before the mentioned time; *a* = an empirically derived constant; and *b* = the *b*-value (Abdelrahman et al., 2015; Abouhussien and Hassan, 2019a; Abouhussien and Hassan, 2020; Colombo et al., 2003; Du et al., 2019).

The constant value “a” was determined for each specimen by plotting log A against log NA and the average value of line intersections with the vertical log NA axis. An average value of “a” (3.57) was used in this study (Colombo et al., 2003; ElBatanouny et al., 2014; Li et al., 2015).

### 3.3.9 AE Intensity analysis

Intensity analysis, which is another parameter-based method, was also adapted to the signal strength of the collected AE signals. This analysis yielded two more ancillary parameters, namely: the historic index  $H(t)$  and severity ( $S_r$ ), which were originally developed to categorize the damage of fiber-reinforced polymer vessels (Fowler, 2003). These parameters have also been used in damage evaluation in many concrete-related applications (Abdelrahman et al., 2015; Abouhussien and Hassan, 2015; Abouhussien and Hassan, 2017; Li et al., 2015; Vélez et al., 2015). These two parameters are very sensitive to the progress of damage, which made them convenient for the quantifiable assessment of the different damage mechanisms of concrete in the aforementioned investigations. In our study, these parameters were utilized in a trial to highlight the effects of varying temperatures, C/F, and rubber particle size and content on the AE data parameters and be correlated to the damage.

The  $H(t)$  could measure any sudden peaks in the CSS versus time and be calculated using **Eq. 2** below:

$$H(t) = \frac{N}{N-K} \frac{\sum_{i=K+1}^N S_{oi}}{\sum_{i=1}^N S_{oi}} \quad \text{Eq. 2}$$

Where N = the cumulative number of hits until the time (t),  $S_{oi}$  = the signal strength of the  $i^{\text{th}}$  event. On the other hand, the severity ( $S_r$ ) was calculated according to **Eq. 3** below:

$$S_r = \sum_{i=1}^J \frac{S_{oi}}{J} \quad \text{Eq. 3}$$

Severity ( $S_r$ ) value was based on the average signal strength of the J number of hits. The constants (K and J) in **Eqs. 2** and **3** used in this study were determined based on previous studies concerning

AE analysis in concrete (Abdelrahman et al., 2015; Abouhussien and Hassan, 2017; ElBatanouny et al., 2014; Nair and Cai, 2010).

Constant  $K$  used in **Eq. 2** may affect the magnitude of  $H(t)$  and subsequently highlights the damage progression in terms of capturing any pronounced AE activity. In this analysis,  $K$ -value was calculated as follows:

- b)  $K = 0$ : if  $N \leq 50$ , b)  $K = N - 30$ : if  $51 \leq N \leq 200$ , c)  $K = 0.85 N$ : if  $201 \leq N \leq 500$ , and
- d)  $K = N - 75$ : if  $N \geq 501$ .

The previously mentioned ranges of  $K$  are dependent on the type of material under testing (Vélez et al. 2015), and they were adapted from the first standard AE intensity analysis made by Fowler (2003). The values of  $J$  have a similar effect on the  $S_r$  to what  $K$  has on  $H(t)$ . Based on previous studies conducted by the authors (Abouhussien and Hassan, 2019a; Abouhussien and Hassan, 2015; Abouhussien and Hassan, 2017; Abouhussien and Hassan, 2019a; Abouhussien and Hassan, 2020; Ridgley et al., 2018), A range of values of  $J$  (25–75) has been studied to calculate  $S_r$ , and  $J$  was set to an average constant value of 50.

### **3.3.10 AE Rise time vs. Average frequency (RA) analysis**

Rise time-amplitude (RA) analysis represents rise time (RT) divided by average signal amplitude. The RA method listed in RILEM recommendation TC 212-ACD (Ohtsu et al., 2010) and other related studies (Ohtsu et al., 2007; Ono, 2011) is one of the crack classification methods based on the fact that each crack mode is associated with a type of waveform. For instance, according to RILEM recommendation TC 212-ACD (Ohtsu et al., 2010), tensile cracks should release waveforms with a short RT and high average frequency (AF), whereas shear cracks should result in waveforms with a longer RT and lower AF (as shown in **Fig. 3-3**). The RT and peak signal

amplitudes were used to calculate RA value according to **Eq. 4**, while the AF values were obtained from **Eq. 5** using the counts and the duration for each event (Ohtsu et al., 2010).

$$\text{RA} = \text{rise time (RT)} / \text{the peak amplitude} \quad \text{Eq. 4}$$

$$\text{Average frequency (AF)} = \text{AE ringdown counts} / \text{duration time} \quad \text{Eq. 5}$$

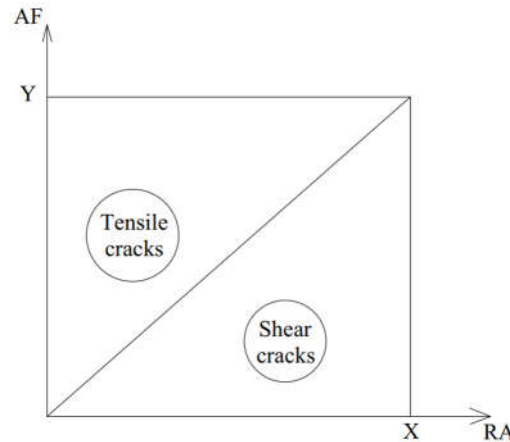


**Fig. 3- 3** RA-value vs. AF-value chart to classify tensile and shear cracks.

Ohno and Ohtsu (Ohno and Ohtsu, 2010) reported that no typical ranges for RA and AF values were set by any standards for each crack type (for instance, NDIS 2421 (NDIS2421, 2000)). In other words, the slope of the diagonal line associated with various crack types (as shown in **Fig. 3**) will be set based on the user's experience. For instance, if Y and X are the maximum AF and RA values, respectively, then the ratio  $M = X/Y$  (s/V/kHz) represents the slope of the diagonal line. M-value depends on material type, specimens' geometry, and load type. **Table 3-6** lists some values of M-ratio reported by many authors who performed a four-point bending load on various concrete mixtures, specimens' dimensions, and load types attempting to classify shear and tensile cracks (Behnia et al., 2014; Calabrese et al., 2010; Prem and Murthy, 2016; Soulioti et al., 2009).

It should be noted that RILEM recommendation TC 212-ACD (Ohtsu et al., 2010) recommends that users calculate RA and AF from the moving average of at least 50 continuous hits to find the variation trends. This study included a trial to utilize RA analysis to classify the micro- and macro-cracking stages using RA and AF charts.

**Table 3- 6** Examples of K-values obtained in concrete-based specimens tested under a four-point flexure test.

Authors	Mixture type	Dimensions (mm)	Loading type	K (s/V/kHz)
Soulioti, Barkoula (Soulioti et al., 2009)	Steel fiber reinforced concrete (SFRC)	100×100×100	Monotonic	0.09
Aggelis (Dimitrios G. Aggelis, 2011)	Plain concrete	100×100×400	Monotonic	0.027
Shahidan, Bunnori (Shahidan, Bunnori, Mohd, Nor, & Johari, 2012)	Steel-reinforced concrete (RC)	150×250×1900	Cyclic	1.0
Aldahdooh and Bunnori (Aldahdooh & Bunnori, 2013)	RC	1500 mm length and various cross-sections dimensions	Monotonic	0.0125
Behnia, Chai (Behnia et al., 2014)	RC, SFRC, polypropylene FRC	200×250×2500	Cyclic	$12.5 \times 10^{-6}$
Prem and Murthy (Prem & Murthy, 2016)	RC	100×200×1500	Monotonic	1.0

### 3.4 Results and Discussion

The values of compressive strength and maximum flexure load/strength for all tested mixtures at both temperatures (25°C and -20°C) are listed in **Table 3-7**. Micro- and macro-crack onset loads and the associated AE parameters for all prism samples are summarized in **Tables 3-8** and **3-9**.

The experimental results and the visual notices, along with AE parametric analysis, are discussed in the following section:

**Table 3- 7** Average results of cylinder compressive strength, first micro-crack loads, maximum flexure load, and flexure strength for all mixtures at 25°C and -20°C.

Mixture No.	Mixture type	Testing temperature	Compressive strength (MPa)	Maximum flexure load (KN)	Flexure strength (MPa)
M1	500-2C/F-0.4w/b	25°C	56.48	15.6	4.68
		-20°C	73.36	21.46	7.32
M2	500-0.7C/F-0.4w/b	25°C	64.42	18.2	5.76
		-20°C	79.64	24.33	7.92
M3	550-MK/FA-control	25°C	73.65	19.14	5.74
		-20°C	82.84	26.81	8.94
M4	550-10%CR	25°C	62.48	17.06	5.12
		-20°C	71.91	22.93	7.18
M5	550-20%CR	25°C	42.4	15.26	4.58
		-20°C	53.13	19.71	6.51
M6	550-30%CR	25°C	31.86	12.96	3.89
		-20°C	42.23	16.16	5.45
M7	550-20%PR	25°C	48.21	16.3	4.89
		-20°C	59.84	21.6	7.08

**Table 3- 8** AE parameters at the micro-cracking stage at 25°C and -20°C.

Mixture no.	Mixture type	Testing temperature	Average signal amplitude (dB)		Number of hits		CSS (pV.s)*10 <sup>4</sup>		$H(t)$		$S_r$ (mV/s)		$b$ -value		First micro-crack load (KN)	First micro-crack stress (MPa)
			CH-1	CH-2	CH-1	CH-2	CH-1	CH-2	CH-1	CH-2	CH-1	CH-2	CH-1	CH-2		
M1	500-2C/F-0.4w/b	25°C	82	80	107	113	0.99	1.01	1.91	1.88	2.25	2.31	0.75	0.77	6.51	1.95
		-20°C	81	80	148	157	1.13	1.19	2.13	2.29	2.81	2.86	0.71	0.68	7.68	2.30
M2	500-0.7C/F-0.4w/b	25°C	82	81	126	121	1.19	1.23	2.31	2.36	2.73	2.77	0.69	0.72	7.58	2.27
		-20°C	80	81	161	167	1.43	1.49	2.48	2.53	2.85	3.02	0.61	0.66	8.72	2.62
M3	550-MK/FA-control	25°C	81	79	143	131	1.76	1.68	2.63	2.57	3.08	2.96	0.63	0.70	7.93	2.38
		-20°C	80	81	177	181	2.01	1.99	3.06	2.91	3.27	3.31	0.49	0.54	9.11	2.73
M4	550-10%CR	25°C	74	73	90	96	0.89	1.01	1.69	1.76	1.72	1.84	0.81	0.77	7.51	2.25
		-20°C	76	77	113	117	1.67	1.61	2.19	2.28	2.38	2.31	0.69	0.66	8.92	2.68
M5	550-20%CR	25°C	67	69	77	74	0.91	0.87	1.63	1.61	1.51	1.45	0.81	0.84	6.12	1.84
		-20°C	72	73	98	101	1.23	1.17	1.96	1.88	1.79	1.83	0.71	0.74	6.87	2.06
M6	550-30%CR	25°C	61	59	67	64	0.81	0.79	1.49	1.47	1.21	1.23	0.86	0.89	5.91	1.77
		-20°C	70	69	89	83	1.16	1.13	1.87	1.81	1.52	1.57	0.75	0.72	6.68	2.00
M7	550-20%PR	25°C	69	70	83	81	0.96	0.94	1.71	1.74	1.59	1.55	0.77	0.74	6.54	1.96
		-20°C	72	74	104	99	1.26	1.31	2.39	2.44	1.89	1.93	0.66	0.63	7.23	2.17

**Table 3- 9** AE parameters at the macro-cracking stage at both temperatures.

Mixture no.	Mixture type	Testing temperature	Average signal amplitude (dB)		Number of hits		CSS (pV.s)*104		$H(t)$		$S_r$ (mV/s)		$b$ -value		Macro-crack load (KN)	Macro-crack strength (MPa)
			CH-1	CH-2	CH-1	CH-2	CH-1	CH-2	CH-1	CH-2	CH-1	CH-2	CH-1	CH-2		
M1	500-2C/F-0.4w/b	25°C	81	80	671	682	9.71	9.84	4.14	4.23	9.83	10.13	0.31	0.28	15.6	4.68
		-20°C	79	80	1161	1143	11.81	11.74	5.49	5.61	12.76	12.61	0.14	0.13	21.46	6.44
M2	500-0.7C/F-0.4w/b	25°C	82	81	933	951	12.95	12.78	4.66	4.78	11.36	11.51	0.26	0.23	18.2	5.46
		-20°C	81	81	1365	1323	13.11	13.26	6.11	6.04	13.88	13.51	0.11	0.12	24.33	7.30
M3	550-MK/FA-control	25°C	79	81	1235	1246	14.83	14.77	4.67	4.39	13.42	13.32	0.17	0.15	19.14	5.74
		-20°C	80	82	1911	1897	15.42	15.59	6.48	6.33	16.47	16.68	0.09	0.10	26.81	8.04
M4	550-10%CR	25°C	76	77	736	739	11.08	10.98	4.32	4.28	10.81	10.87	0.26	0.28	17.06	5.12
		-20°C	77	79	1108	1087	13.26	13.34	6.03	5.89	15.06	14.89	0.13	0.14	22.93	6.88
M5	550-20%CR	25°C	74	72	601	591	8.86	9.09	4.04	4.33	8.97	9.05	0.33	0.29	15.26	4.58
		-20°C	76	75	823	806	10.76	10.59	5.54	5.62	12.79	12.55	0.21	0.19	21.71	6.51
M6	550-30%CR	25°C	68	66	409	398	7.23	7.09	3.92	3.87	8.45	8.36	0.29	0.34	12.96	3.89
		-20°C	72	71	876	859	9.82	9.91	4.53	4.67	9.12	9.35	0.26	0.27	15.16	4.55
M7	550-20%PR	25°C	72	71	646	659	9.05	9.18	4.13	4.19	9.46	9.61	0.31	0.29	16.3	4.89
		-20°C	74	74	978	902	13.72	13.55	5.83	5.76	14.89	14.66	0.19	0.21	21.6	6.48

### 3.4.1 Micro- and macro-crack onset detection by AE analysis

The average values of the AE parameters, including the number of hits, CSS,  $H(t)$ ,  $S_r$ , and  $b$ -value were compared to the applied flexure load along with time for all specimens. For instance, Fig. 3-4 shows the variation of the previously mentioned AE parameters during the flexure test for sample-2 of the M4 mixture (550-10%CR) collected by sensor-2 when testing at  $-20^{\circ}\text{C}$ . As shown in Fig. 3-4a, b, c, the cumulative number of hits, CSS, and  $S_r$  followed an overall increase pattern along with the evolution of cracks until the occurrence of a large visible crack in the specimen. In contrast, the values of  $H(t)$  fluctuated throughout the test with an overall increasing pattern until reaching the peak right before failure. Meanwhile,  $b$ -values kept fluctuating with a decreasing pattern, reaching their minimum value towards the end of the test.

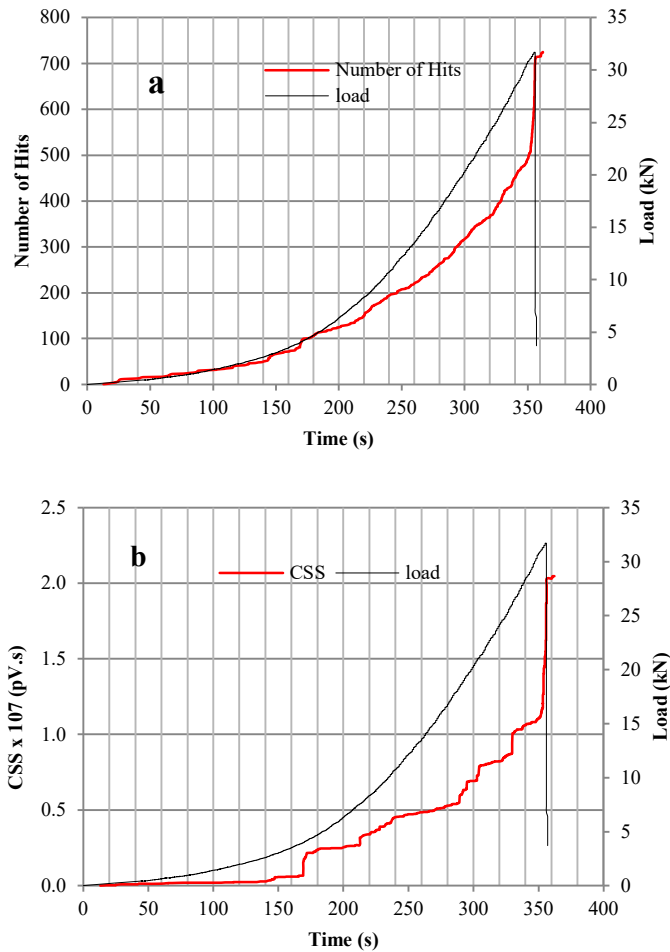


**Fig. 3- 4** The change in AE parameters throughout flexure test versus applied load on sensor-1 sample-1 mixture 20%CR tested at  $-20^{\circ}\text{C}$ : a) Number of hits, b) CSS, c)  $S_r$ , d)  $H(t)$ , e)  $b$ -value

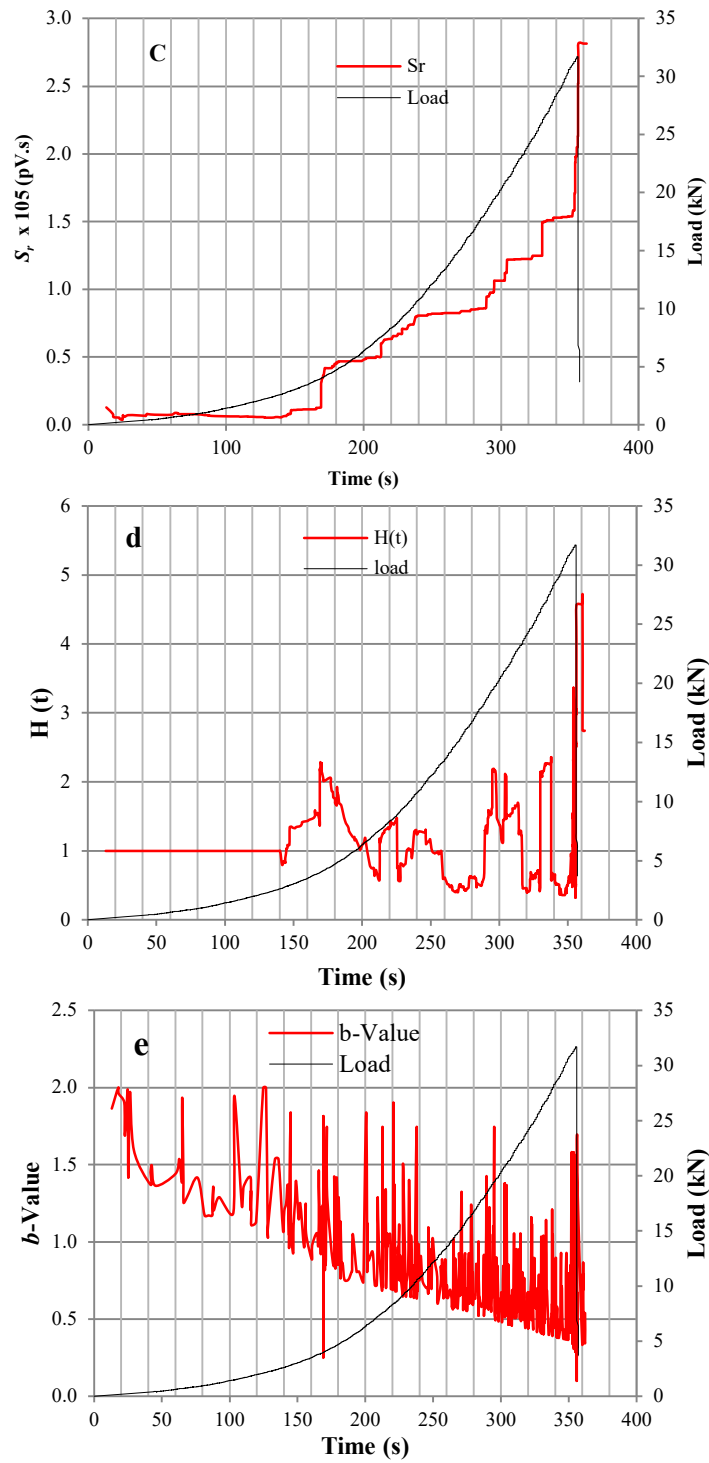


**Fig. 3- 5** The change in AE parameters throughout flexure test versus applied load on sensor-1 sample-1 mixture 20%CR tested at -20°C: a) Number of hits, b) CSS, c)  $S_r$ , d)  $H(t)$ , e)  $b$ -value (cont')

Previous studies related the sharp variations in the number of hits, CSS, and  $S_r$  curves to different damage mechanisms (Du et al., 2019; Mistrass Group, 2007; Nair and Cai, 2010; Shahidan et al., 2012). Other authors related the damage progress to sudden increases in the  $H(t)$  values and the locations of high fluctuations in the  $b$ -value of the AE events released throughout loading (Abouhussien and Hassan, 2015, Abouhussien and Hassan, 2016, Abouhussien and Hassan, 2017; Colombo et al., 2003; ElBatanouny et al., 2014; D. Li et al., 2015; Sagar et al., 2012; Vélez et al., 2015). In particular, a previous study noticed that the onset of the first micro-crack was accompanied by the first slope change in the  $S_r$  curve versus time, the occurrence of the first sudden jumps in the  $H(t)$  curve versus time, and the first drastic fluctuation in  $b$ -value curve versus time (ASTM E1316, 2014).

As shown in **Fig. 3-4b, c, d, and e**, a sharp change in CSS,  $H(t)$ ,  $S_r$ , and  $b$ -value curves was noticed after approximately 169 seconds. At this specific time, this point witnessed the first noticeable slope change in the curves of CSS and  $S_r$  (see **Fig. 3-4b and c**), the first sudden jump in the  $H(t)$  curve (see **Fig. 3-4d**), and the first sudden dip in the  $b$ -value curve (see **Fig. 3-4e**) followed by a general decline trend. This sharp AE activity coincided with a 4.74 KN flexure load, which was about 25% of the failure load of that sample (see **Fig. 3-4**). Therefore, based on this approach, this point of AE activity could be associated with the onset of the first micro-crack in this specimen.

Afterward, further increase in the applied load appeared to yield an overall increase in the number of hits, CSS,  $H(t)$ , and  $S_r$ , and an overall decrease in  $b$ -values, as shown in **Fig. 3-4**. Noticeably, the maximum values of the number of hits, CSS,  $S_r$ , and  $H(t)$  were recorded right before reaching the failure load, as seen in **Fig. 3-4**. That failure load also coincided with the minimum recorded  $b$ -values for this sample. A large flexure crack near the mid-span of the tested sample was visually noticed just before failure, and almost all other tested samples failed

after showing a similar crack before failure. The high AE events at this stage can be attributed to the further propagation of micro-cracks, which eventually led to the creation of macro-cracks. Therefore, these variation trends in the AE parameters can be used to detect the development of macro-cracks in specimens.

It should also be highlighted that, at the onset of macro-cracks, the recorded AE events were higher than the recordings at the micro-cracking stage, as shown in **Tables 8** and **9**. The above AE data analyses enabled the detection of micro-cracks at approximately 25%–40% and 35%–50% of the failure load when samples were tested at 25°C and -20°C, respectively. These results support the validity of the previously described AE analyses in the detection of micro- and macro-cracking in the various mixtures tested in this investigation. The results of the first cracking loads, failure loads, and the corresponding studied AE parameters at both the times of micro- and macro-cracking detection for all tested samples are summarized in **Tables 3-8** and **3-9**.

#### **3.4.2 Effect of cold temperature on micro- and macro-crack onset load and associated AE parameters**

Generally, cooling down concrete mixtures to -20°C was found to enhance the compressive and flexure strength and to increase the threshold at which micro- and macro-cracks appeared (**Tables 3-7–3-9**). For instance, mixture 550-20%CR (M5) showed 42.4 MPa compressive strength when tested at 25°C, and this value increased by 25% to reach 53.13 MPa when tested at -20°C. The flexure strengths for the same mixture showed 4.58 MPa at 25°C and then increased to 6.51 MPa at -20°C. This mixture also experienced the first micro-crack at 1.84 MPa when tested at 25°C and 2.06 MPa when tested at -20°C. The first macro-crack for this mixture was also delayed due to cooling down to -20°C. At 25°C, the first macro-crack was detected at 4.58 MPa and this value increased by 29.2% to reach 6.51 MPa at -20°C.

The increase in resistance and threshold limits due to reducing the temperature to  $-20^{\circ}\text{C}$  was also reflected in an overall increase in the associated cumulative AE parameters, as listed in **Tables 3-8** and **3-9**. For instance, the AE parameters collected until the onset of the first visible micro-crack for mixture M5 (as shown in **Table 3-8**) witnessed an average increase of 33% in the cumulative number of hits, 35% in CSS, 19% in  $H(t)$ , 22% in  $S_r$ , and an average decrease of 12% in  $b$ -values as a result of cooling down samples from  $25^{\circ}\text{C}$  to  $-20^{\circ}\text{C}$ . The same pattern was noticed until the onset of the macro-cracking stage for the same mixture, as shown in **Table 3-9**. For instance, the AE parameters collected until the onset of the first macro-crack witnessed an average increase of 37% in the cumulative number of hits, 19% in CSS, 35% in  $H(t)$ , 41% in  $S_r$ , and an average decrease of 35% in  $b$ -values when testing samples at  $-20^{\circ}\text{C}$  compared to  $25^{\circ}\text{C}$ . This pattern in the collected AE parameters is attributed to the increase in flexure resistance that made the mixtures resist higher loads at  $-20^{\circ}\text{C}$ .

#### **3.4.3 Effect of C/F ratio on micro- and macro-crack onset loads and associated AE parameters at a sub-freezing temperature.**

Using a higher C/F ratio was found to decrease the micro- and macro-crack onset loads and times and the associated cumulative AE parameters of micro- and macro-cracking stages regardless of testing temperatures (see **Tables 3-8** and **3-9**). For instance, as shown in **Table 3-8**, mixture M1 (with a C/F ratio of 2.0) witnessed the first visible micro-crack at 6.51 KN and 7.68 KN flexure loads when tested at  $25^{\circ}\text{C}$  and  $-20^{\circ}\text{C}$ , respectively, and these loads were 16.4% and 13.5% less than that of mixture M2 (with C/F ratio of 0.7) when tested at the same temperatures. Besides, the collected AE parameters till the first visible micro-crack for mixture M1 (with C/F ratio of 2.0) were, on average, 11.8% lower cumulative number of hits, 21% less CSS, 22.6% lower  $H(t)$ , 20.6% lower  $S_r$ , and 7% higher  $b$ -value than that of mixture M2 (with C/F ratio of 0.7) when both mixtures were tested at  $25^{\circ}\text{C}$  (see **Table 3-8**). The higher loads resisted by samples with lower C/F ratio (see **Table 3-8**) could be the reason that led to the

development of more micro- and/or macro-cracks before failure, thus creating additional AE events. On the contrary, changing the C/F ratio did not result in any change in the recorded signal amplitudes throughout the test for both cracking stages and at both temperature conditions (as shown in **Fig. 3-5**). This finding could be limited to the range of C/F ratios included in this paper.

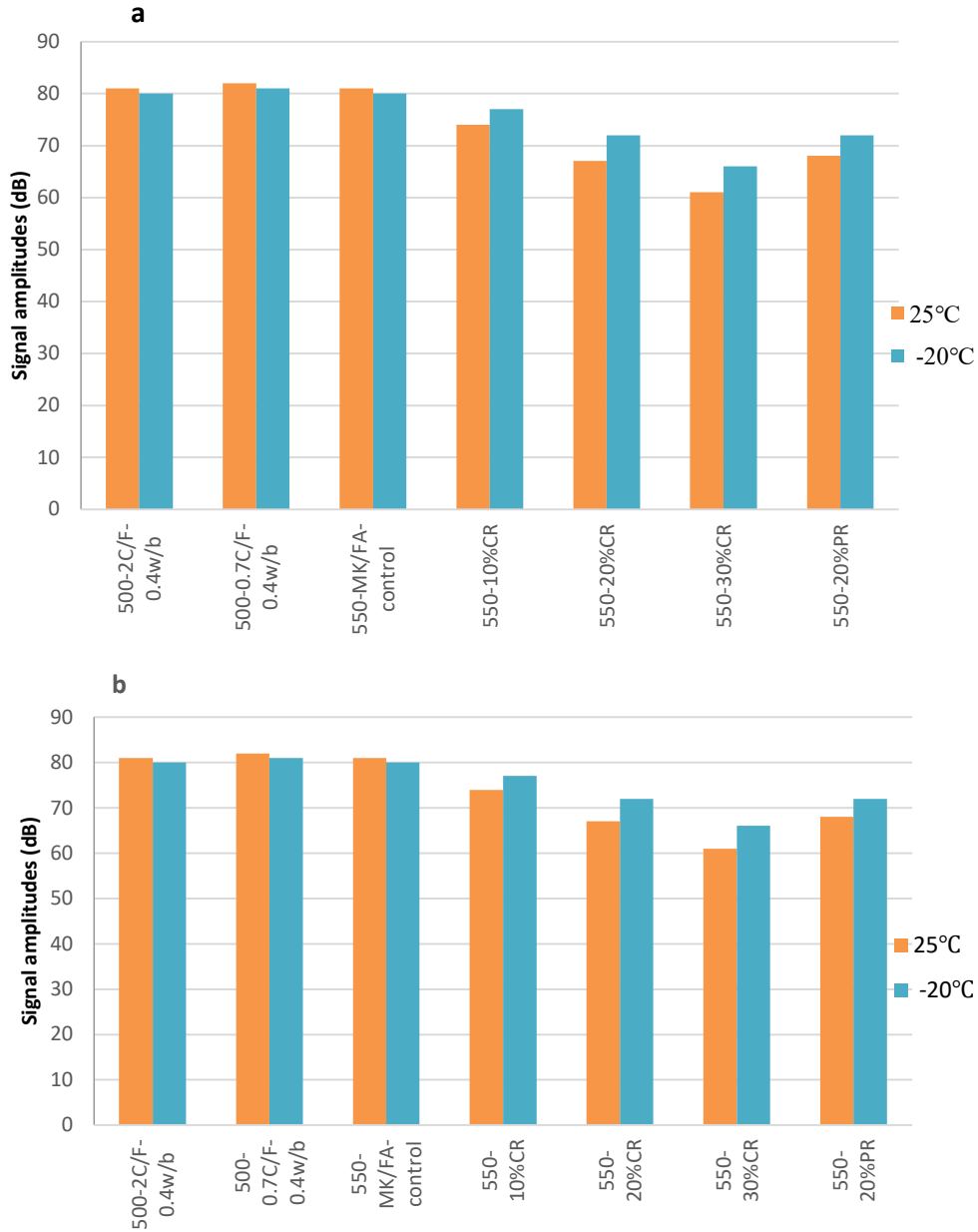


**Fig. 3- 6** Average values of signal amplitudes at 25°C and -20°C at the onset of: a) micro-crack stage, b) macro-crack stage.

### 3.4.4 Effect of CR content on micro- and macro-crack onset load and associated AE parameters at a sub-freezing temperature

Increasing CR content was generally found to decrease the first visible micro- and macro-crack onset loads and the cumulative AE parameters emitted until the onset of each stage, regardless of the samples' temperature. For instance, increasing the CR content from 0% to 10%, 20%, and 30% in mixtures M3-M6, respectively, decreased the onset load for the first visible micro-crack from 7.93 KN in M3 (0% CR) to 5.91 KN in M6 (30% CR) when these mixtures were tested at 25°C (see **Table 3-7**). This reduction in the first visible micro-crack onset was accompanied by a reduction in the collected AE parameters. For example, when both mixtures were tested at 25°C, mixture M6 with 30% CR witnessed, on average, 51.8% lower cumulative number of hits, 53.4% lower CSS, 43% lower  $H(t)$ , 59.6% lower  $S_r$ , and 33.3% higher average  $b$ -values than those values in the non-rubberized mixture M3 (see **Table 3-8**). This behavior could be attributed to the degradation in the compressive and flexure strengths due to having increased the CR content (see **Table 3-7**).

It should also be highlighted that increasing CR content from 0% in mixture M3 to 30% in mixture M6 decreased the signal amplitudes by 25% at the micro-cracking stage and by 16.3% at the macro-cracking stage, as shown in **Fig. 3-5**. The reduction of the signal amplitudes was more pronounced at the micro-cracking stage than it was at the macro-cracking stage. This finding may be related to the fact that micro-cracks are normally associated with a higher number of events having lower amplitudes than macro-cracks, which normally release a smaller number of AE hits with higher amplitudes (Abouhussien and Hassan, 2020).

### 3.4.5 Effect of rubber particle size on micro- and macro-crack onset load and associated AE parameters at a sub-freezing temperature

Decreasing the size of rubber particles yielded higher micro- and macro-cracking onset load compared to mixtures with larger rubber particles. For instance, mixture M7 with 0.4 mm rubber particles experienced the first visible micro-crack at 6.54 KN and 7.23 KN when it was tested at 25°C and -20°C, respectively, compared to 6.12 KN and 6.87 KN for mixture M5 with 4.5 mm CR when tested at the same temperatures, as shown in **Tables 3-8** and **3-9**. It is worth noting that the effect of using smaller rubber particles on cracking onset limits was more pronounced when tested at 25°C compared to the results when tested at -20°C. For instance, decreasing the rubber particle size (mixture M7 compared to mixture M5) yielded a 7% higher micro-crack onset load at 25°C compared to only 2% when tested at -20°C. This behavior could be attributed to the increased stiffness of large CR particles (less compressibility) due to freezing, which alleviated the negative effect of CR on the mixture's strength (Shahidan et al., 2012). And this effect was more pronounced in larger rubber particles compared to smaller ones.

The higher cracking limits were also associated with a higher cumulative number of hits, CSS,  $H(t)$ ,  $S_r$ , and lower  $b$ -values. For instance, until the first visible macro-crack detection, at 25°C, mixture M7 (with 0.4 mm rubber particles) witnessed 8% higher number of hits, 7% more CSS, 7% more  $H(t)$ , 6% more  $S_r$ , and 8.4% lower  $b$ -values compared to mixture M5 (with 4.5 mm CR). This increase in AE activity is attributed to the higher macro-cracking limit (in M7 compared to M5), which allowed more micro-crack formation until failure.

It should be noted that changing the size of rubber particles did not show a noticeable change in the signal amplitude values of the collected AE waves at both temperature conditions. For

instance, the AE signal amplitudes of the waves emitted during the micro-cracking stage for mixtures M5 and M7 were 72 and 72 when tested at 25°C and 73 and 74 when tested at -20°C.

#### **3.4.6 Crack level detection chart based on intensity analysis parameters.**

Based on the findings of the preceding sections, intensity analysis parameters ( $H(t)$  and  $S_r$ ) were strongly related to damage progression and the cracking level. Both  $H(t)$  and  $S_r$  were useful in detecting the propagation of micro- and macro-cracks, and as a result, they had the potential to highlight the extent of cracking in the tested mixtures. To identify the cracking level, the values of the calculated intensity analysis parameters for all tested prisms were correlated to the counterpart cracking stage in order to develop the chart shown in **Fig. 3-6**. The average values of  $H(t)$  and  $S_r$  plotted in **Fig. 3-6** were obtained from the two sensors attached to each prism for all mixtures at both temperatures (listed in **Tables 3-8** and **3-9**). The ranges of the values of  $H(t)$  and  $S_r$  were 1.47–3.06 and  $1.21–3.27 \times 10^4$  (pV.s), respectively, for the micro-cracks that were detected during the micro-cracking stage (**Table 3-8**). Meanwhile, these ranges were 3.87–6.48 and  $8.36–16.68 \times 10^4$  (mV/s) at the macro-cracking stage for  $H(t)$  and  $S_r$ , respectively (**Table 3-9**). It can be noticed that the dots plotted in the chart (**Fig. 3-6**) are clustered in two zones related to the cracking stage at which they were recorded. For example, if the AE intensity analysis parameters were calculated as 2.5 for  $H(t)$  and  $3.0 \times 10^4$  (pV.s)  $S_r$ , then micro-cracks are anticipated at the time these signals were recorded. This chart has the potential to identify the cracking level and give an early warning based on the AE signals collected by the sensors within the range of the mixtures included in this study.

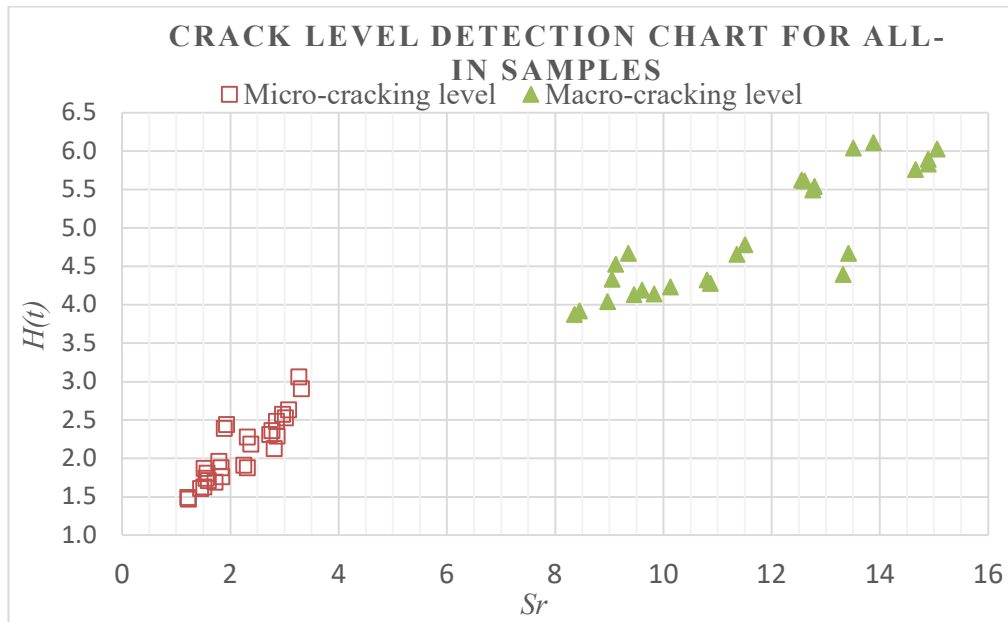


**Fig. 3- 7** Crack level classification chart using intensity analysis parameters for all-in mixtures.

### 3.4.7 Micro- and macro-crack classification using RA analysis.

As previously discussed, the micro- and macro-crack onset times and the associated AE events were identified using the AE parameters including intensity and  $b$ -value analyses. Alternatively, **Figs. 3-7** and **3-8** show the values of RA vs. AF for the non-rubberized mixtures (M1-M3) and the rubberized mixtures (M4-M7), respectively. It can be observed from **Figs. 3-7** and **3-8** that micro-crack events have relatively higher average frequency values and lower RA values. Meanwhile, macro-crack events have relatively higher RA values and lower AF values. In both charts, both point clusters were separated by a straight line (diagonal threshold) with a slope value “k” that was determined as indicated in **section 5.3**. The M-values were  $3.55 \times 10^{-3}$  and  $3.83 \times 10^{-3}$  s/V/kHz for the non-rubberized and rubberized mixtures, respectively. These results confirmed the effectiveness of the RA vs. AF analysis for classifying the crack level in all samples regardless of the mixture type or testing temperature. It should be kept in mind that the obtained M-values are exclusively related to these mixtures, loading type, and loading configuration.

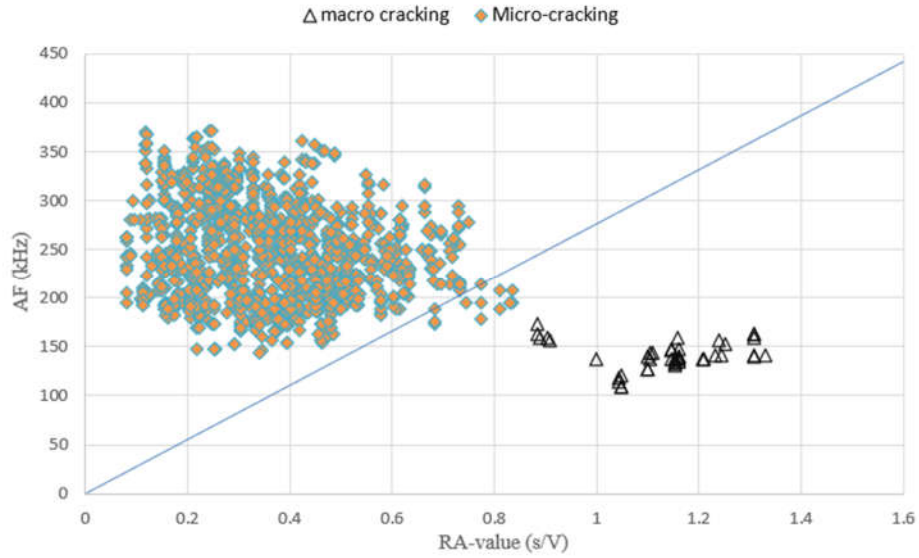


**Fig. 3- 8** Crack level classification chart based on average values of RA and A-FRQ for the non-rubberized mixtures.

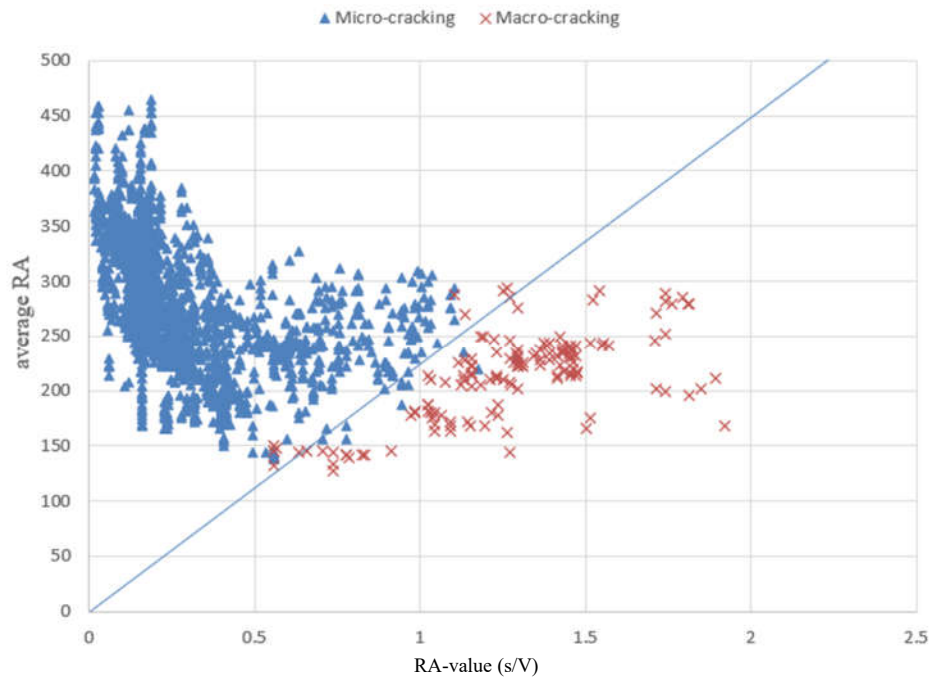


**Fig. 3- 9** Crack level classification chart based on average values of RA and average frequency for the rubberized mixtures.

### 3.5 Conclusions

To evaluate the cracking behavior of rubberized and non-rubberized concretes and the emitted AEs at 25°C and -20°C, prisms from seven mixtures with various C/F ratios, rubber contents,

and rubber particle sizes were developed and underwent a four-point load flexure test for comparison. The collected AE data underwent multiple AE parameter-based analysis methods correlated to applied load history and the visually inspected cracks. The following conclusions were drawn:

1. Analyzing the variation in the emitted AE parameters (the number of hits, CSS,  $H(t)$ ,  $S_r$ , and  $b$ -values) during the flexure test enabled early detection of the first micro-crack initiation, regardless of the samples' temperature. The first micro-crack was associated with the first significant slope change in the number of hits, CSS, and  $S_r$  curves, a sudden jump in the  $H(t)$  curve, and an extreme dip in the  $b$ -value curve. The onset of the micro-cracking stage ranged from 25%–40% and 35%–50% of the failure flexure load for the prisms when tested at 25°C and -20°C, respectively.
2. Visually detected macro-cracks were accompanied by the maximum values of the number of hits, CSS,  $S_r$ ,  $H(t)$ , and the minimum of  $b$ -values. These values were recorded right before reaching the highest load and then the split of prisms near the mid-span.
3. Decreasing samples' temperature was shown to increase the threshold limit of both micro- and macro-crack loads. On average, the onset of the micro-cracking stage for the tested samples ranged from 25%–40% of the maximum flexure load when tested at 25°C compared to 35%–50% at -20°C. Besides, macro-cracks at -20°C appeared at loads almost 25%–40% higher than those at 25°C. This increase in limits was associated with an average increase in the number of hits, CSS,  $H(t)$ ,  $S_r$ , and a decrease in  $b$ -values for the signals collected at -20°C compared to 25°C.
4. Increasing the C/F ratio yielded lower micro- and macro-cracking load thresholds, fewer number of hits, CSS,  $H(t)$ ,  $S_r$ , and higher  $b$ -values until the onset of the first visible macro-crack at both temperature conditions. In addition, changing the C/F ratio did not seem to

affect the signal amplitudes of the emitted signals at 25°C and -20°C, which implies similar wave propagation characteristics in various C/F ratio mixtures.

5. Increasing CR content was accompanied by a decrease in the number of hits, CSS,  $H(t)$ ,  $S_r$ , and an increase in the  $b$ -values for the collected signals emitted until the onset of the first visible macro-crack. This decrease in AE activity could be related to the low cracking load threshold that did not allow more crack propagation. Noticeably, increasing the CR volume decreased the signal amplitudes of the emitted AE waves as a sign of wave attenuation phenomenon. In addition, the cold temperature was found to relieve the attenuation effect.
6. Decreasing the size of rubber particles was found to increase micro- and macro-cracking onset load limits, the associated number of hits, CSS,  $H(t)$ ,  $S_r$ , and decrease the  $b$ -values for signals emitted during the four-point flexure test. The study also did not reveal any change in the amplitudes for signals emitted during the micro- or macro-cracking levels along with changing CR size. Furthermore, cold temperature increased the AE events in mixtures with larger CR sizes and had a more noticeable effect on increasing the micro- and macro-cracking load limits.
7. A damage identification chart was developed to identify the cracking level (micro- or macro-cracking) based on an intensity analysis performed on the collected AE parameters. Using the collected signals' strength/calculated values of  $H(t)$  and  $S_r$ , the charts can predict the severity of damage for the mixtures included in this study, whether at room or sub-freezing temperatures.
8. The study confirmed that RA analysis has the potential to identify the AE events associated with micro- or macro-cracking onset in the studied rubberized and non-rubberized mixtures. Two RA vs. AF charts were developed to classify the AE events associated with micro- or macro-cracks in both the rubberized and non-rubberized mixtures, respectively.

### 3.6 Chapter References

- Abdelrahman, M., ElBatanouny, M. K., Ziehl, P., Fasl, J., Larosche, C. J., and Fraczek, J. (2015). "Classification of alkali-silica reaction damage using acoustic emission: A proof-of-concept study." *Construction & building materials*, 95, 406-413.
- Abdelrahman, M., ElBatanouny, M. K., and Ziehl, P. H. (2014). "Acoustic emission based damage assessment method for prestressed concrete structures: Modified index of damage." *Engineering Structures*, 60, 258-264.
- Abouhussien, A. A., and Hassan, A. A. A. (2015). "Evaluation of damage progression in concrete structures due to reinforcing steel corrosion using acoustic emission monitoring." *Journal of civil structural health monitoring*, 5(5), 751-765.
- Abouhussien, A. A., and Hassan, A. A. A. (2016). "Detection of bond failure in the anchorage zone of reinforced concrete beams via acoustic emission monitoring." *Smart materials and structures*, 25(7), 75034-75046.
- Abouhussien, A. A., and Hassan, A. A. A. (2017). "Acoustic emission monitoring for bond integrity evaluation of reinforced concrete under pull-out tests." *Advances in structural engineering*, 20(9), 1390-1405.
- Abouhussien, A. A., and Hassan, A. A. A. (2019a). "Crack Growth Monitoring in Fiber-Reinforced Self-Consolidating Concrete via Acoustic Emission." *ACI Materials Journal*, 116(5), 181-191.
- Abouhussien, A. A., and Hassan, A. A. A. (2019b). "Assessment of Crack Development in Engineered Cementitious Composites Based on Analysis of Acoustic Emissions." *Journal of materials in civil engineering*, 31(6).
- Abouhussien, A. A., and Hassan, A. A. A. (2020). "Classification of damage in self-consolidating rubberized concrete using acoustic emission intensity analysis." *Ultrasonics*, 100, 105999-105999.
- Aggelis, D. G. (2011). "Classification of cracking mode in concrete by acoustic emission parameters." *Mechanics research communications*, 38(3), 153-157.

- Aggelis, D. G., Soulioti, D. V., Barkoula, N. M., Paipetis, A. S., and Matikas, T. E. (2012). "Influence of fiber chemical coating on the acoustic emission behavior of steel fiber reinforced concrete." *Cement and Concrete Composites*, 34(1), 62-67.
- Aggelis, D. G., Soulioti, D. V., Gatselou, E. A., Barkoula, N. M., and Matikas, T. E. (2013). "Monitoring of the mechanical behavior of concrete with chemically treated steel fibers by acoustic emission." *Construction and Building Materials*, 48, 1255-1260.
- Aldahdooh, M., and Bunnori, N. M. (2013). "Crack classification in reinforced concrete beams with varying thicknesses by mean of acoustic emission signal features." *Construction and Building Materials*, 45, 282-288.
- ASTM C1611-09, (2009) "Standard Test Method for Slump Flow of Self-Consolidating Concrete," *ASTM International*, West Conshohocken.
- ASTM C150-12, (2012) "Standard Specification for Portland Cement," *ASTM International*, West Conshohocken.
- ASTM C39-12, (2012) "Standard Test Method for Compressive Strength of Cylindrical Concrete Specimens," *ASTM International*, West Conshohocken.
- ASTM C618, (2012) "Standard Specification for Coal Fly Ash and Raw or Calcined Natural Pozzolan for Use in Concrete," *ASTM International*, West Conshohocken, PA, USA.
- ASTM C494-13, (2013) "Standard Specification for Chemical Admixtures for Concrete," *ASTM International*, West Conshohocken.
- ASTM E1316-14, (2014) "Standard Terminology for Nondestructive Examinations," *ASTM International*, West Conshohocken.
- ASTM C78/C78M. (2016). "Standard Test Method for Flexural Strength of Concrete (Using Simple Beam with Third-Point Loading), PA." *ASTM International: West Conshohocken*.
- Behnia, A., Chai, H., Yorikawa, M., Momoki, S., Terazawa, M., and Shiotani, T. (2014). "Integrated non-destructive assessment of concrete structures under flexure by acoustic emission and travel time tomography." *Construction and Building Materials*, 67, 202-215.
- Bisby, L., Eng, P., Banthia, N., Bisby, L., Britton, R., Cheng, R., Mufti, A., Neale, K., Newhook, J., and Soudki, K. (2005). "An Introduction to Structural Health Monitoring."

- Calabrese, L., Campanella, G., and Proverbio, E. (2010). "use of cluster analysis of acoustic emission signals in evaluating damage severity in concrete structures." *Journal of Acoustic Emission*, 28.
- Colombo, I. S., Main, I., and Forde, M. (2003). "Assessing damage of reinforced concrete beam using "b-value" analysis of acoustic emission signals." *Journal of materials in civil engineering*, 15(3), 280-286.
- Du, F., Li, D., and Li, Y. (2019). "Fracture mechanism and damage evaluation of FRP/steel–concrete hybrid girder using acoustic emission technique." *Journal of Materials in Civil Engineering*, 31(7), 04019111.
- ElBatanouny, M. K., Mangual, J., Ziehl, P. H., and Matta, F. (2014). "Early Corrosion Detection in Prestressed Concrete Girders Using Acoustic Emission." *Journal of materials in civil engineering*, 26(3), 504-511.
- Fowler, T. B., J. and Conslik, P (2003). "New Directions in testing." *Proceedings, Int. Conf. of Acoustic Emission from composite materials*, K. Ono, ed., *Acoustic emission working group Memphis*, 15(3), 280-286.
- Garrick, G. M. (2005). "Analysis and testing of waste tire fiber modified concrete."
- Mistrass Group, (2007). "PCI-2 based AE system 1 user's manual." *Physical Acoustics Corporation, Princeton Junction, NJ, USA*.
- Ismail, M. K., and Hassan, A. A. A. (2016). "Use of metakaolin on enhancing the mechanical properties of self-consolidating concrete containing high percentages of crumb rubber." *Journal of cleaner production*, 125, 282-295.
- Li, D., Chen, Z., Feng, Q., and Wang, Y. (2015). "Damage analysis of CFRP-confined circular concrete-filled steel tubular columns by acoustic emission techniques." *Smart materials and structures*, 24(8), 85017-85011.
- Li, G., Zhang, L., Zhao, F., and Tang, J. (2020). "Acoustic Emission Characteristics and Damage Mechanisms Investigation of Basalt Fiber Concrete with Recycled Aggregate." *Materials*, 13(18), 4009.
- Mohammed, B. S., Anwar Hossain, K. M., Eng Swee, J. T., Wong, G., and Abdullahi, M. (2012). "Properties of crumb rubber hollow concrete block." *Journal of Cleaner Production*, 23(1), 57-67.

- Nair, A., and Cai, C. S. (2010). "Acoustic emission monitoring of bridges: Review and case studies." *Engineering Structures*, 32(6), 1704-1714.
- Najim, K. B., and Hall, M. R. (2012). "Mechanical and dynamic properties of self-compacting crumb rubber modified concrete." *Construction and Building Materials*, 27(1), 521-530.
- NDIS2421 (2000). "Recommended Practice for In-Situ Monitoring of Concrete Structures by AE." *Japanese Society for Nondestructive Inspection*.
- Ohno, K., and Ohtsu, M. (2010). "Crack classification in concrete based on acoustic emission." *Construction and Building Materials*, 24(12), 2339-2346.
- Ohtsu, M. (1987). "Acoustic emission characteristics in concrete and diagnostic applications." *Journal of Acoustic Emission*, 6(2), 99-108.
- Ohtsu, M., Isoda, T., and Tomoda, Y. (2007). "Acoustic emission techniques standardized for concrete structures." *Journal of Acoustic Emission*, 25(2007), 21-32.
- Ohtsu, M., Shiotani, T., Shigeishi, M., Kamada, T., Yuyama, S., Watanabe, T., Suzuki, T., van Mier, J. G. M., Vogel, T., Grosse, C., Helmerich, R., Forde, M. C., Moczko, A., Breyse, D., Ivanovich, S. A., Sajna, A., Aggelis, D., and Lacidogna, G. (2010). "Recommendation of RILEM TC 212-ACD: acoustic emission and related NDE techniques for crack detection and damage evaluation in concrete: Measurement method for acoustic emission signals in concrete." *Materials and structures*, 43(9), 1177-1181.
- Ono, K. (2011). "Application of acoustic emission for structure diagnosis." *Diagnostyka*, 3-18.
- Physical Acoustics. (2005). "R6I-AST sensor." *Physical Acoustics Corporation*, Princeton Junction, NJ, USA.
- Prem, P. R., and Murthy, A. R. (2016). "Acoustic emission and flexural behavior of RC beams strengthened with UHPC overlay." *Construction and Building Materials*, 123, 481-492.
- Rao, M., Lakshmi, K. P., Rao, G. N., Vijayakumar, K., and Udayakumar, S. (2011). "Precursory microcracking and brittle failure of Latur basalt and migmatite gneiss under compressive loading." *Current Science*, 1053-1059.

- Ridgley, K. E., Abouhussien, A. A., Hassan, A. A., and Colbourne, B. (2018). "Evaluation of abrasion resistance of self-consolidating rubberized concrete by acoustic emission analysis." *Journal of Materials in Civil Engineering*, 30(8), 04018196.
- Sadek, D. M., and El-Attar, M. M. (2015). "Structural behavior of rubberized masonry walls." *Journal of Cleaner Production*, 89, 174-186.
- Sagar, R. V., Prasad, B. R., and Kumar, S. S. (2012). "An experimental study on cracking evolution in concrete and cement mortar by the *b*-value analysis of acoustic emission technique." *Cement and Concrete Research*, 42(8), 1094-1104.
- Shahidan, S., Bunnori, N. M., Mohd, S., Nor, N. M., and Johari, M. A. M. "Analysis of the AE signals parameter at the critical area on the concrete beam." *Proc., 2012 IEEE Symposium on Industrial Electronics and Applications*, IEEE, 386-391.
- Shang, H.-s., Yi, T.-h., and Guo, X.-x. (2014). "Study on Strength and Ultrasonic Velocity of Air-Entrained Concrete and Plain Concrete in Cold Environment." *Advances in materials science and engineering*, 2014, 1-7.
- Soulioti, D., Barkoula, N., Paipetis, A., Matikas, T., Shiotani, T., and Aggelis, D. (2009). "Acoustic emission behavior of steel fiber reinforced concrete under bending." *Construction and Building Materials*, 23(12), 3532-3536.
- Standard, A. (2012). "Standard specification for coal fly ash and raw or calcined natural pozzolan for use in concrete." *ASTM Standard C*, 618.
- Vélez, W., Matta, F., and Ziehl, P. (2015). "Acoustic emission monitoring of early corrosion in prestressed concrete piles." *Structural control and health monitoring*, 22(5), 873-887.
- Wang, H., Dang, Z., Li, L., and You, Z. (2013). "Analysis on fatigue crack growth laws for crumb rubber modified (CRM) asphalt mixture." *Construction & building materials*, 47, 1342-1349.
- Xu, J., Fu, Z., Han, Q., Lacidogna, G., and Carpinteri, A. (2018). "Micro-cracking monitoring and fracture evaluation for crumb rubber concrete based on acoustic emission techniques." *Structural Health Monitoring*, 17(4), 946-958.

Youssf, O., Mills, J. E., Benn, T., Zhuge, Y., Ma, X., Roychand, R., and Gravina, R. (2020).

"Development of Crumb Rubber Concrete for Practical Application in the Residential Construction Sector – Design and Processing." *Construction & building materials*, 260, 119813.

Zaki, R. A., AbdelAleem, B. H., Hassan, A. A., and Colbourne, B. (2020). "Abrasion Resistance of Fiber-Reinforced Concrete under Cold Temperatures." *ACI Materials Journal*, 117(5), 221-232.

## 4. Assessment of Abrasion Resistance of Fiber-Reinforced Concrete at Cold Temperature via Acoustic Emission Analysis

### 4.1 Abstract

This study investigated utilizing acoustic emission (AE) monitoring to assess the abrasion performance of fiber-reinforced self-consolidating concrete at cold temperatures (-20°C). In addition, the study targeted correlating the abrasion damage to AE data through AE intensity analysis parameters. Seven concrete mixtures were developed with variable water-binder (W/B) ratios (0.4 and 0.55), fiber types (steel and polypropylene synthetic fibers), fiber lengths (19 mm and 38 mm), and fiber volumes (0.2% and 1%). Testes on 100-mm cubic samples were conducted at -20°C and 25°C, for comparison, according to the rotating cutter technique in conjunction with AE monitoring. Characteristics of the AE signals, such as signal amplitudes, number of hits, and signal strength, were collected and underwent  $b$ -value and intensity analyses resulting in three subsidiary parameters:  $b$ -value, severity ( $S_r$ ), and the historic index ( $H(t)$ ). A clear correlation between abrasion damage progress and AE parameters was noticed. Analyzing AE parameters along with experimental measurements generally revealed a better abrasion resistance for all mixtures when tested at -20°C compared to that at room temperature. The mixtures with steel fibers, lower W/B values, shorter fibers, and higher fiber volume showed improved abrasion resistance irrespective of temperature. Noticeably, the mixtures containing longer fibers, higher W/B values, or lower fiber dosage experienced a more pronounced enhancement ratio in the abrasion resistance when cooled down to sub-zero temperature. Two damage classification charts were developed to infer the mass loss percentage and wear depth due to abrasion using intensity analysis parameters:  $S_r$  and  $H(t)$ .

### 4.2 Introduction

Core infrastructure such as harbors, bridges, and roads suffer inevitably from abrasive erosion. The high wind speed, severe wave hits, and ship/iceberg collisions further aggravate the

situation in the Arctic region, which is also characterized by extremely low temperatures. Such circumstances may lead to premature aging and could decrease the predicted service life of concrete structures in these areas. Therefore, the abrasion performance of concrete in such structures should be given great attention (Zaki et al. 2020).

Abrasion resistance is defined as the materials' ability to resist being rubbed off due to friction. To evaluate the abrasion resistance of concrete, various standard destructive techniques by the American Society for Testing and Materials (ASTM) are available. These methods included the rotating desk test (C779/C779M-12 2012b), sandblasting test (C418-12 2012c), and the rotating cutter test (C944/C944M-12 2012a). Selecting the proper standard test method mainly depends on simulating the configuration of forces that the structure is exposed to. Many factors contribute to the abrasion performance of concrete, such as the percentage of coarse aggregate in the mixture (Pyo et al. 2018) and the cement paste/aggregate quantity (Horszczaruk 2005). Hence, engineers can mitigate abrasion damage by selecting the proper concrete type and constituents. For instance, self-consolidating concrete (SCC), which usually has a low coarse aggregate fraction and high fine materials volume (Lachemi et al. 2003), was found to have a better abrasion resistance over normal vibrated concrete (NVC) (Ghafoori 2014).

SCC is a highly flowable and non-segregating concrete type. It can flow and enclose the reinforcement bars without any vibration effort (ACI237R-07 2007). Using SCC has gained wide acceptance in Japan since the late 1980s, and its use in North America has grown drastically since 2000, especially in the precast industry (ACI237R-07 2007). In an attempt to improve the mechanical performance of SCC, previous studies investigated adding steel fibers (SFs) and/or synthetic fibers (SynF) to the mixture (AbdelAleem et al. 2017; AbdelAleem et al. 2018; Ismail and Hassan 2017; Khayat et al. 2014). The inclusion of fibers in concrete allows omnidirectional crack control by transferring tensile stresses over crack faces, which adds extra strength to the cementitious composites (AbdelAleem and Hassan 2019; jun Li et al. 2016; jun

Li et al. 2017). Fibers also increase the ductility of concrete, which in turn makes it harder for parts of the concrete to be pulled off by the abrasion action. Ridgley et al. (Ridgley et al. 2018) reported that adding synthetic polypropylene fibers to SCC generally enhanced the abrasion performance in terms of the percentage of weight loss and wearing depth. Their results also indicated that flexible and short fibers exhibited better abrasion performance on average than rigid and longer ones.

At below-freezing temperatures, the performance of fibrous concretes could be quite different than at room temperature. Previous studies supported that exposure to cold temperatures increased compressive strength, tensile strength, flexural toughness, and impact resistance with more brittle failure for various types of fiber-reinforced concretes (Duthil 2015; Lee et al. 1988; Pigeon and Cantin 1998; Zaki et al. 2021). Omar et al. (2020) investigated the impact and mechanical performance of developed lightweight fiber-reinforced SCC mixtures at varying temperatures (+20°C, 0°C, and -20°C). The study also showed an enhancement in the mechanical and impact performance of all mixtures when decreasing the temperature. In addition, the study revealed that the inclusion of fibers in the mixture compensated for the brittle behavior of concrete that resulted from decreasing the temperature. Omar et al. (Omar et al. 2020) attributed this behavior to that water in pores freezes at sub-zero temperatures leading to an increase in strength since the capillary pores will be filled with a solid substance that has an extra load capacity. They (Omar et al. 2020) also attributed the improved strength of fiber-reinforced SCC to the increased bond between the fibers and the hardened cementitious matrix due to shrinkage of concrete at low temperatures.

Non-destructive techniques (NDT) such as visual inspection, ultrasonic waves, and eddy-current methods are of high importance for the ongoing condition assessment of concrete structures, especially in harsh environments. Meanwhile, for hard-to-reach areas and continuous monitoring cases, acoustic emission (AE) monitoring was proved to be a more

convenient candidate taking advantage over other traditional forms of NDT (Vidya Sagar et al. 2012). AE is a phenomenon that occurs in a solid material under stress when it is cracked or damaged. This event emits strain energy waves that can be collected by attached AE sensors. The sensors convert the picked-up waves into electrical signals and then feed them into a data acquisition system for recording and processing to detect and quantify the damage (Zaki et al. 2015; Ziehl et al. 2008). AE has been successfully employed in many concrete-related studies. For instance, to classify the fracture process of steel fiber reinforced concrete (Aggelis et al. 2011); monitor the alkali-silica reaction expansion damage (Abdelrahman et al. 2015); evaluate the performance of a simple span pre-stressed concrete bridge during a proof test (Anay et al. 2016); assess abrasion damage of SCC containing synthetic fibers or rubberized materials under room temperature (Ridgley et al. 2018; Ridgley et al. 2018); and to identify initial yielding and the failure onset of bonded post-tensioned concrete elements (Salamone et al. 2012).

Preliminary studies were performed by Ridgley et al. (Ridgley et al. 2018; Ridgley et al. 2018) to assess the abrasion damage of different concrete types by means of AE analysis. The outcomes of these studies demonstrated the capability of AE parameters to state the extent of abrasion damage in terms of both mass loss and wear depth when samples were tested at room temperature. To date, there are no studies in the literature that utilized AE monitoring to assess the abrasion performance of concrete under sub-zero temperatures. It is anticipated that the changes in the microstructure of concrete as a result of exposure to sub-zero temperatures could lead to an impact on the AE wave propagation and spread following the behavior of ultrasonic waves (Shang et al. 2014). Consequently, further investigations are warranted to examine this effect and confirm the validity of the AE analysis in evaluating the abrasion resistance of concrete at cold temperatures. This study examined the use of AE continuous monitoring as a potential NDT technique to assess the cold temperature abrasion performance

of fiber-reinforced concrete containing various types, lengths, and dosages of fibers. The study also aimed to provide a method to roughly infer the abrasion mass loss and wearing depth using AE intensity analysis parameters.

### **4.3 Experimental Investigation**

#### **4.3.1 Materials properties and mixture design**

A total of seven mixtures were prepared and tested. The full details of all mixture proportions tested in this study are shown in **Table 4-1**. Mixtures include two SCC mixtures with 500 kg/m<sup>3</sup> binder (cement) content (M1 and M2) but different W/B ratios. The behavior of AE waves is related to the properties of the transfer medium. Upon this, mixtures M1-M2 were implemented to check the effect of turning a high amount of water (such that in mixture M1 with W/B of 0.55 compared to mixture M2 with W/B of 0.4) into ice on the propagation of AE waves at -20°C and to evaluate AE's ability to detect the change in abrasion performance. In addition, five mixtures with 550 kg/m<sup>3</sup> binder content. The five mixtures are as follows: one SCC mixture without fibers (control) (M3); two SCC mixtures with 0.2% polypropylene SynFs (19 mm and 38 mm lengths); one normal vibrated mixture with 1% polypropylene SynFs (38 mm length), and one SCC mixture with 0.2% steel fiber (SF) (35 mm length). The geometrical and mechanical characteristics of these fibers are described in **Table 4-2**. Mixtures M2-M5 were adopted from a previous study performed by the authors (Ridgley et al. 2018). Meanwhile, various trial mixtures were performed to develop mixtures M1, M6, and M7. The fresh properties of the mixtures were evaluated by conducting V-funnel, L-box, and T<sub>50</sub>, and the results were summarized in **Table 4-3**. The steel and synthetic fibers included in this study are the most commercially common in the market and were implemented to evaluate the change in the AE parameters due to changing fiber type. The volume of fibers ( $V_f$ ) was set as 0.2% for all mixtures except for mixture M6, where  $V_f$  was taken as 1%. In SCC mixtures, 0.2% was found to be the maximum possible dosage of fibers that satisfied the requirements of

fresh properties for SCC, while the 1% fiber in mixture M6 was the maximum percentage of fibers that ensured a homogeneous mixture with no fiber balling. Mixtures M5 with 38 mm long synthetic polypropylene fibers and M7 with 35 mm long steel fibers have the same fiber content of 0.2% and almost the same fiber length. Comparing the parameters of the AE waves emitted in both mixtures could address the effect of fiber material on the AE wave characteristics. Mixture M6 was included to study the effect of increasing fiber content on the behavior of the AE parameters and to assess AE monitoring ability to detect the variation in abrasion performance. Besides, the high dose of synthetic polypropylene fibers is anticipated to have some attenuation effect on signal amplitudes since the fiber's material (polypropylene) has some acoustic absorption properties.

**Table 4- 1** Mixture proportions.

Mixture no.	Mixture type	Cement (kg/m <sup>3</sup> )	MK (kg/m <sup>3</sup> )	FA (kg/m <sup>3</sup> )	C/F	W/B	C.A. (kg/m <sup>3</sup> )	F.A. (kg/m <sup>3</sup> )	Water content (kg/m <sup>3</sup> )	V <sub>f</sub> %	HRWRA (kg/m <sup>3</sup> )
M1	500-0.55w/b	500	-	-	0.7	0.55	606.24	866.1	275	-	-
M2	500-0.4w/b	500	-	-	0.7	0.4	686.54	980.77	200	-	2.13
M3	550-control	275	110	165	0.7	0.4	620.3	886.1	220	-	3.43
M4	550-SynF19	275	110	165	0.7	0.4	620.3	886.1	220	0.2	4.35
M5	550-SynF38	275	110	165	0.7	0.4	620.3	886.1	220	0.2	4.69
M6	550-1%SynF38	275	110	165	0.7	0.4	620.3	886.1	220	1	5.8
M7	550-SF35	275	110	165	0.7	0.4	620.3	886.1	220	0.2	4.6

Note: 1 kg/m<sup>3</sup> = 0.06243 lb/ft<sup>3</sup>

Regarding the mixtures designation:

- 500-0.55w/b means a concrete mixture with a binder content of 500 kg/m<sup>3</sup> and 0.55 water-binder ratio.
- “SynF” stands for synthetic fibers, and “SF” stands for steel fibers.
- 550-SynF38 means a concrete mixture with a binder content of 550 kg/m<sup>3</sup> and reinforced with synthetic fibers 38 mm in length.

**Table 4- 2** The physical and mechanical properties of fibers.

Fiber type	Material	Length (mm)	Diameter (mm)	Specific gravity	Tensile Strength (MPa)	Fiber's shape
SF-35	Steel	35	0.55	7.85	1150	Hooked end
SynF-19	polypropylene	19	0.66	0.91	300	Straight
SynF-38	polypropylene	38	0.64	0.91	515	Straight

Notes: 1 mm = 0.039 in.; 1 MPa = 145 psi

**Table 4- 3** Average values of L-box ratio, T<sub>50</sub>, V-funnel time, compressive strength, and wear depth of all samples at room and cold temperatures.

Mixture no.	Mixture type	Testing temperature	L-box (H <sub>2</sub> /H <sub>1</sub> )	T <sub>50</sub> (sec)	V-funnel time (sec)	Compressive strength (MPa)	Wear depth (mm)	Rate of mass loss (gms/min)	Weight loss / compressive strength (gms/MPa)
M1	500-0.55w/b	Room	0.75	3.8	15	61.63	1.21	1.63	0.16
		Cold				76.55	1.02	1.27	0.10
M2	500-0.4w/b	Room	0.89	2.1	8	66.54	1.04	1.41	0.13
		Cold				79.74	0.98	1.23	0.09
M3	550-control	Room	0.92	2.0	7.2	74.56	0.82	1.29	0.10
		Cold				89.73	0.72	1.17	0.08
M4	550-SynF19	Room	0.88	2.3	8.5	78.85	0.57	0.96	0.07
		Cold				90.97	0.46	0.89	0.06
M5	550-SynF38	Room	0.82	2.6	11.4	76.26	0.62	1.12	0.09
		Cold				88.11	0.54	0.97	0.07
M6	550-1%SynF38	Room	--	--	--	51.92	0.52	1.08	0.12
		Cold				63.85	0.46	0.88	0.08
M7	550-SF35	Room	0.79	2.5	10.9	78.96	0.46	0.81	0.06
		Cold				89.74	0.40	0.69	0.05

Notes: 1 MPa = 145 psi; 1 mm = 0.039 in.

All tested mixtures contained type GU cement, which was in compliance with ASTM Type I (C150 2012) and had a specific gravity of 3.15. Two supplementary cementing materials: fly ash (FA) and metakaolin (MK), were used in five mixtures. These SCMs had a specific gravity of 2.5 and 2.27, respectively. Both coarse aggregate (C.A.) and fine aggregate (F.A.) used in this investigation had a specific gravity of 2.6 and water absorption of 1%. The coarse-to-fine aggregate ratio was taken at 0.7 in all mixtures to achieve acceptable fresh properties of the SCC mixtures. The W/B ratio was kept constant at 0.4 in all mixtures except for one mixture (M2) where a W/B of 0.55 was used to study the effect of increasing water content (that will turn into ice after freezing) on the abrasion performance and the characteristics of the emitted AE waves at -20°C. To obtain successful SCC mixtures (in terms of fresh properties), a high range water reducing admixture (HRWRA) was added to all SCC mixtures to achieve the desired slump flow of 700 ± 50 mm, as per ASTM C1611 (ASTM C1611/C1611M, 2009). The HRWRA used was similar to that described in ASTM Type F (C494-13 2013) and had a specific gravity of 1.2 and a pH level of 9.5.

### 4.3.2 Abrasion test setup

For each mixture, six cylinders (100 mm height and 200 mm diameter) and four prisms (100 mm square cross-section and 400 mm length) were cast to test the compressive strength and abrasion resistance, respectively. All specimens were cured in a moisture curing room at approximately 25°C for 28 days. When samples reached 28 days of maturity, the prisms were cut into 100 mm cubes (to obtain six cubes from each mixture) for abrasion testing. A group of three cylinders and three cubes from each mixture was kept at ambient room temperature, and another group was kept in a freezer at -20°C for at least 48 hours before testing to reach a steady-state temperature before testing (Zaki et al. 2020). The compressive strength was determined for each mixture by testing three cylinders at both room and -20°C temperature according to ASTM C39 (ASTM C39-12, 2012f). For the abrasion test, the rotating-cutter standard ASTM C944 method (C944/C944M-12, 2012a) was implemented on three faces (one from each cubic specimen). This ASTM standard abrasion test uses a drill press with a rotating chuck that carries 10 kg applied directly on the chosen face of cubic samples (C944/C944M-12, 2012a). The used abrasion test setup is shown in **Fig. 4-1**. In this study, each face was tested for six intervals (1 min each), and weight loss was measured after each interval. Besides, the wear depth due to abrasion was measured for each face at the end of the test (after 6 mins) using electronic calipers having a sensitivity of 0.01 mm.



**Fig. 4- 1** AE and rotating cutter abrasion test setup.

In this study, piezoelectric AE sensors (model number R6I-AST) with an integral preamplifier were used (Group 2007). During the abrasion tests, one piezoelectric sensor was attached to each cube specimen using a two-part epoxy adhesive. The AE system monitored and recorded the signals being emitted during the abrasion testing (see **Fig. 4-1** for AE system setup). These sensors have high sensitivity and low resonant frequency, making them more convenient for multiple applications, including metals, FRPs, and concrete structures (Abouhussien and Hassan, 2017). The sensors attached to the specimens were connected to a cable and then to a data acquisition system.

#### **4.3.3 AE data filtering**

AE software called AEwin was utilized to record the AE data and control the data acquisition system during the tests. An amplitude threshold of 40 dB was set to record different AE signal parameters emitted during the abrasion testing period. A full list of the AE parameters determined in the system can be seen in **Table 4-4**. The pre-testing analog and digital filter ranges shown in **Table 4-4** were selected based on a preliminary study completed by the authors to evaluate the abrasion damage in concrete using AE analysis (Ridgley et al. 2018;

Ridgley et al. 2018). This AE data acquisition setup, shown in **Table 4-4** has also been implemented in other previous studies conducted by the authors and allowed the detection of various damage mechanisms in concrete (Abouhussien and Hassan 2017; Group 2007). The collected AE parameters included signal amplitude, signal strength, duration, absolute energy, number of hits, rise time, average frequency, and peak frequency. A full description of these parameters is discussed in ASTM E1316 (E1316 2014).

**Table 4- 4** AE system details.

<b>AE hardware setup</b>	
Threshold	40 dB <sub>AE</sub>
Sample rate	1 MSPS
Pre-trigger	256 μs
Length	1 k points
Preamp gain	40 dB
Preamp voltage	28
Analog filter	1-50 kHz
Digital filter	100-400 kHz
Peak definition time	200 μs
Hit definition time	800 μs
Hit lockout time	1000 μs
Maximum duration	1000 μs

#### 4.3.4 AE *b*-value analysis

The signal amplitudes and number of hits of AE signals were collected, filtered, and underwent a *b*-value analysis to evaluate abrasion damage progress for all samples. The *b*-value is based on seismic equations in the first place and was effectively utilized in many studies to indicate the changes in the frequency level of the AE waves to assess several damage mechanisms in concrete ((Colombo et al. 2003; ElBatanouny et al. 2014; Ohtsu and Tomoda 2008; Vidya Sagar and Raghu Prasad 2013). The *b*-value was calculated throughout the abrasion tests for all specimens according to **Eq. 1**.

$$\text{Log } N_A = a - b \log A \quad \text{Eq. 1}$$

In this equation,  $N_A$  = the number of hits prior to the specific time having amplitudes larger than  $A$ ;  $A$  = the signal amplitude of the specific hit at the specific time (dB),  $a$  = an empirically derived constant; and  $b$  = the  $b$ -value (ElBatanouny et al. 2014; Ohtsu and Tomoda 2008; Vidya Sagar and Raghu Prasad 2013)

The constant  $a$  was determined for each specimen by plotting  $\log A$  against  $\log N_A$ , and the average value of  $\log N_A$  axis intercept was taken as the value of  $a$ .

#### 4.3.5 AE Intensity analysis

In addition to the  $b$ -value analysis, an intensity analysis was performed on the signal strength of the collected AE signals to calculate more parameters that could be correlated to the damage and to study the effects of varying temperatures, W/B ratio, and fiber type, length, and dosage on the AE data characteristics variation. The intensity analysis included calculating two additional AE parameters: the historic index ( $H(t)$ ) and severity ( $S_r$ ). These two parameters are very sensitive to the progress of damage, making them convenient for the quantifiable assessment of the different damage mechanisms of concrete in several different studies (Abouhussien and Hassan 2017; ElBatanouny et al. 2014; FOWLER et al. 1989; Nair and Cai 2010; Vélez et al. 2015). The  $H(t)$  could measure any sudden peaks or troughs in the cumulative signal strength (CSS) versus time and was calculated using **Eq. 2** below:

$$H(t) = \frac{N}{N-K} \frac{\sum_{i=K+1}^N S_{oi}}{\sum_{i=1}^N S_{oi}} \quad \text{Eq. 2}$$

In this equation,  $N$  = the cumulative number of hits until time ( $t$ ),  $S_{oi}$  = the signal strength of the  $i^{\text{th}}$  event. On the other hand, the severity ( $S_r$ ) was calculated according to **Eq. 3**.

$$S_r = \sum_{i=1}^J \frac{S_{oi}}{J} \quad \text{Eq. 3}$$

Severity ( $S_r$ ) value measures any changes in the recorded signal strengths. Hence, highlighting any severe damage or excessive cracking damage.  $S_r$  value was based on the average signal

strength of the  $J$  number of hits. The constants ( $K$  and  $J$ ) in Equations 2 and 3 used in this study were determined based on previous studies concerning AE analysis in concrete (Abdelrahman et al. 2014; FOWLER et al. 1989; Nair and Cai 2010; Vélez et al. 2015).

Constant  $K$  used in Equation 2 may affect the magnitude of  $H(t)$  and subsequently highlight the damage progression in terms of capturing any pronounced AE activity. In this analysis,  $K$  was calculated as follows:

- c)  $K = 0$ : if  $N \leq 50$ , b)  $K = N - 30$ : if  $51 \leq N \leq 200$ , c)  $K = 0.85 N$ : if  $201 \leq N \leq 500$ , and  
d)  $K = N - 75$ : if  $N \geq 501$ .

The previously mentioned ranges of  $K$  are dependent on the type of the material under testing (ElBatanouny et al. 2014; Nair and Cai 2010; Vélez et al. 2015) and were adapted from the first standard AE intensity analysis made by Fowler et al (FOWLER et al. 1989).

The values of  $J$  have a similar effect on the  $S_r$  to that  $K$  has on  $H(t)$ . A range of values of  $J$  of 25-75 has been studied to calculate  $S_r$ , which was also followed in previous studies (Abdelrahman et al. 2015; Abdelrahman et al. 2014; Nair and Cai 2010). In this study,  $J$  was set to an average constant value of 50 based on an analysis performed in preliminary studies conducted by the authors (Ridgley et al. 2018; Ridgley et al. 2018).

#### **4.4 Experimental Results and Discussion**

The experimental measurements regarding abrasion weight loss and the associated AE parameters collected during the abrasion tests were analyzed and discussed in further detail in the following sections to assess the abrasion performance and reliability of AE analysis. It's worth noting that the values of abrasion weight loss measured at both room and cold temperatures were found to be close to another similar study that adopted the same abrasion test (Ridgley et al. 2018). The implications of the studied AE parameters are as follows: the cumulative number of hits indicates the number of cracks induced in concrete, CSS implies both the number and width of cracks induced in concrete, the intensity analysis parameters ( $S_r$

and  $H(t)$  are sensitive to damage and cracks progression, and  $b$ -value implies the change in the frequency of the AE events (cracks) emitted in concrete hence addressing damage progression.

#### 4.4.1 Validity of the built-in and post-processing filters to eliminate noise data.

A smooth roller abrasion test was performed on sample-1 from mixture 550-SynF38 (M5) at 25°C while being monitored via an AE sensor, as shown in **Fig. 4-2**. Smooth rollers were adopted to simulate the test conditions and eliminate abrasion action to check the validity of the filter's ranges adopted in this study. The sample's weight loss for sample-1 from mixture M5 was measured after each 1 min interval at both the rotating cutter and smooth roller abrasion tests (as shown in **Table 4-5**). **Fig. 4-3** shows two samples "a and b" of mixture M5 after 6 minutes of abrasion testing under the rotating cutter and the smooth roller abrasion test, respectively. The figure shows the significant abrasion damage due to the rotating cutter effect on sample "a". Meanwhile sample "b" has barely been affected by any abrasion damage due to the smooth roller abrasion test.



**Fig. 4- 2** Verification abrasion test setup using a smooth roller.

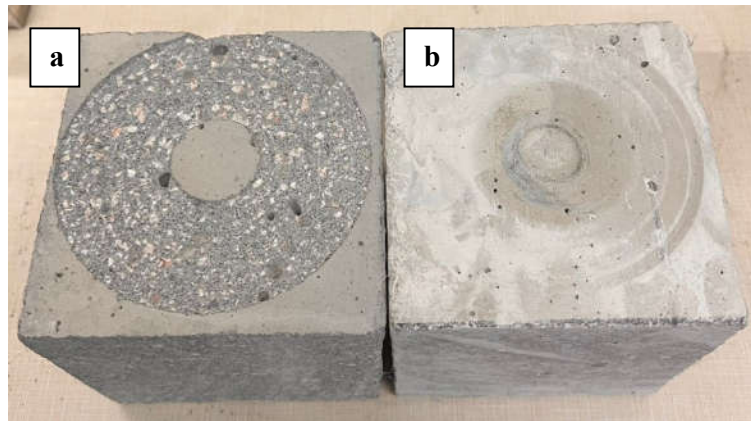


**Fig. 4- 3** Mixture M5 samples after 6 minutes of testing under a) rotating cutter abrasion test, b) smooth roller abrasion test.

**Table 4- 5** The percentage of weight loss after testing sample-2 of mixture 550-SynF38 (M5) at 25°C under smooth-roller and rotating cutter test.

Test type	The average percentage of weight loss (%)					
	1 min	2 min	3 min	4 min	5 min	6 min
Smooth roller test	0.0	0.001	0.0018	0.002	0.0024	0.0031
Rotating cutter test	0.05	0.12	0.17	0.22	0.26	0.29

The associated AE parameters emitted at both tests were collected and analyzed, as shown in **Table 4-6**. As can be noticed in **Table 4-6**, the abrasion damage induced under the smooth roller test was negligible compared to the damage induced under the effect of the rotating cutter test. For instance, after 6 minutes of abrasion, the sample experienced 0.0031% weight loss under the smooth-roller test compared to 0.29% under the rotating cutter test. The AE parameters collected by the AE monitoring system experienced the same pattern. For example, the signal amplitude for the hits emitted under the smooth-roller test was around 43 dB, barely exceeding the amplitude threshold in the adopted filters (40 dB). Besides, under the smooth roller abrasion test, the collected total number of hits was 24 compared to 336 in the case of the rotating cutter abrasion test. Moreover, the CSS recorded by the end of the test was 0.063 mV.s

in the case of the smooth roller test compared to 1.39 mV.s in the case of the rotating cutter test.

**Table 4- 6** Average AE parameters collected when testing sample-2 of mixture 550-SynF38 at 25°C under smooth-roller and rotating cutter test.

Test type	Average signal amplitude (dB)		Number of hits		CSS * 10 <sup>12</sup> (mV.s)		<i>H (t)</i>		<i>S<sub>r</sub></i> (mV.s)	
	1 min	6 min	1 min	6 min	1 min	6 min	1 min	6 min	1 min	6 min
Smooth roller test	42	44	8	24	0.014	0.063	0.11	0.21	0.11	0.24
Rotating cutter test	84	81	68	336	0.18	1.39	1.13	1.23	2.06	3.27

These results manifest the validity of the adopted filter range to eliminate most of the AE noise data induced throughout the abrasion test.

#### 4.4.2 Correlation between the abrasion damage and AE parameters at cold temperature

After checking the validity of the adopted filter ranges to eliminate most of the noise data. Any AE hit and its signal strength (energy) recorded by the sensors should be related to a crack or damage induced inside the testing sample. Hence, the cumulative number of hits or CSS should imply the damage severity in the tested samples. It has been concluded in a previous study performed by the authors that AE parameters can be correlated to abrasion damage of fiber-reinforced concrete at room temperature (Ridgley et al. 2018; Ridgley et al. 2018).

**Figs. 4-4a and b** show the percentage of weight loss throughout the 6 minutes rotating cutter abrasion test at 25°C and -20°C, respectively. The AE parameters emitted throughout the test were collected and analyzed to find a pattern that correlates abrasion damage to the corresponding emitted AE signals. Sample S2 (SCC-500-0.55w/b mixture) is presented in **Fig. 4-5** as an example of all other tested mixtures. **Fig. 4-5** shows the changes in the number of hits, CSS, *b*-value, *H (t)*, and *S<sub>r</sub>* versus time of the selected sample (S2) tested at -20°C. The change in the percentage of weight loss due to abrasion versus time was also displayed on each graph for comparison. The sections with smaller slopes or that are flat in the graphs of **Fig. 4-5a, b** represent the time between tests when the abrasion was stopped and resumed after each

minute to measure the weight loss following each 1 min interval. The graph shows that the abrasion damage follows a semi-linear trend in the average percentage of weight loss versus time in contrast to the variations in some of the studied AE parameters.

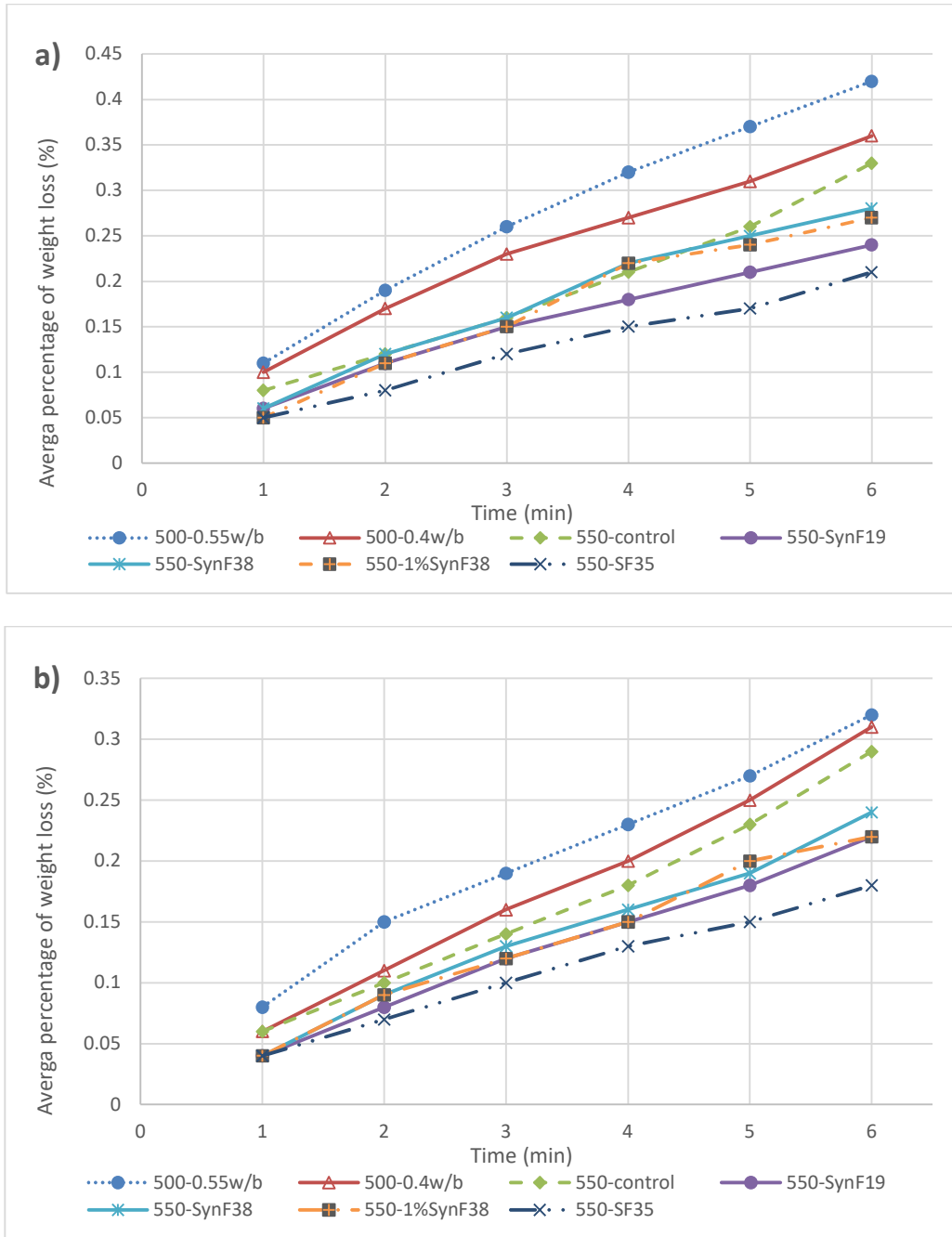


**Fig. 4- 4** Average percentage of weight loss (%) of all mixtures at: a) Room temperature (25°C) and b) Cold temperature (-20°C).

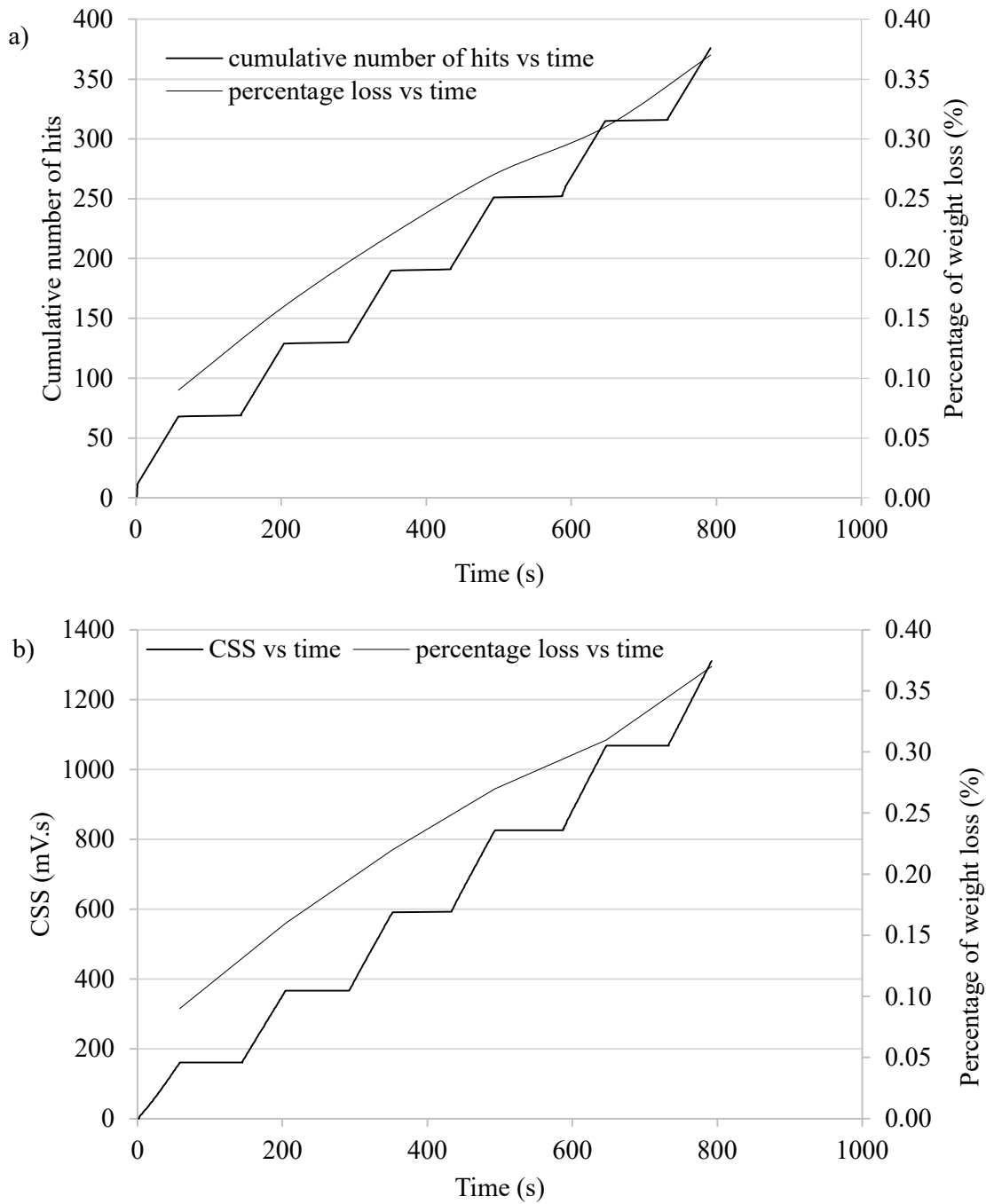


**Fig. 4- 5** Variations in AE parameters for 500-0.55w/b (S2) tested at cold temperature: a) Number of hits, b) CSS c)  $b$ -value, d)  $H(t)$ , and e)  $S_r$

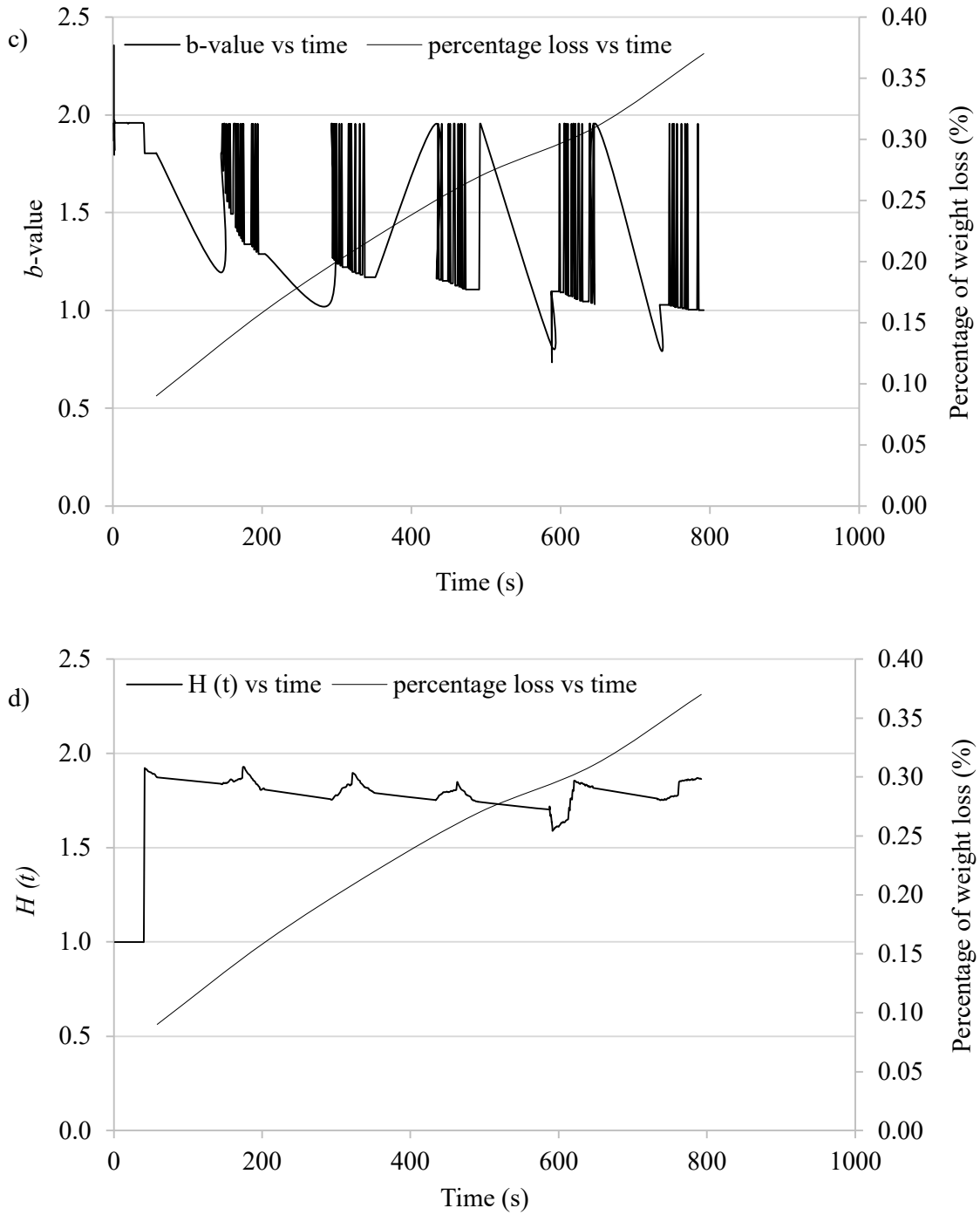


**Fig. 4- 6** Variations in AE parameters for 500-0.55w/b (S2) tested at cold temperature: a) Number of hits, b) CSS c)  $b$ -value, d)  $H(t)$ , and e)  $S_r$  (cont')

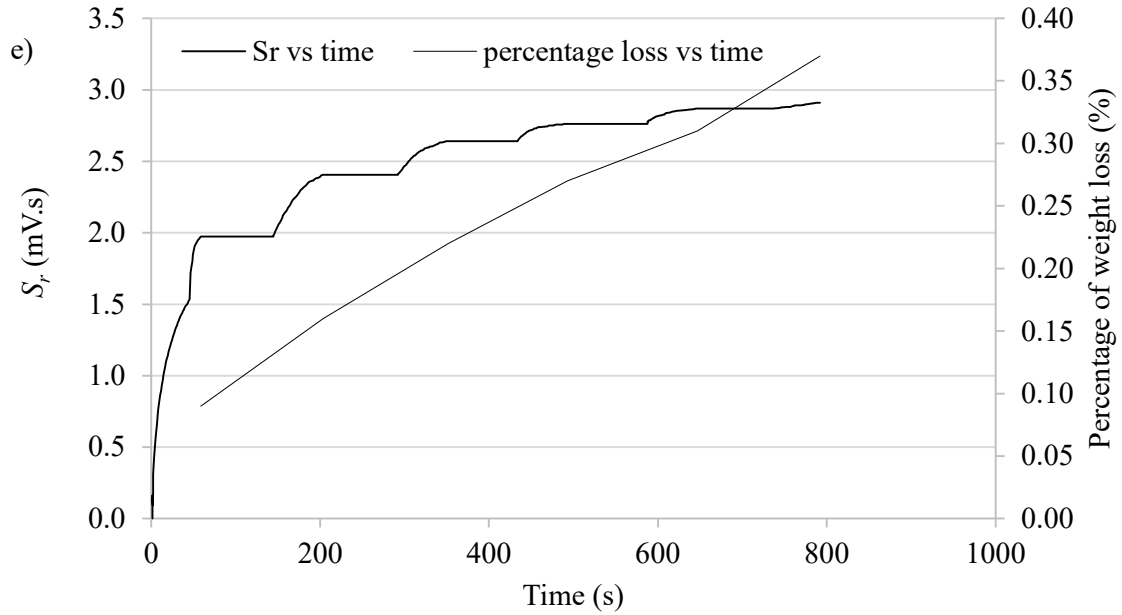


**Fig. 4- 7** Variations in AE parameters for 500-0.55w/b (S2) tested at cold temperature: a) Number of hits, b) CSS c)  $b$ -value, d)  $H(t)$ , and e)  $S_r$ (cont')

**Fig. 4-5a** (for the selected S2 sample tested at  $-20^{\circ}\text{C}$ ) shows that the cumulative number of hits increased over time throughout the test period. For this sample, the number of hits after 1 min was 68 and increased to reach 376 after 6 min. This AE activity coincided with an increase in the percentage of weight loss from 0.09% to reach 0.37% during the same period. CSS followed a similar trend to that of the number of hits versus time, as seen in **Fig. 4-5b**. Specifically, CSS values linearly increased from 161 to 1311 mV.s as the abrasion damage increased from 0.09 to 0.37%. In contrast, the  $b$ -value curve fluctuated over the test and followed an overall descending trend as the abrasion weight loss increased. For instance, the  $b$ -value decreased from 1.8 to 1.0 in accordance with an increase in the weight loss for the same sample from 0.09% to 0.37%, as seen in **Fig. 4-5c**. It is worth noting that the locations of the higher fluctuations in the  $b$ -value chart (**Fig. 4-5c**) corresponded to the times that have higher AE activity (linear increase in the number of hits and CSS) and greater abrasion damage.

Similarly, the  $H(t)$  magnitudes experienced slightly sudden peaks and drops throughout the test while constantly fluctuating at a value of around 1.8 with a maximum value of 1.92, as seen in **Fig. 4-5d**. The sudden increases in the  $H(t)$  values coincided with an increased AE activity corresponding to the locations of the slope change in the CSS variation. All these previous events can be related to the rising linear trend in the abrasion damage after each test interval. This increased AE activity (in terms of variation of the values of  $H(t)$ ) can be attributed to the particle exfoliation associated with abrasion damage (Ridgley et al. 2018).<sup>17</sup> In contrast,  $S_r$  spiked in the first testing interval to reach a value of 1.9 mV.s and showed a gradual increase for the rest of the test, reaching its peak value of 2.9 mV.s at the end of the test, as seen in **Fig. 4-5e**. The continual increase in the  $S_r$  during the test could be attributed to the abrasion damage progression leading to more cracks and AE strain energy release.

**Fig. 4-6** displays the  $b$ -values obtained by the end of each testing interval, at which the  $b$ -value almost reached the minimum value. The figure displays the relationship between the  $b$ -value and weight loss percentage for the same mixture (S2) tested at room and  $-20^{\circ}\text{C}$ . It is shown that the increase in weight loss due to abrasion was accompanied by an almost linear decline in the  $b$ -value. These relationships of the S2 sample (presented in **Fig. 4-6**) also indicate the existence of a correlation between abrasion damage and  $b$ -value at both cold and room temperatures.

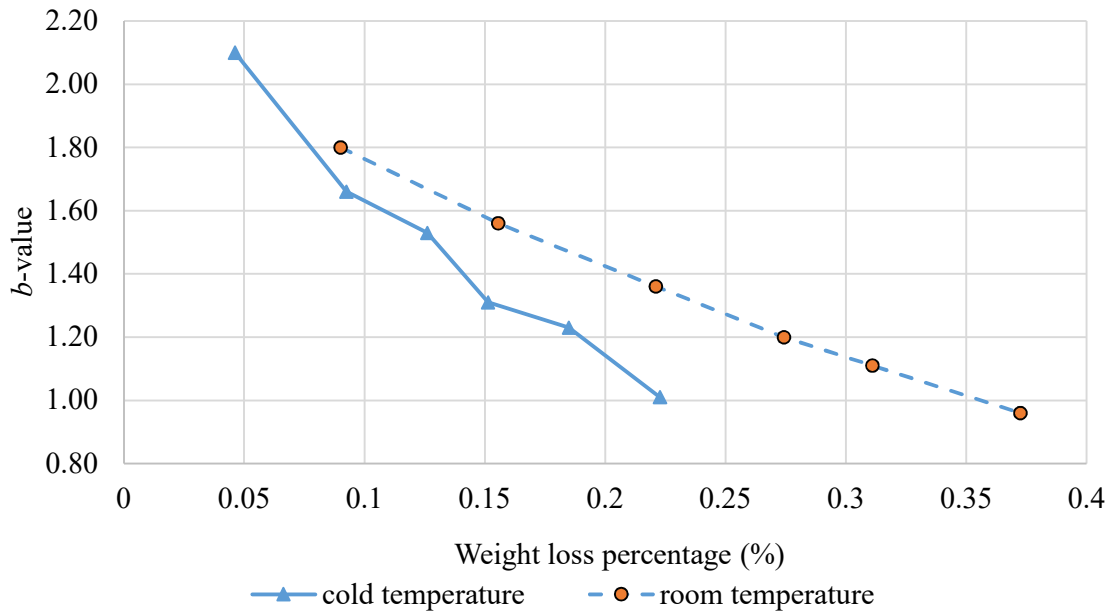


**Fig. 4- 8** Relation between  $b$ -value and weight loss for 550-0.55W/B (S2) at cold and room temperatures.

On the other hand, the values of signal amplitudes for the same sample (S2 sample tested at -20°C) throughout the test were analyzed and found to experience insignificant changes in accordance with the damage progression, except for a slight increase in the amplitude values for samples tested at cold temperature compared to those tested at room temperature samples. For example, for sample (SCC-500-0.55w/b-S2), the average amplitude values corresponding to each testing interval from 1 to 6 min were 87, 88, 88, 86, 87, and 88 dB, respectively. Other samples tested in this study showed a similar trend in the variations in the previously noted AE parameters as the sample graphed in **Figs. 4-5 and 4-6** demonstrate. Subsequently, it can be concluded that the analysis of these AE parameters could be used as a tool to identify the abrasion damage progress in the tested mixtures regardless of temperature. The values of the selected AE parameters (number of hits, CSS,  $b$ -value,  $H(t)$ ,  $S_r$ ) at the end of the first and last 1 min intervals were summarized in **Table 4-7**. The AE parameters in **Table 4-7** were utilized on a comparative basis to assess the abrasion resistance of the tested SCC mixtures, as discussed in the following sections.

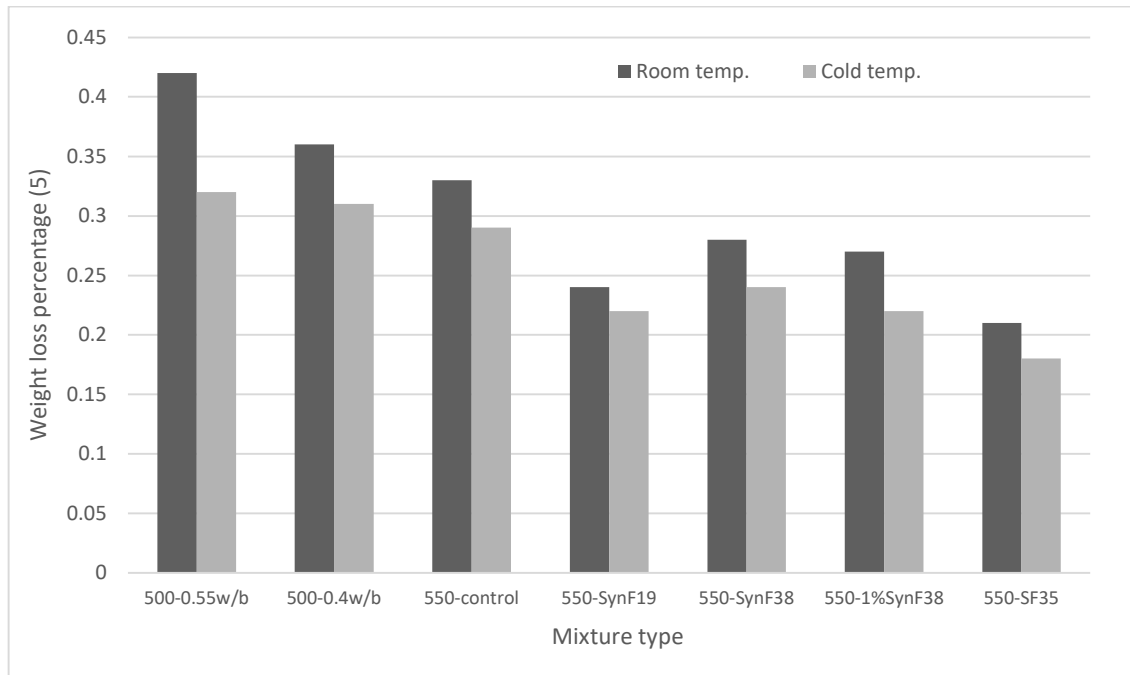


**Fig. 4- 9** Average percentage of weight loss of all samples after 6 mins abrasion at room and cold temperatures.

#### **4.4.3 Effect of cold temperature on the abrasion performance and AE data**

Lab measurements and the collected AE parameters supported that cold temperature generally enhanced the compressive strength and abrasion resistance of all mixtures, as displayed in **Fig. 4-7** and **Tables 4-3, 4-7, and 4-8**. For example, experimental measurements showed that mixture M1 experienced 24% less weight loss when tested at  $-20^{\circ}\text{C}$  compared to room temperature ( $25^{\circ}\text{C}$ ) after 6 minutes of abrasion. Similarly, the reduction in weight loss was 14% for M2, 13.7% for M3, 8.3% for M4, 14.3% for M5, 7.4% for M6, and 14.3% for M7 compared with room temperature. In terms of wear depth, as expected, lab testing showed a decrease of 16% for M1, 6% for M2, 12% for M3, 19.3% for M4, 13% for M5, 11.5% for M6, 13% for M7 at cold temperature versus room one. The values of abrasion mass loss rate (gms/min) listed in **Table 4-3** confirm the same observations. For instance, the rate of mass loss for the mixtures when tested at cold temperature compared to room temperature dropped from 1.63 gm/min to 1.27 gm/min for mixture M1 and from 1.29 gm/min to 1.17 gm/min for mixture M3. This behavior could be attributed to the fact that when water in pores began to

freeze, the strength increased since the capillary pores were filled with a solid substance, which added an extra load-bearing capacity.<sup>1</sup> The effect of variation in the compressive strength of the tested mixtures was also considered by presenting the values of normalized mass loss with respect to the compressive strength in **Table 4-3**.

**Table 4- 7** Average values of AE parameters after 1 min & 6 min abrasion testing of all samples at room and cold temperatures.

Mixture no.	Mixture type	Testing temperature	Average signal amplitude (dB)		Number of hits		CSS * 10 <sup>12</sup> (mV.s)		H (t)		S <sub>r</sub> (mV.s)		b-value	
			1 min	6 min	1 min	6 min	1 min	6 min	1 min	6 min	1 min	6 min	1 min	6 min
M1	500-0.55w/b	Room	85	85	104	604	0.29	1.91	1.77	2.72	2.62	4.08	1.43	0.94
		Cold	87	86	95	532	0.21	1.29	1.52	2.55	2.45	3.73	1.88	1.07
M2	500-0.4w/b	Room	87	83	96	519	0.26	1.85	1.70	2.51	2.55	3.85	1.8	1.15
		Cold	84	86	83	506	0.15	1.11	1.56	2.0	2.40	3.41	1.85	1.63
M3	550-control	Room	81	82	81	381	0.24	1.8	1.49	1.45	2.14	3.81	1.88	1.32
		Cold	84	86	66	367	0.14	1.28	1.54	1.29	2.25	3.35	2.0	1.39
M4	550-SynF19	Room	80	78	68	341	0.17	1.21	0.95	1.05	1.94	3.22	2.83	1.91
		Cold	86	87	57	327	0.13	1.06	0.92	1.03	1.83	2.72	2.97	1.99
M5	550-SynF38	Room	84	79	61	345	0.2	1.37	1.09	1.2	2.05	3.29	2.42	1.71
		Cold	83	85	60	337	0.18	1.13	1.03	1.17	1.94	3.11	2.71	1.83
M6	550-1%SynF38	Room	87	84	55	321	0.18	1.29	1.39	1.18	2.75	2.92	2.48	1.83
		Cold	87	85	47	309	0.14	1.09	0.98	1.14	1.79	2.83	2.81	1.95
M7	550-SF35	Room	87	85	54	336	0.17	1.11	0.96	1.14	1.92	2.69	2.60	1.85
		Cold	87	85	51	318	0.13	1.07	1.01	1.13	1.66	2.37	2.71	1.91

**Table 4- 8** Average percentage of weight loss after testing at room and cold temperatures for all samples.

Mixture no.	Mixture type	The average percentage of weight loss (%)											
		1 min		2 min		3 min		4 min		5 min		6 min	
		Room	Cold	Room	Cold	Room	Cold	Room	Cold	Room	Cold	Room	Cold
M1	500-0.55w/b	0.11	0.08	0.19	0.15	0.26	0.19	0.32	0.23	0.37	0.27	0.42	0.32
M2	500-0.4w/b	0.10	0.06	0.17	0.11	0.23	0.16	0.27	0.20	0.31	0.25	0.36	0.31
M3	550-control	0.08	0.06	0.12	0.10	0.16	0.14	0.21	0.18	0.26	0.23	0.33	0.29
M4	550-SynF19	0.06	0.04	0.11	0.08	0.15	0.12	0.18	0.15	0.21	0.18	0.24	0.22
M5	550-SynF38	0.06	0.04	0.12	0.09	0.16	0.13	0.22	0.16	0.25	0.19	0.28	0.24
M6	550-1%SynF38	0.05	0.04	0.11	0.09	0.15	0.12	0.22	0.20	0.24	0.20	0.27	0.22
M7	550-SF35	0.05	0.04	0.08	0.07	0.12	0.10	0.15	0.13	0.17	0.15	0.21	0.18

Another reason is that the ice may have bridged the cracks and limited crack growth in the matrix, which can add more strength to the concrete matrix. The shrinkage of concrete at  $-20^{\circ}\text{C}$  may also have positively affected the bond between the fibers and the hardened cementitious matrix (Zaki et al. 2020), which is another reason that may have contributed to increasing the strength at cold temperatures. The aforementioned reasons could be further confirmed by the result of mixture 500-0.55w/b (M1), which had the highest W/B ratio compared to all other tested mixtures. This mixture experienced the most pronounced enhancement ratio in the abrasion resistance when frozen (24% reduction in weight loss and 16% reduction in wear depth).

The same behavior could be found from the AE collected parameters shown in **Table 4-7**. For example, the reduction in weight loss due to freezing of 500-0.55w/b mixture (M1) was accompanied by an average reduction of 12% in the number of hits, 32.5% in CSS, 43% in  $H(t)$ , and 13.5% in  $S_r$ , and an average increase of 13.8% in  $b$ -value. Regarding the signal amplitudes, there was a slight increase in the average signal amplitudes for samples tested at  $-20^{\circ}\text{C}$  compared with those at room temperature, as shown in **Fig. 4-8**. This amplitude trend could be attributed to the fact that water inside the pores turned into ice and decreased signal attenuation. Another reason could be that cooling down samples to  $-20^{\circ}\text{C}$  was accompanied by higher strength and more brittle behavior, resulting in higher values of strain energy released during damage progress.

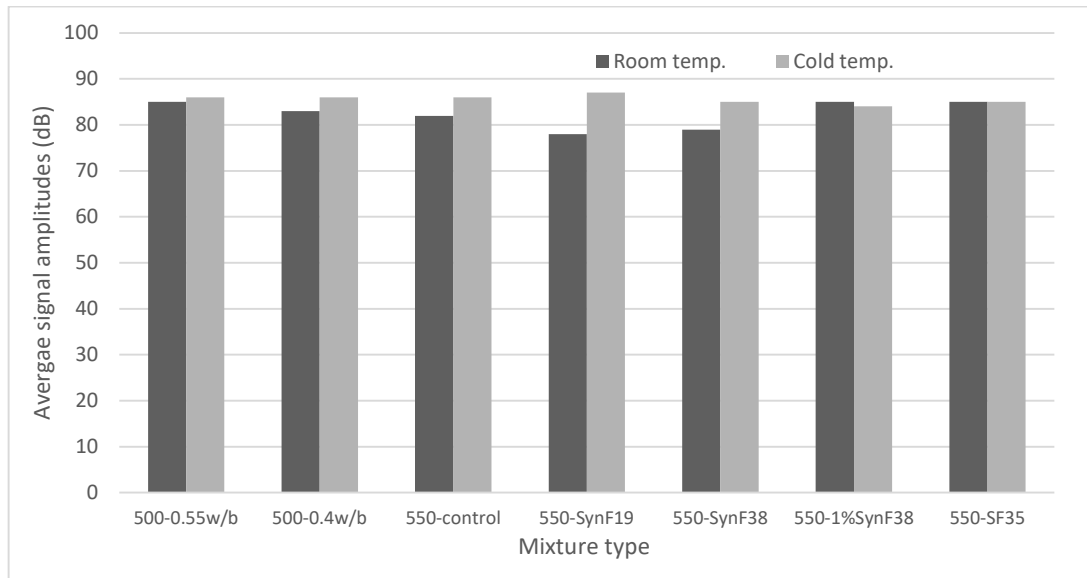


**Fig. 4- 10** Average signal amplitude values of all samples at room and cold temperature.

#### **4.4.4 Effect of W/B ratio on the abrasion performance and AE data at room and cold temperatures**

Two SCC mixtures were developed with two different W/B ratios, 0.4 and 0.55 (M1 and M2). The results in **Table 4-3** indicated that increasing the W/B ratio negatively affected the abrasion wear depth at normal temperatures. The cold temperature, however, alleviated these reductions. Samples with a higher W/B ratio (0.55) experienced a more pronounced enhancement ratio in the abrasion resistance when cooled down to -20°C. For instance, mixture M2 (0.4 W/B) experienced a weight loss of 0.36% compared to 0.42% for mixture M1 (0.55 W/B ratio) when tested at room temperature. Whilst mixture M2 (0.4 W/B ratio) experienced a weight loss of 0.31% compared to 0.32% for mixture M1 (0.55 W/B ratio) when tested at cold temperature. Regarding wear depth, mixture M2 (0.4 W/B) experienced 1.04 mm compared to 1.21 mm for mixture M1 (0.55 W/B) when tested at room temperature. On the other hand, mixture M2 (0.4 W/B) experienced 0.98 mm compared to 1.02 mm for mixture M1 (0.55 W/B) when tested at cold temperature. This enhancement ratio in the abrasion resistance of the mixture with a higher W/B ratio at cold temperature could be related to the fact that more

amount of water converted to ice in higher W/B ratio mixtures, which filled the micro-cracks in the matrix. This led to a relatively higher strength, as discussed in Section 5.2.

The same behavior in the abrasion performance could be noticed from the AE parameter values (see **Table 4-7**). For example, when testing at room temperature, increasing the W/B ratio from 0.4 (M2) to 0.55 (M1) yielded an average increase of 16% in the number of hits, 3% in CSS, 8% in  $H(t)$  values, and 6% in  $S_r$ , and a decrease of 18% in  $b$ -value, indicating lower abrasion resistance. On the other hand, increasing the W/B ratio at  $-20^{\circ}\text{C}$  resulted in an increase in the number of hits by 5%, in CSS by 16%, in  $H(t)$  by 27%, in  $S_r$  by 6%, and a decrease in  $b$ -value by 34%, indicating slightly lower abrasion resistance.

#### **4.4.5 Effect of fibers on the abrasion performance and AE data at room and cold temperatures**

A control SCC mixture without fibers (M3) was developed, and four other mixtures (M4-M7), including different types, lengths, and volumes of fibers, were included and tested at room and cold temperatures for comparison. The results in **Tables 4-7** and **4-8** showed an overall improvement in the abrasion performance for the different fiber-reinforced mixtures compared to the control mixture, irrespective of temperature. For instance, the control mixture without fibers (M3) experienced an average weight loss of 0.33% and 0.29% at room and cold temperatures, respectively, while these numbers were 0.27, 0.23% (on average) in mixtures containing fibers (M4-M7). Similarly, the control mixture without fibers (M3) showed an average wear depth of 0.82 mm, and 0.72 mm at room and cold temperatures, respectively, and these numbers were 0.52 mm, and 0.42 mm (on average) in mixtures containing fibers (M4-M7).

The same enhancement in the abrasion performance could be noticed from the AE parameter values (see **Table 4-7**). For example, incorporating fibers in the mixtures (M4-M7) yielded an average decrease of 13.4% in the number of hits, 30.5% in CSS, 21.4% in  $H(t)$  values, and

20.4% in  $S_r$ , and an increase of 37% in  $b$ -value for fiber-reinforced mixtures compared to the results of the control mixture (M3) at  $-20^{\circ}\text{C}$ . This result could be attributable to the fact that fibers provide more crack control and prevent particles from pulling out as a result of abrasion. Besides, the shrinkage of concrete under cold temperatures promoted the bond between fibers and the surrounding matrix (Zaki et al. 2021).<sup>1</sup>

#### **4.4.6 Effect of fiber volume on the abrasion and AE data at room and cold temperature**

The study included two mixtures containing the same fiber type and length at different dosages: 0.2 and 1% (M5 and M6, respectively). The results in **Tables 4-3** and **4-8** indicated that increasing the fiber volume yielded slightly lower values of weight loss and wearing depth under both cold and room temperatures, indicating better abrasion resistance. For example, the M5 mixture with 0.2% fibers experienced mass losses of 0.28% and 0.24%, and wear depths of 0.62mm and 0.54mm at room and cold temperatures, respectively. Alternatively, the M6 mixture (with 1% fibers) showed 0.27% and 0.22% mass loss, as well as 0.52 mm and 0.46 mm, wear depth at room and cold temperatures, respectively. This enhancement in the abrasion resistance could be attributed to the additional crack control accompanied by using higher fiber volumes.

The above experimental results were further confirmed by analyzing the calculated AE parameters shown in **Table 4-7**. For example, when tested at  $-20^{\circ}\text{C}$ , increasing the fiber volume from 0.2% to 1% was accompanied by a reduction in the number of hits from 337 to 309, in CSS from 1130 mV.s to 1090 mV.s, in  $H(t)$  from 1.17 to 1.14, and in  $S_r$  from 3.11 to 2.83, and an increase in  $b$ -value from 1.83 to 1.95 (which indicates an improved abrasion resistance when a higher volume of fibers was used).

#### **4.4.7 Effect of fiber type on the abrasion and AE data at room and cold temperatures**

Two types of fibers were used in this investigation: 38mm polypropylene synthetic fibers (M5) and 35mm steel fibers (M7). For mixture M5, the average percentages of abrasion weight loss

at room and cold temperatures were 0.28%, and 0.24%, respectively. These numbers dropped to 0.21%, and 0.18%, respectively, when using steel fibers (M7), indicating better abrasion resistance. Similarly, in the mixture with polypropylene synthetic fibers (M5) the average wear depths were 0.62 mm and 0.54 mm at room and cold temperature, respectively, and these numbers also dropped to 0.46 mm and 0.40 mm, respectively, in the mixture with steel fibers (**Table 4-3**). These results show that the steel fiber mixture encouraged better abrasion resistance than polypropylene synthetic fiber at both room and sub-zero temperatures.

The calculated AE parameters showed a similar trend to that observed from the experimental results for the two mixtures. For example, in the case of steel fiber mixture, the average values of the number of hits, CSS,  $H(t)$ , and  $S_r$  were lower, and the average  $b$ -values were higher than in the case of synthetic polypropylene fiber mixture. The average magnitudes of these parameters in the same order in case of room temperature were 336, 1110 mV.s, 1.14, 3.65, and 1.85 at room temperature and 318, 1070 mV.s, 1.13, 3.11, and 1.91 at -20°C for the steel fiber mixture compared to 345, 1370 mV.s, 1.2, 3.81, and 1.71 at room temperature and 337, 1130 mV.s, 1.17, 3.31, and 1.83 at -20°C for polypropylene synthetic fiber mixture, as seen in **Table 4-7**. Unlike other AE parameters, the signal amplitude did not show a significant difference when fiber materials changed from steel to polypropylene, and hence no attenuation effect was detected. This conclusion is limited to the fiber content used in this study (0.2%).

#### **4.4.8 Effect of fiber length on the abrasion and AE data under different temperatures**

Two SCC mixtures were developed with two different lengths of synthetic polypropylene fiber (19 and 38mm). Experimental measurements showed that shorter fiber enhances the abrasion resistance compared to longer fiber, irrespective of sample temperature. At room and cold temperatures, the 19 mm fiber mixture (M4) experienced an average percentage of weight loss of 0.24% and 0.22%, respectively, compared to 0.28% and 0.24 %, in the mixture with 38 mm fibers (M5). Also, at room and cold temperatures, the 19 mm fiber mixture (M4) had an

average wear depth of 0.57 and 0.46 mm, respectively, compared to 0.62 and 0.54, respectively, in the 38 mm fiber mixture (**Tables 4-3 and 4-8**). This result could be attributed to the increased value of compressive strength as a result of decreasing the fiber length as can be seen in **Table 4-3**. Another significant reason could be that, at the same volume of fiber (0.2%), increasing the fiber length reduces the number of fibers distributed in the mixture, which leads to a lower effect on controlling the crack growth or confining the concrete.

The analyzed AE parameters, including the number of hits, CSS,  $b$ -value,  $H(t)$ , and  $S_r$  showed a similar trend, as expected (**Table 4-7**). For instance, changing the fiber length from 19 mm to 38 mm yielded a 4% higher average number of hits, 13% higher average CSS, 14% higher average  $H(t)$ , 3% higher average  $S_r$ , and 11% lower average  $b$ -value, at room temperature (which matched an increase in the mass loss due to abrasion). At  $-20^{\circ}\text{C}$ , the collected AE parameters of the 38 mm mixture reported a 3% average increase in the number of hits, 7% average increase in CSS, 13% average increase in  $H(t)$ , 2% average increase in  $S_r$ , and 8% average decrease in  $b$ -value, compared to the 19 mm fiber counterpart mixture. It is worth noting that the 38 mm fiber mixture witnessed a more pronounced enhancement ratio in the abrasion resistance when frozen compared to the 19 mm mixture. For instance, the 38 mm mixture witnessed a 14.3% decrease in mass loss compared to an 8% decrease for the 19 mm fiber mixture when decreasing the sample temperature to  $-20^{\circ}\text{C}$ . This result could be attributed to the improved bond strength between fibers and cement matrix due to concrete shrinkage at freezing temperature, and this effect is more pronounced in longer fibers compared to shorter ones. The AE signals amplitude witnessed no significant change as a result of changing the fiber length in the synthetic polypropylene fiber mixtures, as can be seen in **Fig. 4-8**.

#### **4.4.9 Abrasion damage quantification charts using AE intensity analysis parameters.**

One of the major targets of this study was to evaluate the extent of abrasion damage in various fiber-reinforced concrete mixtures via the analysis of AE characteristics throughout the tests.

Two damage quantification charts were developed in terms of weight loss and wear depth (**Figs. 4-9 and 4-10**, respectively) using the  $H(t)$  and  $S_r$  values at the end of the abrasion test for all mixtures. These charts were developed by combining the calculated AE intensity analysis parameters and experimental results presented in **Tables 4-3, 4-7, and 4-8** at both cold and room temperatures. Using the pair of values of the  $H(t)$  and  $S_r$ , resulting from the intensity analysis, the user can predict the range of mass loss percentage as well as the wear depth from the charts in **Figs. 4-9 and 4-10**. The mass loss attained from all tested mixtures falls into three ranges: 0.15-0.24%, 0.25-0.34%, and 0.35-0.45%, as seen in **Fig. 4-7**. Likewise, the wear depth values in **Fig. 4-10** were classified into three groups: 0.38-0.64, 0.65-0.91, and 0.92-1.26 mm. For example, if the calculated values of  $H(t)$  and  $S_r$  were 1.6 and 3.5 mV.s, respectively, the predicted mass loss could be in the range of 0.25-0.35%, and the predicted wear depth would be 0.65-0.91 mm (**Figs. 4-9 and 4-10**). It is worth noting that these charts are limited to the range of mixtures compositions used in this study tested at room temperature (25°C) and -20°C. Further studies on various SCC mixtures reinforced with other types, lengths, and volumes of fibers are recommended to refine the abrasion damage prediction charts presented herein.

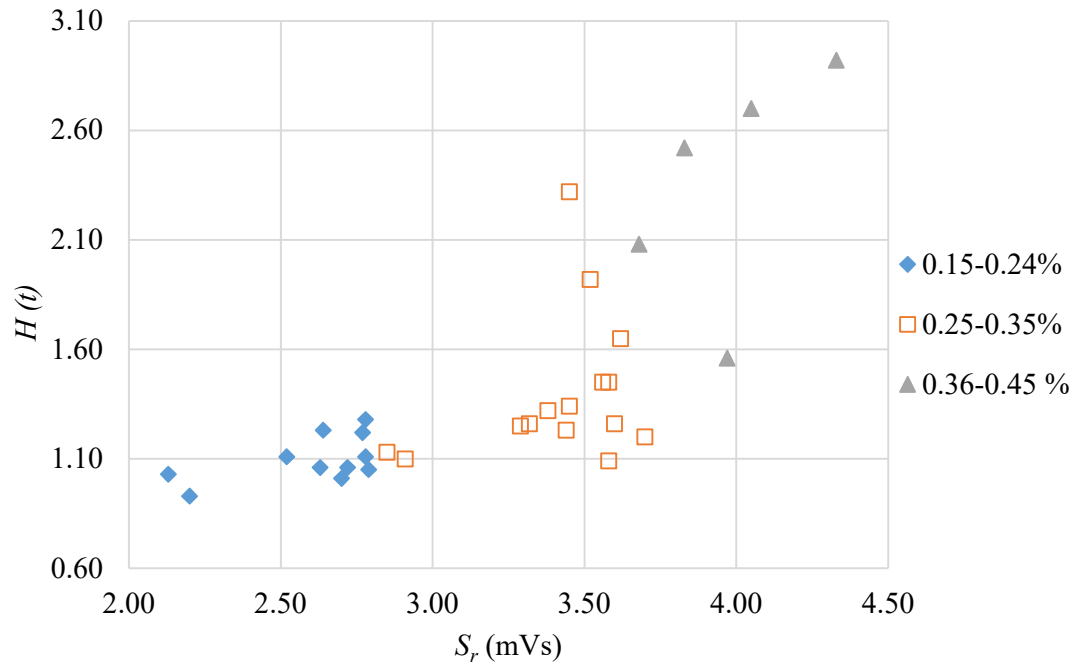


**Fig. 4- 11** Percentage of weight loss (%) quantification chart.

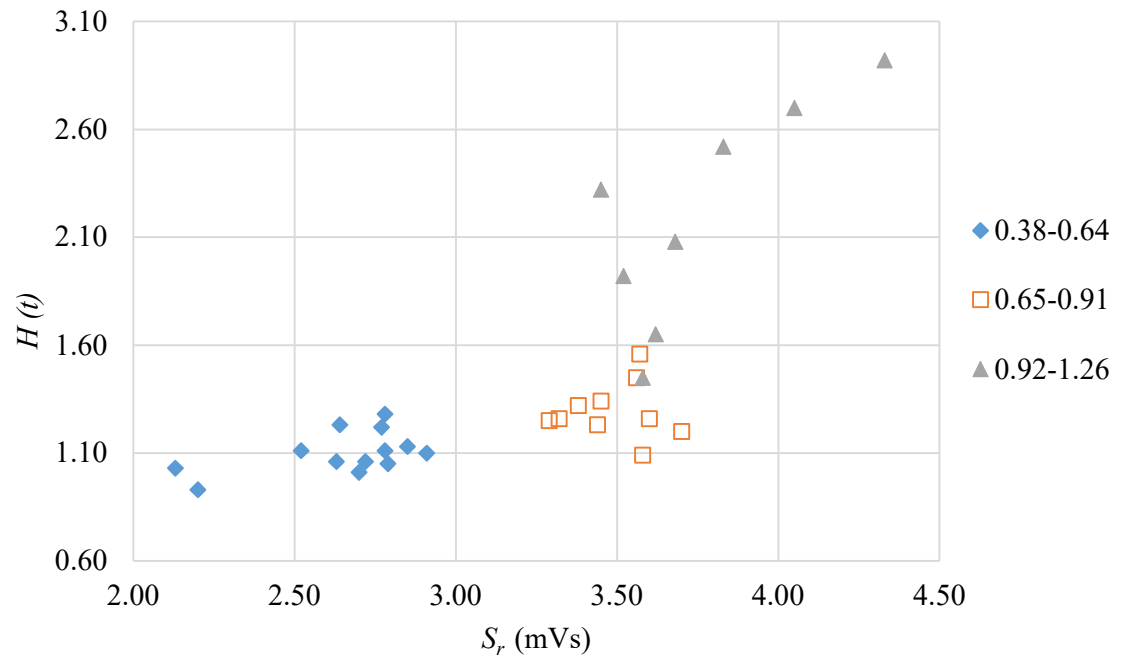


**Fig. 4- 12** Wear depth (mm) quantification chart.

## 4.5 Conclusions

The scope of this study was to evaluate the abrasion performance at a sub-zero temperature of various concrete mixtures reinforced with different types, lengths, and dosages of fibers and different W/B ratios. Cubic samples were tested using the rotating cutter abrasion method along with piezoelectric sensors to collect the AE signals generated during the tests. It should be noted that the scope of this current paper focused on the laboratory examination of the application of AE monitoring. For the potential implementation in the field, further verifications are warranted to confirm the effectiveness of the studied AE parameters for the condition evaluation of existing structures undergoing continuous SHM using the AE technique.

1. The AE parameters, including the number of hits, CSS,  $H(t)$ ,  $S_r$ , and  $b$ -value, were found to be directly correlated to the abrasion damage at both cold and room temperatures. Comparing the experimental and AE results, it was noticed that the increase in both mass loss and wear depth was accompanied by an overall increase in the number of hits, CSS, and  $S_r$  and by an overall decrease in the  $b$ -values. The values of  $H(t)$  kept fluctuating over the test period at a specific value as an indication of the propagation of the abrasion damage.
2. Adding different types, lengths, or volumes of fibers or changing the W/B ratio did not seem to significantly affect the AE signal amplitude as they kept fluctuating with no recognized pattern at both sub-zero and room temperatures. However, it was noticed that the signals collected at sub-zero temperatures seemed to have slightly higher average amplitudes than those obtained at room temperature. The other studied AE parameters (number of hits, CSS,  $H(t)$ ,  $S_r$ , and  $b$ -value) were found to be more sensitive to the abrasion damage progression regardless of concrete mix design or testing temperature.

3. All tested mixtures experienced an overall enhancement in their abrasion performance when tested at cold temperature ( $-20^{\circ}\text{C}$ ) compared to their abrasion performance at room temperature. In addition, the improvement of the abrasion resistance due to cold temperature was more pronounced in mixtures with a higher W/B ratio (0.55) compared to ones with a lower W/B ratio (0.4)
4. Using a higher volume of fibers in the mixture resulted in a slight increase in the abrasion resistance in terms of mass loss and wear depth at both cold and room temperatures compared to the counterpart mixture with a lower volume. This could be attributed to the enhanced crack control in higher fiber volume mixture compared to the lower volume fiber mixture.
5. Using steel fibers in the mixture improved the abrasion performance (lower values of mass loss and wear depth) than using polypropylene synthetic fibers at both cold and room temperatures. The analysis of the values of the calculated AE parameters throughout the tests supported the same outcome.
6. Increasing the length of fibers led to higher average values of mass loss and wear depth compared to mixtures with shorter fibers at both cold and room temperatures, indicating lower abrasion resistance. The retrogression in the abrasion resistance of mixtures with longer fibers versus those with shorter fibers matched an increase in the values of the number of hits, CSS,  $H(t)$ , and  $S_r$ , and a decrease in the  $b$ -value. On the other hand, the mixture with longer fiber experienced a more significant enhancement in the abrasion performance when cooled down to  $-20^{\circ}\text{C}$  compared to that with shorter fiber.
7. The results of this study supported the sensitivity of the AE analysis to assess the abrasion damage of various mixtures with and without fibers at cold temperatures. This study also proposed damage prediction charts which could facilitate the application of AE monitoring to classify the abrasion wear extent. The charts were developed based on the AE intensity

analysis parameters together with the abrasion mass loss and wear depth of all samples tested at room and cold temperatures.

#### **4.6 Chapter References**

AbdelAleem, B. H., and Hassan, A. A. (2019). "Cyclic Behavior of Rubberized Beam-Column Joints Reinforced with Synthetic Fibers." *ACI Materials Journal*, 116(2), 105-118.

AbdelAleem, B. H., Ismail, M. K., and Hassan, A. A. (2017). "Properties of self-consolidating rubberised concrete reinforced with synthetic fibres." *Magazine of Concrete Research*, 69(10), 526-540.

AbdelAleem, B. H., Ismail, M. K., and Hassan, A. A. (2018). "The combined effect of crumb rubber and synthetic fibers on impact resistance of self-consolidating concrete." *Construction and Building Materials*, 162, 816-829.

Abdelrahman, M., ElBatanouny, M. K., Ziehl, P., Fasl, J., Larosche, C. J., and Fraczek, J. (2015). "Classification of alkali-silica reaction damage using acoustic emission: A proof-of-concept study." *Construction & building materials*, 95, 406-413.

Abdelrahman, M., ElBatanouny, M. K., and Ziehl, P. H. (2014). "Acoustic emission-based damage assessment method for prestressed concrete structures: Modified index of damage." *Engineering Structures*, 60, 258-264.

Abouhussien, A. A., and Hassan, A. A. (2017). "Application of acoustic emission monitoring for assessment of bond performance of corroded reinforced concrete beams." *Structural Health Monitoring*, 16(6), 732-744.

Abouhussien, A. A., and Hassan, A. A. A. (2017). "Acoustic emission monitoring for bond integrity evaluation of reinforced concrete under pull-out tests." *Advances in structural engineering*, 20(9), 1390-1405.

ACI237R-07 (2007). "Self-consolidating concrete." 30.

- Aggelis, D., Soulioti, D., Sapouridis, N., Barkoula, N., Paipetis, A., and Matikas, T. (2011). "Acoustic emission characterization of the fracture process in fibre reinforced concrete." *Construction and Building Materials*, 25(11), 4126-4131.
- Anay, R., Cortez, T. M., Jáuregui, D. V., ElBatanouny, M. K., and Ziehl, P. (2016). "On-site acoustic-emission monitoring for assessment of a prestressed concrete double-tee-beam bridge without plans." *Journal of Performance of Constructed Facilities*, 30(4), 04015062.
- ASTM C150, A. (2012). "Standard specification for Portland cement." ASTM international (West Conshohocken, PA).
- ASTM C1611/C1611M, A. (2009). "Standard test method for slump flow of self-consolidating concrete." *Annual book of ASTM standards*, 4, 850-855.
- ASTM C39-12, A. (2012f). "Standard Test Method for Compressive Strength of Cylindrical Concrete Specimens." ASTM International (West Conshohocken).
- ASTM C418-12, A. (2012c). "Standard Test Method for Abrasion Resistance of Concrete by Sandblasting." ASTM International (West Conshohocken).
- ASTM C494-13, A. (2013). "Standard Specification for Chemical Admixtures for Concrete." ASTM International (West Conshohocken).
- ASTM C779/C779M-12, A. (2012b). "Standard Test Method for Abrasion Resistance of Horizontal Concrete Surfaces." ASTM International (West Conshohocken).
- ASTM C944/C944M-12, A. (2012a). "Standard Test Method for Abrasion Resistance of Concrete or Mortar Surfaces by the Rotating-Cutter Method." ASTM International (West Conshohocken).
- Colombo, I. S., Main, I., and Forde, M. (2003). "Assessing damage of reinforced concrete beam using " *b*-value" analysis of acoustic emission signals." *Journal of materials in civil engineering*, 15(3), 280-286.
- Duthil, P. (2015). "Material properties at low temperature." arXiv preprint arXiv:1501.07100.

- E1316, A. (2014). " Terminology for nondestructive examinations." ASTM International (west conshohocken, PA).
- ElBatanouny, M. K., Mangual, J., Ziehl, P. H., and Matta, F. (2014). "Early Corrosion Detection in Prestressed Concrete Girders Using Acoustic Emission." *Journal of materials in civil engineering*, 26(3), 504-511.
- FOWLER, T., BLESSING, J., and CONLISK, P. "New directions in testing." Proc., AECM-3: International Symposium on Acoustic Emission from Composite Materials, 3 rd, Paris, France, 16-27.
- Ghafoori, N., Najimi, M., and Aqel, M. A. (2014). "Abrasion resistance of self-consolidating concrete." *Journal of materials in civil engineering*, 26(2), 296-303.
- Group, M. (2007). "PCI-2 based AE system 1 user's manual." Physical Acoustics Corporation, Princeton Junction, NJ, USA.
- Horszczaruk, E. (2005). "Abrasion resistance of high-strength concrete in hydraulic structures." *Wear*, 259(1), 62-69.
- Ismail, M. K., and Hassan, A. A. (2017). "Impact resistance and mechanical properties of self-consolidating rubberized concrete reinforced with steel fibers." *Journal of Materials in Civil Engineering*, 29(1), 04016193.
- jun Li, J., gang Niu, J., jun Wan, C., Jin, B., and liu Yin, Y. (2016). "Investigation on mechanical properties and microstructure of high-performance polypropylene fiber reinforced lightweight aggregate concrete." *Construction and Building Materials*, 118, 27-35.
- jun Li, J., jun Wan, C., gang Niu, J., feng Wu, L., and chao Wu, Y. (2017). "Investigation on flexural toughness evaluation method of steel fiber reinforced lightweight aggregate concrete." *Construction and Building Materials*, 131, 449-458.

- Khayat, K. H., Kassimi, F., and Ghoddousi, P. (2014). "Mixture design and testing of fiber-reinforced self-consolidating concrete." *ACI Materials Journal*, 111(2), 143.
- Lachemi, M., Hossain, K. M., Lambros, V., and Bouzoubaa, N. (2003). "Development of cost-effective self-consolidating concrete incorporating fly ash, slag cement, or viscosity-modifying admixtures." *Materials Journal*, 100(5), 419-425.
- Lee, G., Shih, T., and Chang, K.-C. (1988). "Mechanical properties of concrete at low temperature." *Journal of cold regions engineering*, 2(1), 13-24.
- Nair, A., and Cai, C. (2010). "Acoustic emission monitoring of bridges: Review and case studies." *Engineering structures*, 32(6), 1704-1714.
- Ohtsu, M., and Tomoda, Y. (2008). "Phenomenological model of corrosion process in reinforced concrete identified by acoustic emission." *ACI materials journal*, 105(2), 194-199.
- Omar, A. T., Sadek, M. M., and Hassan, A. A. (2020). "Impact resistance and mechanical properties of lightweight self-consolidating concrete under cold temperatures." *ACI Materials Journal*, 117(5), 81-91.
- Pigeon, M., and Cantin, R. (1998). "Flexural properties of steel fiber-reinforced concrete at low temperatures." *Cement and Concrete Composites*, 20(5), 365-375.
- Pyo, S., Abate, S. Y., and Kim, H.-K. (2018). "Abrasion resistance of ultra-high performance concrete incorporating coarser aggregate." *Construction & building materials*, 165, 11-16.
- Ridgley, K. E., Abouhussien, A. A., Hassan, A. A., and Colbourne, B. (2018). "Assessing abrasion performance of self-consolidating concrete containing synthetic fibers using acoustic emission analysis." *Materials and Structures*, 51, 1-17.
- Ridgley, K. E., Abouhussien, A. A., Hassan, A. A., and Colbourne, B. (2018). "Evaluation of abrasion resistance of self-consolidating rubberized concrete by acoustic emission analysis." *Journal of Materials in civil Engineering*, 30(8), 04018196.

- Salamone, S., Veletzos, M. J., Lanza di Scalea, F., and Restrepo, J. I. (2012). "Detection of initial yield and onset of failure in bonded post-tensioned concrete beams." *Journal of Bridge Engineering*, 17(6), 966-974.
- Shang, H.-s., Yi, T.-h., and Guo, X.-x. (2014). "Study on Strength and Ultrasonic Velocity of Air-Entrained Concrete and Plain Concrete in Cold Environment." *Advances in materials science and engineering*, 2014, 1-7.
- Vélez, W., Matta, F., and Ziehl, P. (2015). "Acoustic emission monitoring of early corrosion in prestressed concrete piles." *Structural control and health monitoring*, 22(5), 873-887.
- Vidya Sagar, R., and Raghu Prasad, B. (2013). "Laboratory investigations on cracking in reinforced concrete beams using online acoustic emission monitoring technique." *Journal of Civil Structural Health Monitoring*, 3, 169-186.
- Vidya Sagar, R., Raghu Prasad, B., and Sharma, R. (2012). "Evaluation of damage in reinforced concrete bridge beams using acoustic emission technique." *Nondestructive Testing and Evaluation*, 27(2), 95-108.
- Zaki, A., Chai, H. K., Aggelis, D. G., and Alver, N. (2015). "Non-destructive evaluation for corrosion monitoring in concrete: A review and capability of acoustic emission technique." *Sensors*, 15(8), 19069-19101.
- Zaki, R. A., AbdelAleem, B. H., Hassan, A. A., and Colbourne, B. (2020). "Abrasion Resistance of Fiber-Reinforced Concrete under Cold Temperatures." *ACI Materials Journal*, 117(5), 221-232.
- Zaki, R. A., AbdelAleem, B. H., Hassan, A. A., and Colbourne, B. (2021). "Impact resistance of steel fiber reinforced concrete in cold temperatures." *Cement and Concrete Composites*, 122, 104116.

Ziehl, P. H., Galati, N., Nanni, A., and Tumialan, J. G. (2008). "In-situ evaluation of two concrete slab systems. II: evaluation criteria and outcomes." *Journal of Performance of Constructed Facilities*, 22(4), 217-227.

## 5. Summary and Recommendations

### 5.1 Summary

The research project listed in this thesis was divided into three separate studies listed in detail in chapters 2, 3, and 4. The project aimed to investigate the change in the parameters of AE waves emitted in various concrete mixtures when the temperature decreases to sub-freezing levels under special monitoring conditions. Seventeen concrete mixtures were developed, and cubic and prismatic samples were taken and tested under rotating-cutter abrasion and monotonic four-point flexure test. The acoustic activity throughout testing was monitored and collected. The experimental measurements, the AE data analyses results, and the visual notices at both 25°C and -20°C were analyzed and the following conclusions were drawn:

#### **The results of rotating-cutter abrasion test indicated that:**

- Along with abrasion damage progress, the recorded values of cumulative number of hits, CSS,  $H(t)$ , and  $S_r$  witnessed an increase. Meanwhile,  $b$ -values fluctuated with an overall declining trend which indicates a clear correlation between the recorded AE parameters and abrasion damage progression.
- Generally, the AE parameters at -20°C had higher values of cumulative number of hits, CSS,  $H(t)$ , and  $S_r$  and lower  $b$ -values compared to that at 25°C.
- Overall, AE signals' amplitudes significantly decreased along with increasing CR content regardless of samples temperatures throughout testing, as a clear indication of attenuation phenomenon occurrence. Meanwhile, in rubberized concretes, signal attenuation was less noticeable at -20°C. This effect could be attributed to the increase in CR stiffness at sub-zero temperatures.
- Neither rubber particles' size, C/F, W/C, nor different fiber types, lengths, or volumes were found to affect signal amplitudes values in the tested mixtures which proved the inexistence of attenuation phenomenon due to these factors.

- The experimental measurements, AE data analysis, and the visual notices revealed an overall enhanced abrasion performance of concrete mixtures at cold temperature (-20°C) compared to that at 25°C. The enhancement in the abrasion resistance was more pronounced in mixtures with higher C/F, larger CR particles, higher CR contents, higher W/B, and longer fibers.
- The AE intensity analysis parameters  $H(t)$ , and  $S_r$  could be utilized to roughly estimate the ranges of abrasion mass loss and wear depth in plain, rubberized, and fiber reinforced concrete mixtures regardless of samples temperature during the test.

**The results of monotonic four-point flexure test indicated that:**

- Analyzing the variation in the emitted AE parameters during the flexure test enabled early detection of the first micro- and macro-crack onsets, regardless of the samples' temperature.
- The first micro-crack onset was associated with the first significant slope change in the number of hits, CSS, and  $S_r$  curves, a sudden jump in the  $H(t)$  curve, and an extreme dip in the  $b$ -value curve. The onset of the micro-cracking stage ranged from 25%–40% and 35%–50% of the failure flexure load for the prisms when tested at 25°C and -20°C, respectively.
- Visually detected macro-cracks were accompanied by the maximum values of the number of hits, CSS,  $S_r$ ,  $H(t)$ , and the minimum  $b$ -values. These values were recorded right before reaching the highest load and then the split of prisms near the mid-span.
- Decreasing samples' temperature was noticed to increase the threshold limit of both micro- and macro-crack loads. Macro-cracks at -20°C appeared at loads almost 25%–40% higher than those at 25°C. This increase in limits was associated with an average increase in the number of hits, CSS,  $H(t)$ ,  $S_r$ , and a decrease in  $b$ -values for the signals collected at -20°C compared to 25°C.
- Increasing the C/F or CR particle size yielded lower micro- and macro-cracking load thresholds, lower number of hits, CSS,  $H(t)$ ,  $S_r$ , and higher  $b$ -values until the onset of the first

visible macro-crack at both temperature conditions. In addition, changing the C/F did not seem to affect the signal amplitudes of the emitted signals at 25°C and -20°C, which implies similar wave propagation characteristics in various C/F mixtures.

- Increasing CR content was accompanied by a decrease in the number of hits, CSS,  $H(t)$ ,  $S_r$ , and an increase in the  $b$ -values for the collected signals emitted until the onset of the first visible macro-crack. This decrease in AE activity could be related to the low cracking load threshold that did not allow more crack propagation. Noticeably, increasing the CR volume decreased the signal amplitudes of the emitted AE waves as a sign of wave attenuation phenomenon. In addition, the cold temperature was found to relieve the attenuation effect.
- Decreasing the size of rubber particles was found to increase micro- and macro-cracking onset load limits, the associated number of hits, CSS,  $H(t)$ ,  $S_r$ , and decrease the  $b$ -values for signals emitted during the four-point flexure test. Furthermore, cold temperature increased the AE events in mixtures with larger CR sizes and had a more noticeable effect on increasing the micro- and macro-cracking load limits.
- The study confirmed that RA analysis has the potential to identify the AE events associated with micro- or macro-cracking onset in the studied rubberized and non-rubberized mixtures. Two RA vs. AF charts were developed to classify the AE events associated with micro- or macro-cracks in both the rubberized and non-rubberized mixtures.

## **5.2 Potential Applications and Recommendations for Future Research**

The charts developed in this study can be applied in extremely cold regions on offshore structures, bridges, and other civil infrastructure where typical visual inspections for extended periods of time are not possible.

Abrasion and flexure tests were performed in a controlled lab condition on small-scale samples (100 mm cubes and 100 mm\* 100 mm\* 400 mm prisms). Hence, it's recommended that more research be performed on large-scale samples to generate and redefine the quantification charts that were developed in this study. Increasing the size of concrete samples and the existence of reinforcing steel would slightly alter the AE parameters. In addition, the distance between damage sources and acoustic probes is anticipated to increase in larger samples which is anticipated to affect the presented AE results. Besides, the wave reflection phenomenon is anticipated to be more present in larger samples. Testing larger samples would allow for a better understanding of variations in acoustic emission signatures. Lastly, investigating the effects of ice abrasion on concrete samples would also be greatly recommended to better understand the interactions between concrete offshore structures and sea ice.

## Bibliography

- AbdelAleem, B. H., and Hassan, A. A. (2018). "Development of self-consolidating rubberized concrete incorporating silica fume." *Construction and Building Materials*, 161, 389-397.
- AbdelAleem, B. H., and Hassan, A. A. (2019). "Cyclic Behavior of Rubberized Beam-Column Joints Reinforced with Synthetic Fibers." *ACI Materials Journal*, 116(2), 105-118.
- AbdelAleem, B. H., Ismail, M. K., and Hassan, A. A. (2017). "Properties of self-consolidating rubberised concrete reinforced with synthetic fibres." *Magazine of Concrete Research*, 69(10), 526-540.
- AbdelAleem, B. H., Ismail, M. K., and Hassan, A. A. (2018). "The combined effect of crumb rubber and synthetic fibers on impact resistance of self-consolidating concrete." *Construction and Building Materials*, 162, 816-829.
- Abdelrahman, M., ElBatanouny, M. K., Ziehl, P., Fasl, J., Larosche, C. J., and Fraczek, J. (2015). "Classification of alkali-silica reaction damage using acoustic emission: A proof-of-concept study." *Construction & building materials*, 95, 406-413.
- Abdelrahman, M., ElBatanouny, M. K., and Ziehl, P. H. (2014). "Acoustic emission based damage assessment method for prestressed concrete structures: Modified index of damage." *Engineering Structures*, 60, 258-264.
- Abouhussien, A. A., and Hassan, A. A. (2017). "Application of acoustic emission monitoring for assessment of bond performance of corroded reinforced concrete beams." *Structural Health Monitoring*, 16(6), 732-744.
- Abouhussien, A. A., and Hassan, A. A. (2019). "Crack Growth Monitoring in Fiber-Reinforced Self-Consolidating Concrete via Acoustic Emission." *ACI Materials Journal*, 116(5), 181-191.

- Abouhussien, A. A., and Hassan, A. A. A. (2015). "Evaluation of damage progression in concrete structures due to reinforcing steel corrosion using acoustic emission monitoring." *Journal of civil structural health monitoring*, 5(5), 751-765.
- Abouhussien, A. A., and Hassan, A. A. A. (2016). "Detection of bond failure in the anchorage zone of reinforced concrete beams via acoustic emission monitoring." *Smart materials and structures*, 25(7), 75034-75046.
- Abouhussien, A. A., and Hassan, A. A. A. (2017). "Acoustic emission monitoring for bond integrity evaluation of reinforced concrete under pull-out tests." *Advances in structural engineering*, 20(9), 1390-1405.
- Abouhussien, A. A., and Hassan, A. A. A. (2019). "Assessment of Crack Development in Engineered Cementitious Composites Based on Analysis of Acoustic Emissions." *Journal of materials in civil engineering*, 31(6).
- Abouhussien, A. A., and Hassan, A. A. A. (2020). "Classification of damage in self-consolidating rubberized concrete using acoustic emission intensity analysis." *Ultrasonics*, 100, 105999-105999.
- ACI237R-07. (2007). "Self-consolidating concrete." *American Concrete Institute, Farmington Hills, MI, USA*, 30.
- Acoustics, P. (2005). "R6I-AST sensor." *Physical Acoustics Corporation, Princeton Junction, NJ, USA*.
- Aggelis, D., Soulioti, D., Sapouridis, N., Barkoula, N., Paipetis, A., and Matikas, T. (2011). "Acoustic emission characterization of the fracture process in fibre reinforced concrete." *Construction and Building Materials*, 25(11), 4126-4131.
- Aggelis, D. G. (2011). "Classification of cracking mode in concrete by acoustic emission parameters." *Mechanics research communications*, 38(3), 153-157.

- Aggelis, D. G., Soulioti, D. V., Barkoula, N. M., Paipetis, A. S., and Matikas, T. E. (2012). "Influence of fiber chemical coating on the acoustic emission behavior of steel fiber reinforced concrete." *Cement and Concrete Composites*, 34(1), 62-67.
- Aggelis, D. G., Soulioti, D. V., Gatselou, E. A., Barkoula, N. M., and Matikas, T. E. (2013). "Monitoring of the mechanical behavior of concrete with chemically treated steel fibers by acoustic emission." *Construction and Building Materials*, 48, 1255-1260.
- Aldahdooh, M., and Bunnori, N. M. (2013). "Crack classification in reinforced concrete beams with varying thicknesses by mean of acoustic emission signal features." *Construction and Building Materials*, 45, 282-288.
- Anay, R., Cortez, T. M., Jáuregui, D. V., ElBatanouny, M. K., and Ziehl, P. (2016). "On-site acoustic-emission monitoring for assessment of a prestressed concrete double-tee-beam bridge without plans." *Journal of Performance of Constructed Facilities*, 30(4), 04015062.
- ASTM C150-12, (2012) "Standard Specification for Portland Cement," *ASTM International*, West Conshohocken.
- ASTM C1611-09, (2009) "Standard Test Method for Slump Flow of Self-Consolidating Concrete," *ASTM International*, West Conshohocken.
- ASTM C39-12, (2012) "Standard Test Method for Compressive Strength of Cylindrical Concrete Specimens," *ASTM International*, West Conshohocken.
- ASTM C418-12, "Standard Test Method for Abrasion Resistance of Concrete by Sandblasting," *ASTM International*, West Conshohocken (2012c).
- ASTM C494-13, (2013) "Standard Specification for Chemical Admixtures for Concrete," *ASTM International*, West Conshohocken.
- ASTM C618, (2012) "Standard Specification for Coal Fly Ash and Raw or Calcined Natural Pozzolan for Use in Concrete," *ASTM International*, West Conshohocken, PA, USA.

- ASTM C779/C779M-12, "Standard Test Method for Abrasion Resistance of Horizontal Concrete Surfaces," *ASTM International*, West Conshohocken (2012b).
- ASTM C78/C78M. (2016). "Standard Test Method for Flexural Strength of Concrete (Using Simple Beam with Third-Point Loading), PA." *ASTM International: West Conshohocken*.
- ASTM E1316-14, (2014) "Standard Terminology for Nondestructive Examinations," *ASTM International*, West Conshohocken.
- Banthia, N., Yan, C., and Sakai, K. (1998). "Impact resistance of fiber reinforced concrete at subnorma temperatures." *Cement and Concrete Composites*, 20(5), 393-404.
- Behnia, A., Chai, H., Yorikawa, M., Momoki, S., Terazawa, M., and Shiotani, T. (2014). "Integrated non-destructive assessment of concrete structures under flexure by acoustic emission and travel time tomography." *Construction and Building Materials*, 67, 202-215.
- Bignozzi, M., and Sandrolini, F. (2006). "Tyre rubber waste recycling in self-compacting concrete." *Cement and concrete research*, 36(4), 735-739.
- Bisby, L., Eng, P., Banthia, N., Bisby, L., Britton, R., Cheng, R., Mufti, A., Neale, K., Newhook, J., and Soudki, K. (2005). "An Introduction to Structural Health Monitoring."
- Cai, X. P., Yang, W. C., Yuan, J., Ge, Y., and Zhang, B. S. "Effect of low temperature on mechanical properties of concrete with different strength grade." *Proc., Key Engineering Materials*, Trans Tech Publ, 308-312.
- Calabrese, L., Campanella, G., and Proverbio, E. (2010). "USE OF CLUSTER ANALYSIS OF ACOUSTIC EMISSION SIGNALS IN EVALUATING DAMAGE SEVERITY IN CONCRETE STRUCTURES." *Journal of Acoustic Emission*, 28.
- Colombo, I. S., Main, I., and Forde, M. (2003). "Assessing damage of reinforced concrete beam using" b-value" analysis of acoustic emission signals." *Journal of materials in civil engineering*, 15(3), 280-286.

- Du, F., Li, D., and Li, Y. (2019). "Fracture mechanism and damage evaluation of FRP/steel-concrete hybrid girder using acoustic emission technique." *Journal of Materials in Civil Engineering*, 31(7), 04019111.
- Duthil, P. (2015). "Material properties at low temperature." *arXiv preprint arXiv:1501.07100*.
- ElBatanouny, M. K., Mangual, J., Ziehl, P. H., and Matta, F. (2014). "Early Corrosion Detection in Prestressed Concrete Girders Using Acoustic Emission." *Journal of materials in civil engineering*, 26(3), 504-511.
- Fowler, T. B., J. and Conslik, P (2003). "New Directions in testing." *Proceedings, Int. Conf. of Acoustic Emission from composite materials*, K. Ono, ed., Acoustic emission working group Memphis, 15(3), 280-286.
- Ghafoori, N., Najimi, M., and Aqel, M. A. (2014). "Abrasion resistance of self-consolidating concrete." *Journal of materials in civil engineering*, 26(2), 296-303.
- Group, M. (2007). "PCI-2 based AE system 1 user's manual." *Physical Acoustics Corporation, Princeton Junction, NJ, USA*.
- Halsall, P., Cavicchia, L., and McDonough, A. (2016). *Canadian Infrastructure Report Card : Informing the Future*, Johnson-Shoyama Graduate School of Public Policy, Regina, SK, CA.
- Horszczaruk, E. (2005). "Abrasion resistance of high-strength concrete in hydraulic structures." *Wear*, 259(1), 62-69.
- Ismail, M. K., and Hassan, A. A. (2016). "Influence of mixture composition and type of cementitious materials on enhancing the fresh properties and stability of self-consolidating rubberized concrete." *Journal of Materials in Civil Engineering*, 28(1), 04015075.
- Ismail, M. K., and Hassan, A. A. (2017). "Impact resistance and mechanical properties of self-consolidating rubberized concrete reinforced with steel fibers." *Journal of Materials in Civil Engineering*, 29(1), 04016193.

- Ismail, M. K., and Hassan, A. A. A. (2016). "Impact resistance and acoustic absorption capacity of self-consolidating rubberized concrete." *ACI materials journal*, 113(6), 725-736.
- Ismail, M. K., and Hassan, A. A. A. (2016). "Use of metakaolin on enhancing the mechanical properties of self-consolidating concrete containing high percentages of crumb rubber." *Journal of cleaner production*, 125, 282-295.
- jun Li, J., gang Niu, J., jun Wan, C., Jin, B., and liu Yin, Y. (2016). "Investigation on mechanical properties and microstructure of high performance polypropylene fiber reinforced lightweight aggregate concrete." *Construction and Building Materials*, 118, 27-35.
- jun Li, J., jun Wan, C., gang Niu, J., feng Wu, L., and chao Wu, Y. (2017). "Investigation on flexural toughness evaluation method of steel fiber reinforced lightweight aggregate concrete." *Construction and Building Materials*, 131, 449-458.
- Khayat, K. H., Kassimi, F., and Ghoddousi, P. (2014). "Mixture design and testing of fiber-reinforced self-consolidating concrete." *ACI Materials Journal*, 111(2), 143.
- Kim, J. J., Kim, D. J., Kang, S. T., and Lee, J. H. (2012). "Influence of sand to coarse aggregate ratio on the interfacial bond strength of steel fibers in concrete for nuclear power plant." *Nuclear Engineering and Design*, 252, 1-10.
- Lachemi, M., Hossain, K. M., Lambros, V., and Bouzoubaa, N. (2003). "Development of cost-effective self-consolidating concrete incorporating fly ash, slag cement, or viscosity-modifying admixtures." *Materials Journal*, 100(5), 419-425.
- Laplante, P., Aitcin, P. C., and Vézina, D. (1991). "Abrasion Resistance of Concrete." *Journal of materials in civil engineering*, 3(1), 19-28.
- Lee, G., Shih, T., and Chang, K.-C. (1988). "Mechanical properties of concrete at low temperature." *Journal of cold regions engineering*, 2(1), 13-24.

- Li, D., Chen, Z., Feng, Q., and Wang, Y. (2015). "Damage analysis of CFRP-confined circular concrete-filled steel tubular columns by acoustic emission techniques." *Smart materials and structures*, 24(8), 85017-85011.
- Li, G., Zhang, L., Zhao, F., and Tang, J. (2020). "Acoustic Emission Characteristics and Damage Mechanisms Investigation of Basalt Fiber Concrete with Recycled Aggregate." *Materials*, 13(18), 4009.
- Liu, H., Li, W., Luo, G., Liu, S., and Lyu, X. (2020). "Mechanical properties and fracture behavior of crumb rubber basalt fiber concrete based on acoustic emission technology." *Sensors (Basel, Switzerland)*, 20(12), 1-21.
- Liu, M., Lu, J., Ming, P., and Yin, Y. (2021). "Study of fracture properties and post-peak softening process of rubber concrete based on acoustic emission." *Construction & building materials*, 313, 125487.
- Liu, T. C. "Abrasion resistance of concrete." *In: Journal Proceedings*, 78, 341-350.
- Lovejoy, S. C. (2003). "Determining Appropriate Fatigue Inspection Intervals for Steel Bridge Members." *Journal of bridge engineering*, 8(2), 66-72.
- Madandoust, R., and Mousavi, S. Y. (2012). "Fresh and hardened properties of self-compacting concrete containing metakaolin." *Construction and building materials*, 35, 752-760.
- Mohammed, B. S., Anwar Hossain, K. M., Eng Swee, J. T., Wong, G., and Abdullahi, M. (2012). "Properties of crumb rubber hollow concrete block." *Journal of Cleaner Production*, 23(1), 57-67.
- Nair, A., and Cai, C. S. (2010). "Acoustic emission monitoring of bridges: Review and case studies." *Engineering Structures*, 32(6), 1704-1714.
- Najim, K. B., and Hall, M. R. (2012). "Mechanical and dynamic properties of self-compacting crumb rubber modified concrete." *Construction and Building Materials*, 27(1), 521-530.

- Nanni, A. (1989). "Abrasion resistance of roller compacted concrete." *ACI materials journal*, 86(6), 559-565.
- NDIS2421 (2000). "Recommended Practice for In-Situ Monitoring of Concrete Structures by AE." *Japanese Society for Nondestructive Inspection*.
- Ohno, K., and Ohtsu, M. (2010). "Crack classification in concrete based on acoustic emission." *Construction and Building Materials*, 24(12), 2339-2346.
- Ohtsu, M. (1987). "Acoustic emission characteristics in concrete and diagnostic applications." *Journal of Acoustic Emission*, 6(2), 99-108.
- Ohtsu, M., Isoda, T., and Tomoda, Y. (2007). "Acoustic emission techniques standardized for concrete structures." *Journal of Acoustic Emission*, 25(2007), 21-32.
- Ohtsu, M., Shiotani, T., Shigeishi, M., Kamada, T., Yuyama, S., Watanabe, T., Suzuki, T., van Mier, J. G. M., Vogel, T., Grosse, C., Helmerich, R., Forde, M. C., Moczko, A., Breyse, D., Ivanovich, S. A., Sajna, A., Aggelis, D., and Lacidogna, G. (2010). "Recommendation of RILEM TC 212-ACD: acoustic emission and related NDE techniques for crack detection and damage evaluation in concrete: Measurement method for acoustic emission signals in concrete." *Materials and structures*, 43(9), 1177-1181.
- Ohtsu, M., and Tomoda, Y. (2008). "Phenomenological model of corrosion process in reinforced concrete identified by acoustic emission." *ACI materials journal*, 105(2), 194-199.
- Omar, A. T., Sadek, M. M., and Hassan, A. A. (2020). "Impact resistance and mechanical properties of lightweight self-consolidating concrete under cold temperatures." *ACI Materials Journal*, 117(5), 81-91.
- Ono, K. (2011). "Application of acoustic emission for structure diagnosis." *Diagnostyka*, 3-18.

- Ozbay, E., Lachemi, M., and Sevim, U. K. (2011). "Compressive strength, abrasion resistance and energy absorption capacity of rubberized concrete with and without slag." *Materials and structures*, 44(7), 1297-1307.
- Pigeon, M., and Cantin, R. (1998). "Flexural properties of steel fiber-reinforced concretes at low temperatures." *Cement and Concrete Composites*, 20(5), 365-375.
- Pollock, A. A. "Material Brittleness and the energetics of acoustic emission." *Proc., Experimental Mechanics on Emerging Energy Systems and Materials, Volume 5: Proceedings of the 2010 Annual Conference on Experimental and Applied Mechanics*, Springer, 73-79.
- Prem, P. R., and Murthy, A. R. (2016). "Acoustic emission and flexural behavior of RC beams strengthened with UHPC overlay." *Construction and Building Materials*, 123, 481-492.
- Pyo, S., Abate, S. Y., and Kim, H.-K. (2018). "Abrasion resistance of ultra-high performance concrete incorporating coarser aggregate." *Construction & building materials*, 165, 11-16.
- Rahman, M., Usman, M., and Al-Ghalib, A. A. (2012). "Fundamental properties of rubber modified self-compacting concrete (RMSCC)." *Construction and Building Materials*, 36, 630-637.
- Rao, M., Lakshmi, K. P., Rao, G. N., Vijayakumar, K., and Udayakumar, S. (2011). "Precursory microcracking and brittle failure of Latur basalt and migmatite gneiss under compressive loading." *Current Science*, 1053-1059.
- Ridgley, K. E., Abouhussien, A. A., Hassan, A. A., and Colbourne, B. (2018). "Assessing abrasion performance of self-consolidating concrete containing synthetic fibers using acoustic emission analysis." *Materials and Structures*, 51, 1-17.
- Ridgley, K. E., Abouhussien, A. A., Hassan, A. A., and Colbourne, B. (2018). "Evaluation of abrasion resistance of self-consolidating rubberized concrete by acoustic emission analysis." *Journal of Materials in Civil Engineering*, 30(8), 04018196.

- Sadek, D. M., and El-Attar, M. M. (2015). "Structural behavior of rubberized masonry walls." *Journal of Cleaner Production*, 89, 174-186.
- Sagar, R. V., Prasad, B. R., and Kumar, S. S. (2012). "An experimental study on cracking evolution in concrete and cement mortar by the b-value analysis of acoustic emission technique." *Cement and Concrete Research*, 42(8), 1094-1104.
- Salamone, S., Veletzos, M. J., Lanza di Scalea, F., and Restrepo, J. I. (2012). "Detection of initial yield and onset of failure in bonded posttensioned concrete beams." *Journal of Bridge Engineering*, 17(6), 966-974.
- Shahidan, S., Bunnori, N. M., Mohd, S., Nor, N. M., and Johari, M. A. M. "Analysis of the AE signals parameter at the critical area on the concrete beam." *Proc., 2012 IEEE Symposium on Industrial Electronics and Applications*, IEEE, 386-391.
- Shang, H.-s., Yi, T.-h., and Guo, X.-x. (2014). "Study on Strength and Ultrasonic Velocity of Air-Entrained Concrete and Plain Concrete in Cold Environment." *Advances in materials science and engineering*, 2014, 1-7.
- Shigeishi, M., and Ohtsu, M. (2001). "Acoustic emission moment tensor analysis: development for crack identification in concrete materials." *Construction and Building Materials*, 15(5), 311-319.
- Sommer, A. M., Nowak, A. S., and Thoft-Christensen, P. (1993). "Probability-Based Bridge Inspection Strategy." *Journal of structural engineering (New York, N.Y.)*, 119(12), 3520-3536.
- Soulioti, D., Barkoula, N., Paipetis, A., Matikas, T., Shiotani, T., and Aggelis, D. (2009). "Acoustic emission behavior of steel fiber reinforced concrete under bending." *Construction and Building Materials*, 23(12), 3532-3536.

- Su, H., Yang, J., Ling, T.-C., Ghataora, G. S., and Dirar, S. (2015). "Properties of concrete prepared with waste tyre rubber particles of uniform and varying sizes." *Journal of Cleaner Production*, 91, 288-296.
- Sukontasukkul, P., and Chaikaew, C. (2006). "Properties of concrete pedestrian block mixed with crumb rubber." *Construction and Building Materials*, 20(7), 450-457.
- Vélez, W., Matta, F., and Ziehl, P. (2015). "Acoustic emission monitoring of early corrosion in prestressed concrete piles." *Structural control and health monitoring*, 22(5), 873-887.
- Vidya Sagar, R., and Raghu Prasad, B. (2013). "Laboratory investigations on cracking in reinforced concrete beams using online acoustic emission monitoring technique." *Journal of Civil Structural Health Monitoring*, 3, 169-186.
- Vidya Sagar, R., Raghu Prasad, B., and Sharma, R. (2012). "Evaluation of damage in reinforced concrete bridge beams using acoustic emission technique." *Nondestructive Testing and Evaluation*, 27(2), 95-108.
- Wang, C., Zhang, Y., and Ma, A. (2011). "Investigation into the fatigue damage process of rubberized concrete and plain concrete by AE analysis." *Journal of Materials in civil engineering*, 23(7), 953-960.
- Wang, H., Dang, Z., Li, L., and You, Z. (2013). "Analysis on fatigue crack growth laws for crumb rubber modified (CRM) asphalt mixture." *Construction & building materials*, 47, 1342-1349.
- Xu, J., Fu, Z., Han, Q., Lacidogna, G., and Carpinteri, A. (2018). "Micro-cracking monitoring and fracture evaluation for crumb rubber concrete based on acoustic emission techniques." *Structural Health Monitoring*, 17(4), 946-958.
- Youssf, O., Mills, J. E., Benn, T., Zhuge, Y., Ma, X., Roychand, R., and Gravina, R. (2020). "Development of Crumb Rubber Concrete for Practical Application in the Residential

Construction Sector – Design and Processing." *Construction & building materials*, 260, 119813.

Yuyama, S., Li, Z.-w., Ito, Y., and Arazoe, M. (1999). "Quantitative analysis of fracture process in RC column foundation by moment tensor analysis of acoustic emission." *Construction and Building Materials*, 13(1), 87-97.

Zaki, A., Chai, H. K., Aggelis, D. G., and Alver, N. (2015). "Non-destructive evaluation for corrosion monitoring in concrete: A review and capability of acoustic emission technique." *Sensors*, 15(8), 19069-19101.

Zaki, R. A., AbdelAleem, B. H., Hassan, A. A., and Colbourne, B. (2020). "Abrasion Resistance of Fiber-Reinforced Concrete under Cold Temperatures." *ACI Materials Journal*, 117(5), 221-232.

Ziehl, P. H., Galati, N., Nanni, A., and Tumialan, J. G. (2008). "In-situ evaluation of two concrete slab systems. II: evaluation criteria and outcomes." *Journal of Performance of Constructed Facilities*, 22(4), 217-227.